

Scenario set-up and forcing data for impact model evaluation and impact attribution within the third round of the Inter-Sectoral Model Intercomparison Project (ISIMIP3a)

Katja Frieler¹, Jan Volkholz¹, Stefan Lange¹, Jacob Schewe¹, Matthias Mengel¹, María del Rocío Rivas López¹, Christian Otto¹, Christopher P.O. Reyer¹, Dirk Nikolaus Karger², Johanna T. Malle², Simon Treu¹, Christoph Menz¹, Julia L. Blanchard³, Cheryl S. Harrison⁴, Colleen M. Petrik⁵, Tyler D. Eddy⁶, Kelly Ortega-Cisneros⁷, Camilla Novaglio³, Yannick Rousseau³, Reg A. Watson³, Charles Stock⁸, Xiao Liu⁹, Ryan Heneghan¹⁰, Derek Tittensor¹¹, Olivier Maury¹², Matthias Büchner¹, Thomas Vogt¹, Tingting Wang¹³, Fubao Sun¹³, Inga J. Sauer^{1,14}, Johannes Koch¹, Inne Vanderkelen^{15,16,17}, Jonas Jägermeyr^{1,18,19}, Christoph Müller¹, Sam Rabin²⁰, Jochen Klar¹, Iliusi D. Vega del Valle¹, Gitta Lasslop²¹, Sarah Chadburn²², Eleanor Burke²³, Angela Gallego-Sala²⁴, Noah Smith²², Jinfeng Chang²⁵, Stijn Hantson²⁶, Chantelle Burton²³, Anne Gädeke¹, Fang Li²⁷, Simon N. Gosling²⁸, Hannes Müller Schmied^{21,29}, Fred Hattermann¹, Jida Wang³⁰, Fangfang Yao³¹, Thomas Hickler²¹, Rafael Marcé^{32,33}, Don Pierson³⁴, Wim Thiery¹⁵, Daniel Mercado-Bettín³², Robert Ladwig³⁵, Ana I. Ayala³⁴, Matthew Forrest²¹, Michel Bechtold³⁶

Affiliations:

¹Potsdam Institute for Climate Impact Research, 14473 Potsdam, Germany

²Swiss Federal Research Institute WSL, Zürcherstrasse 111, 8903 Birmensdorf, Switzerland

³Institute for Marine and Antarctic Studies, University of Tasmania, Hobart, Tasmania, Australia

⁴Department of Ocean and Coastal Science and Center for Computation and Technology, Louisiana State University, Baton Rouge, Louisiana, USA

⁵Scripps Institution of Oceanography, University of California San Diego, CA, USA

⁶Centre for Fisheries Ecosystems Research, Fisheries & Marine Institute, Memorial University, St. John's, NL, Canada

⁷Department of Biological Sciences, University of Cape Town, Rondebosch, Cape Town, 7701, South Africa

⁸NOAA/OAR/Geophysical Fluid Dynamics Laboratory, Princeton, NJ, United States

⁹SAIC@NOAA/NWS/NCEP Environmental Modeling Center, 5830 University Research Court, College Park, MD 20740

¹⁰School of Mathematical Sciences, Queensland University of Technology, Brisbane, QLD, Australia

¹¹Department of Biology, Dalhousie University, Halifax, Nova Scotia, Canada, B3H 4R2

¹²Institute for Research for Development, UMR 248 MARBEC, France.

¹³Key Laboratory of Water Cycle and Related Land Surface Processes, Institute of Geographic Sciences and Natural Resources Research, Chinese Academy of Sciences, Beijing 100101, China

¹⁴Institute for Environmental Decisions, ETH Zurich, Zurich, Switzerland

¹⁵Vrije Universiteit Brussel, Department of Hydrology and Hydraulic Engineering, Brussels, Belgium

¹⁶Wyss Academy for Nature, University of Bern, Bern, Switzerland

¹⁷Climate and Environmental Physics and Oeschger Center for Climate Change Research, University of Bern, Bern, Switzerland

¹⁸NASA Goddard Institute for Space Studies, New York, NY 10025, USA

¹⁹Columbia University, Climate School, New York, NY 10025, USA

47 ²⁰Climate and Global Dynamics Laboratory National Center for Atmospheric Research Boulder, CO
48 80302, USA
49 ²¹Senckenberg Leibniz Biodiversity and Climate Research Centre (SBIK-F), Frankfurt am Main,
50 Germany.
51 ²²Department of Mathematics, University of Exeter, Exeter UK
52 ²³Met Office Hadley Centre, Fitzroy Road, Exeter, UK
53 ²⁴Geography Department, University of Exeter, Exeter, UK
54 ²⁵College of Environmental and Resource Sciences, Zhejiang University, Hangzhou, China
55 ²⁶Faculty of Natural Sciences, Universidad del Rosario, Bogotá, Colombia
56 ²⁷International Center for Climate and Environment Sciences, Institute of Atmospheric Physics, Chinese
57 Academy of Sciences, Beijing, China
58 ²⁸School of Geography, University of Nottingham, Nottingham, UK
59 ²⁹Institute of Physical Geography, Goethe University Frankfurt, Frankfurt am Main, Germany
60 ³⁰Department of Geography and Geospatial Sciences, Kansas State University, Manhattan, Kansas,
61 USA
62 ³¹Environmental Resilience Institute, University of Virginia, Charlottesville, Virginia 22903, USA
63 ³²Catalan Institute for Water Research (ICRA), 17003 Girona, Spain
64 ³³Universitat de Girona, Girona, Spain³⁴Uppsala University, Norbyvägen 18 D, 752 36 Uppsala, Sweden
65 ³⁵Center for Limnology, University of Wisconsin-Madison, Madison, Wisconsin 53706, USA
66 ³⁶KU Leuven, Department of Earth and Environmental Sciences, Leuven, Belgium

67

68 *Correspondence to:* Katja Frieler (katja.frieler@pik-potsdam.de)

69

70 **Abstract.** This paper describes the rationale and the protocol of the first component of the third
71 simulation round of the Inter-Sectoral Impact Model Intercomparison Project (ISIMIP3a,
72 www.isimip.org) and the associated set of climate-related and direct human forcing data (CRF and
73 DHF, respectively). The observation-based climate-related forcings for the first time include high-
74 resolution observational climate forcings derived by orographic downscaling, monthly to hourly coastal
75 water levels, and wind fields associated with historical tropical cyclones. The DHFs include land use
76 patterns, population densities, information about water and agricultural management, and fishing
77 intensities. The ISIMIP3a impact model simulations driven by these observation-based climate-related
78 and direct human forcings are designed to test to what degree the impact models can explain observed
79 changes in natural and human systems. In a second set of ISIMIP3a experiments the participating
80 impact models are forced by the same DHFs but a counterfactual set of atmospheric forcings and
81 coastal water levels where observed trends have been removed. These experiments are designed to
82 allow for the attribution of observed changes in natural, human and managed systems to climate
83 change, rising CH₄ and CO₂ concentrations, and sea level rise according to the definition of the Working
84 Group II contribution to the IPCC AR6.

85

86 **1 Introduction**

87 The Inter-Sectoral Impact Model Intercomparison Project ISIMIP (www.isimip.org) provides a common
88 scenario framework for cross-sectorally consistent climate impact simulations currently covering the
89 following sectors: agriculture (global; in cooperation with AgMIP's Global Gridded Crop Model
90 Intercomparison Project (GGCMI)), water (global and regional), lakes (global and regional), biomes
91 (global), forest (regional), fisheries and marine ecosystems (global and regional), terrestrial biodiversity

92 (global), fire (global), permafrost (global), peat (global), coastal systems (global), energy (global), health
93 (temperature-related mortality; water-borne diseases; vector-borne diseases; and food security and
94 nutrition) (global and local), and labour productivity (global and local). The impact model simulations
95 are made freely available, allowing for all types of follow-up analysis. The consistent design of the
96 simulations does allow for the comparison of climate impact simulations within each sector. However,
97 it also enables the bottom-up integration of impacts across sectors. Thus, it provides a unique basis for
98 the estimation of the effects of climate change on, e.g., the economy, displacement and migration,
99 health, or water quality resolving the mechanisms along different impact channels and fully exploiting
100 the process-understanding represented in the biophysical impact models.

101
102 Initialised in 2012, ISIMIP is organised in individual modelling rounds. The decision about their design
103 and the development of the associated simulation protocols has been developed into an iterative
104 process between stakeholders and users of ISIMIP data, the sectoral coordinators representing
105 participating modelling teams, the Scientific Advisory Board, and the Cross-Sectoral and Coordination
106 Team at PIK (ISIMIP Coordination Team, Sectoral Coordinators, Scientific Advisory Board, 2018).
107 Since its second round the ISIMIP protocols comprise an ‘a’ part describing impact model simulations
108 that cover the historical period forced by observational climate-related and direct human forcings
109 (evaluation set-up), and a ‘b’ part dedicated to impact simulations based on simulated climate-related
110 forcings including future projections. This paper describes the ISIMIP3a simulation framework only
111 where the DHF described here are also used for the historical simulations within ISIMIP3b. Compared
112 to ISIMIP2a the evaluation set-up based on observational forcing data has been extended to now
113 include additional years up to 2021 and sensitivity experiments using high resolution historical climate
114 forcing data to quantify associated improvements of impact simulations (see section 3.1). Besides, the
115 set of historical observation-based direct human forcings has been updated compared to previous
116 ISIMIP simulation rounds (see **Table 1**). For the first time, and closely connected to the evaluation set-
117 up, ISIMIP3a now also includes an ‘impact attribution’ scenario set-up designed to address the question
118 “To what degree have observed changes in the climate-related systems contributed to observed
119 changes in natural, human or managed systems compared to direct human influences?” Here, changes
120 in climate-related systems mean climate change itself, changes in atmospheric CO₂ and CH₄
121 concentration, and sea level changes. The attribution question can both refer to the impacts of individual
122 events (e.g. to what extent has long-term climate change contributed to the observed extent of a specific
123 river flood?) and to long-term changes (e.g. to what extent have long-term climate change and
124 increasing CO₂ fertilisation contributed to an observed change in crop yields?). The IPCC AR5 (Cramer
125 et al., 2014) and AR6 (O’Neill et al., 2022; Hope et al., 2022) have established a framework for impact
126 attribution according to which an ‘observed impact of climate change or change in any other climate-
127 related system’ is defined as the difference between the observed state of the human, natural or
128 managed system and a counterfactual baseline that characterises the system’s behaviour in the
129 absence of changes in the climate-related systems. This counterfactual baseline may be stationary or
130 vary in response to direct human influences such as changes in land use patterns, agricultural or water
131 management or population distribution and economic development affecting exposure and vulnerability

132 to weather-related hazards. While the definition is established for about a decade at least, the number
133 of studies addressing impact attribution based on this basic definition is still relatively small compared
134 to the number of studies addressing climate attribution, i.e. the question to what degree anthropogenic
135 emissions of climate forcers, in particular greenhouse gases, have induced changes in the climate-
136 related systems. While climate attribution is mainly confronted by the challenge of separating the
137 anthropogenically forced changes from the internal variability of the climate-related systems, the focus
138 of climate impact attribution is on separating the impacts of observed changes in these climate-related
139 systems from the effects of other direct (human) drivers of changes in the considered natural, human
140 or managed systems. 'Observed changes in the climate-related systems' does not necessarily imply
141 'changes induced by anthropogenic climate forcing', but only means 'any long-term trend' in line with
142 the IPCC definition of climate change (see Glossary of the AR5 (IPCC, 2014) and AR6 (Matthews et
143 al., 2021)).

144 Impact attribution studies usually face the problem that the counterfactual baseline assuming no long-
145 term changes in the climate-related systems cannot be observed (see (Hansen et al., 2016) for
146 examples). However, impact models such as the ones participating in ISIMIP are well suited to simulate
147 this baseline. As the impact models usually account not only for the changes in climate or the climate-
148 related systems but also for direct human forcings such as land use and irrigation changes, changes in
149 water and agricultural management, population distributions etc. (see **Table 1** for a comprehensive list
150 of direct human forcings provided within ISIMIP3a) they are ideal tools to address the attribution
151 question: In line with the IPCC definition it requires the comparison of a factual simulation based on the
152 observed variations in the climate-related and direct human drivers to a counterfactual simulations
153 where only the climate-related forcings are replaced by counterfactual versions where long-term trends
154 have been removed. While the factual simulations correspond to the evaluation runs within ISIMIP3a
155 (see section 2.1), the protocol now also includes the counterfactual simulations based on the newly
156 generated counterfactual data sets derived from observational data of climate and coastal water levels
157 (see sections 2.2 for the associated concept and scenario design and **Table 3** for a comprehensive list
158 of the counterfactual climate and sea level forcing data that are described in more detail in section 3.1
159 and 3.3, respectively). To allow for an attribution of 'observed changes in natural, human, and managed
160 systems' in contrast to an attribution of simulated changes it has to be demonstrated that the processes
161 represented in the impact model can explain the observed changes in the affected system, i.e. it has to
162 be shown that the model forced by observed changes in the climate-related systems and accounting
163 for the historical development of direct (human) forcings is able to reproduce the observed changes in
164 the affected system. In this way the attribution exercise is closely linked to the ISIMIP3a evaluation
165 exercise. Thereby, models can either explicitly represent known changes in non-climate drivers such
166 as known adjustments of fertiliser input or growing seasons (explicit accounting for non-climate drivers)
167 or implicitly account for their potential contributions by e.g., allowing for non-climate related temporal
168 trends in empirical models as often done in empirical approaches (implicit accounting for non-climate
169 drivers).

170 While the default attribution experiment in ISIMIP3a is designed for the attribution of observed changes
171 in human, natural, and managed systems to observed change in the climate-related systems in

172 combination (in the current ISIMIP3a setting this is changes in atmospheric climate forcing in
173 combination with changes in atmospheric CO₂ and CH₄ concentrations, see **Table 3**), the protocol
174 also includes a sensitivity experiments that allow for the quantification of the influence of increasing
175 CO₂ concentrations separately and for an attribution of observed changes in natural, human and
176 managed systems to historical changes in atmospheric CO₂ concentrations only (see section **2.1**).
177 Here, we consistently define ‘an observed impact of a change in any component of the historical forcing
178 as the difference between the observed state of the system to a counterfactual world where only this
179 specific component of the forcing has not changed. So the ‘observed impact of increasing CO₂
180 concentrations’ is approximated by the difference between a full forcing run and a run where CO₂
181 concentrations are held constant. This is different from the ‘CO₂ only’ experiment considered within
182 TRENDY (Trends in the land carbon cycle, (Sitch et al., 2015, Protocol - TRENDY, 2023)) where the
183 pure effect of increasing CO₂ concentrations on the terrestrial carbon cycle (e.g. net biome production)
184 is estimated by simulations where the Dynamic Global Vegetation Models (as participating in the biomes
185 sector of ISIMIP) are forced by the observed increases in CO₂ concentrations but a time-invariant “pre-
186 industrial” climate and land use mask. In the above sense, other ISIMIP3a experiments can also be
187 considered counterfactual baseline experiments that allow for the attribution of observed changes in
188 human, natural, or managed systems to changes in the direct human forcings as a whole (DHF set to
189 zero or fixed at 1901 and 2015 levels) or to changes in individual components such as changes in water
190 management, irrigation patterns, and riverine influx of nutrients into the ocean (see section **2.1** and
191 **Table 2**). The attribution to changes in direct human forcings is e.g. similar to the comparison of the full
192 forcing run within TRENDY to the ‘CO₂ and climate only’ run where climate change and atmospheric
193 CO₂ concentrations are prescribed according to observations but land use changes are held constant
194 to quantify the contribution of this direct human forcing to observed changes in the carbon cycle for the
195 annual report of the Global Carbon Project (e.g. (Friedlingstein et al., 2022)). However, in this paper
196 the term ‘impact attribution’ is used as a short form of ‘attribution of observed changes in natural, human
197 and managed systems to observed changes in the climate-related systems’ which is the focus of the
198 ISIMIP3a experiments. In other cases the driver to which the changes are attributed is explicitly named.
199 In addition to ISIMIP3a, there are other model intercomparison projects that address different kinds of
200 attribution questions such as Land Use Model Intercomparison Project (LUMIP, (Lawrence et al., 2016))
201 and Detection and Attribution Model Intercomparison Project (DAMIP, (Gillett et al., 2016)) embedded
202 into the sixth phase of the Coupled Model Intercomparison Project (CMIP6). While the phase 2 LUMIP
203 experiments include historical climate model simulations to quantify the contribution of historical land
204 use changes to observed climate change, the AMIP protocol include a counterfactual ‘no anthropogenic
205 climate forcing’ baseline to attribute observed changes in climate to anthropogenic climate forcings.

206

207 The development of the protocol was coordinated by the ISIMIP-Cross-Sectoral Science Team (CSST)
208 at the Potsdam Institute for Climate Impact Research (PIK) and involved the sectoral coordinators,
209 participating modelling teams, and the Scientific Advisory Board. The process was initiated by a
210 proposal for the main research questions to be addressed and an associated scenario set-up
211 accounting for suggestions collected in a stakeholder engagement process (Lejeune et al., 2018).

212 Following ISIMIP’s mission and implementation document (ISIMIP Coordination Team, Sectoral
213 Coordinators, Scientific Advisory Board, 2018), the basic proposal was approved by the ISIMIP strategy
214 group at the cross-sectoral ISIMIP workshop in Potsdam, September 2018 (Outcomes of the ISIMIP
215 Strategy Group Meeting, 2023). Thereby the CSST and the sectoral coordinators were tasked to
216 translate the decisions into a cross-sectorally consistent simulation protocol and to generate, pre-
217 process or collect the required climate-related and direct human forcing data. The provided forcing data
218 sets (e.g. the climate variables or components of atmospheric composition or types of land use) is very
219 much demand driven. The data we describe here represent a core set that is sufficient for the range of
220 models participating so far (see ISIMIP output data table (ISIMIP Output Data Table, 2023) that also
221 provides information about the input data used by the individual models) but may be extended if there
222 were further demands. This paper presents the results of this process and the motivation and reasoning
223 behind the individual steps for ISIMIP3a, while a follow-up paper will provide the same information for
224 ISIMIP3b dedicated to impact projections based on climate model simulations (Frieler, submitted 2023).
225 It provides the point of reference for modelling teams interested in participating in ISIMIP3a but also for
226 users of the impact simulation data, which become freely accessible according to the ISIMIP terms of
227 use (ISIMIP terms of use, 2023). The paper is accompanied by a simulation protocol (ISIMIP3
228 simulation protocol, 2023) providing all technical details such as file and variable naming conventions
229 and sector-specific lists of output variables to be reported by the participating modelling teams. The
230 ISIMIP3 simulation round was officially started on 21st February 2020¹ with the release of the
231 associated protocol. Since then, the protocol has already received some updates through the addition
232 of output variables, correction of errors, and inclusion of new sectors. This paper refers to the protocol
233 version of 14th January 2023. However, the protocol may still receive updates similar to the ones
234 mentioned above. Impact modellers interested in contributing to ISIMIP should therefore refer to
235 (ISIMIP3 simulation protocol, 2023) for the most up to date version for planned impact model
236 simulations. The protocol landing page (protocol.isimip.org) includes a unique version identifier (the
237 commit hash) that links to the latest protocol version on github for traceability.

238
239 In the second round of ISIMIP the observation-based model evaluation part (ISIMIP2a) was temporally
240 separate from the climate model-based second part (ISIMIP2b, (Frieler et al., 2017). This has led to
241 inconsistencies in the models and model versions contributing to ISIMIP2a and ISIMIP2b. Also, not all
242 models providing future projections within ISIMIP2b also provided model evaluation runs for ISIMIP2a.
243 To avoid this problem and ensure that each model’s set of future projections is accompanied by
244 associated historical simulations allowing for model evaluation, in the third simulation round (ISIMIP3),
245 the ISMIP3a and ISIMIP3b protocols were released together and participating in ISIMIP3 means
246 contributing to ISIMIP3a and ISIMIP3b using the same impact model versions.

247
248 In the following section 2 of this paper, we provide the comprehensive list of all ISIMIP3a model
249 evaluation and sensitivity experiments (see **Table 2** within section 2.1) and the counterfactual ‘no
250 climate change’ experiments (see **Table 4** within section 2.2) describe the rationale behind the scenario

¹ announced via email to the ISIMIP mailing list from 21st February 2020

251 set-ups. Detailed description of the climate-related forcing data sets (see CRF section of **Table 1** in
252 section **2.1** and **Table 3** in section **2.2**) are provided in the third section: atmospheric climate data (see
253 section **3.1**); tropical cyclone data (see section **3.2**); coastal water levels (see section **3.3**), and the
254 ocean data (see section **3.4**). Section **4** presents the ISIMIP3a direct human forcing data sets (see DHF
255 section of **Table 1**), comprising population data (see section **4.1**), gross domestic product (see section
256 **4.2**), land use and irrigation patterns (see section **4.3**), fertiliser inputs (see section **4.4**), land
257 transformations (see section **4.5**), nitrogen deposition (see section **4.6**), crop calendar (see section
258 **4.7**), dams and reservoirs (see section **4.8**), fishing intensities (see section **4.9**), regional forest
259 management (see section **4.10**), and desalination (see section **4.11**).

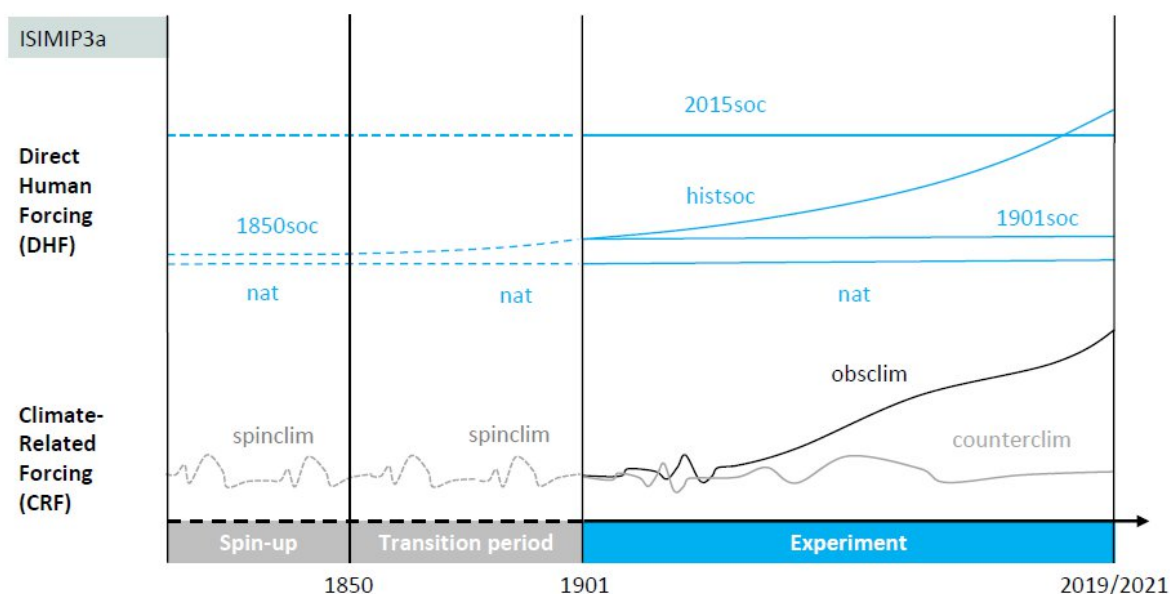
260

261 **2 Experiments and underlying rationale**

262

263 ISIMIP3a includes a core ('default') set of experiments that are specified by a specific set of underlying
264 climate-related forcings and direct human forcings that have to be indicated in the file names when
265 submitting simulation data to the ISIMIP repository. In the following we first introduce these default
266 experiments by defining the combination of both types of forcing data sets. In the subheadings naming
267 the experiments the associated CRF and DHF specifiers to be used in the file names are indicated in
268 brackets where the third sensitivity specifier is set to 'default' (CRF specifier + DHF specifier, default).
269 The different combinations of the default sets of ISIMIP3a CRFs ('obsclim', 'counterclim') and DHFs
270 ('histsoc', '2015soc', '1901soc', '1850soc', 'nat') are sketched in **Figure 1** and defined in more detail
271 below (see **Table 1** for the default 'obsclim' CRF and the default DHFs and **Table 3** for the 'counterclim'
272 CRF). Some of the forcing data sets are mandatory: i.e. if impact models account for the forcing, the
273 specified dataset must be used; if an alternative input data set is used instead, the run cannot be
274 considered an ISIMIP simulation. We also provide 'optional' forcing data that could be used but are not
275 'mandatory' in the above sense (see second column of **Table 1** and **Table 3**). In addition, the protocol
276 includes a set of sensitivity experiments that are described as deviations from the default runs and
277 labelled by the baseline CRF and DHF settings and the third specifier then indicating the deviation from
278 this default setting instead of being set to 'default'. The ISIMIP3a sensitivity runs include experiments
279 with high-resolution climate forcing ('30arcsec', '90arcsec', '300arcsec', or '1800arcsec'), fixed levels
280 of atmospheric CO₂ concentrations ('1901co2'), a scenario assuming no water management
281 ('nowatermgt'), simulations excluding the occurrence of wildfires ('nofire'), keeping irrigation patterns at
282 1901 levels ('1901irr'), and assuming fixed 1955 riverine inputs of freshwater and nutrients into the
283 ocean ('1955-riverine-input') (see **Table 2**). **Table 2** and **Table 4** providing the comprehensive list of all
284 'obsclim' and 'counterclim'-based experiments, respectively, also indicate the priority of the experiments
285 where '1st priority' means that modellers should focus on this set of experiments if their capacities were
286 limited and they wanted to limit the set of experiments. However, this is just an indication trying to ensure
287 the generation of a small set of experiments that is covered by as many impact models as possible. If
288 an impact modeller can only do part of the first priority set-up or has to start from second priority
289 simulations these fragmented data sets can also be submitted to the ISIMIP3a repository.

290



291
 292 **Figure 1: ISIMIP3a scenario design:** Illustration of the default ISIMIP3a forcing data sets. Each experiment is
 293 defined by a combination of a CRF data set with a DHF data set. The considered combinations are listed in **Table**
 294 **2** and **Table 4** and the underlying rationale is described in section 2.1 (evaluation runs based on ‘obsclim’ defined
 295 in **Table 1**) and section 2.2 (attribution runs based on ‘counterclim’ defined in **Table 3**). **Table 1** also lists all data
 296 sets defining the ‘histsoc’ DHF. Solid lines indicate the part of the experiments that should be reported while the
 297 dashed lines illustrate the different spin-up procedures for the models that require a spin-up. Note that the oceanic
 298 climate-related forcing for the *marine ecosystems and fisheries* sector is only available for ‘obsclim’ and the period
 299 1961-2010, i.e. the actual experiments only start from the year 1961. The associated spin-up procedure and the
 300 simulations set-up for a transition period are not illustrated in the Figure but described below for the ‘obsclim +
 301 histsoc, default’, ‘obsclim + nat, default’, ‘obsclim + histsoc, 60arcmin’, and ‘obsclim + nat, 60arcmin’ experiments
 302 considered in this sector.
 303

304 2.1 Model evaluation and sensitivity experiments based on observed CRFs (‘obsclim’)

305 The experiments described in this section are all based on observational (factual) climate data, coastal
 306 water levels, and atmospheric CO₂ as well as CH₄ concentrations including observed trends. The only
 307 exception are the sensitivity experiments where CO₂ concentrations are fixed at 1901 levels
 308 (‘1901co2’). However, as these experiments only deviate in this one aspect from the factual CRF they
 309 are also described by the ‘obsclim’ CRF specifier but the ‘1901co2’ sensitivity specifier to indicate the
 310 deviation. So all experiments described in this section share the common ‘obsclim’ CRF specifier in the
 311 file names. In contrast, all experiments described in section 2.2 can be identified by the ‘counterclim’
 312 specifier in the names of the output files containing the impact model simulations.
 313

314 2.1.1 Default evaluation experiments based on observed CRFs (‘obsclim’)

315 In this first part of section 2.1 we describe the default ISIMIP3a experiments (sensitivity specifier in the
 316 file names set to ‘default’) that are based on the standard observed climate-related forcings (‘obsclim’,
 317 see CRF part of **Table 1**) in combination with different assumptions regarding direct human forcings
 318 (‘histsoc’, ‘2015soc’, ‘1901soc’, and ‘nat’) illustrated in **Figure 1**.
 319

320 **Standard evaluation experiment (obsclim + histsoc; default).** The first set of observation-based
 321 simulations is dedicated to impact model evaluation, i.e., to test our ability to reproduce and explain

322 observed long-term changes or variations in impact indicators such as crop yields, river discharge,
 323 changes in natural vegetation carbon, vegetation types, and peatland moisture conditions. To this end,
 324 we provide the climate-related ('obsclim'), direct human ('histsoc'), and static geographical forcings
 325 listed in **Table 1**. They are described in more detail in sections **3** and **4**.

326
 327 For impact model simulations that require a spin-up to e.g. balance carbon stocks, 100 years of climate
 328 data ('spinclim') are provided that represent stable 1900 climate conditions. The spinclim data is
 329 equivalent to the first 100 years of the counterfactual climate data that are described in section **3.1**. If
 330 more than 100 years of spin-up are needed, the spinclim data can be repeated as often as needed. For
 331 the spin-up, CO₂ concentrations and direct human forcing should be kept constant at 1850 levels. To
 332 get to the historical reporting period starting in 1901, modellers should simulate a transition period from
 333 1850 to 1900 using spinclim climate data and the observed increase in CO₂ concentrations and
 334 historical changes in socioeconomic forcings (from 1850-1900).

335
 336 The temporal coverage of the evaluation experiment is limited to 1961-2010 in the *marine ecosystems*
 337 *and fisheries* sector due to the availability of reanalysis-based oceanic forcing data (Liu et al., 2021).
 338 As spin-up + transition period for the 'obsclim + histsoc, default' experiments starting in 1961 the models
 339 should be run through six cycles of 1961-1980 '1955-riverine-input' CRFs (120 years, see **Table 1**)
 340 assuming reconstructed fishing efforts from 1861-1960 and constant 1861 levels before during 1841-
 341 1860 (see **Table 1** and **Figure 3** in section **4.9**). If more years of spin-up are required, additional cycles
 342 of the 1961-1980 '1955-riverine-input' CRFs should be added, assuming constant 1861 fishing efforts.

343
 344 **Table 1: Climate-related, direct human, and static geographic forcing data provided for the model**
 345 **evaluation and sensitivity experiments within ISIMIP3a.** The CRFs are grouped according to the definition of
 346 the default 'obsclim' CRF (30 arcmin for the atmospheric data and 15 arcmin for the oceanic data), the higher
 347 resolution '30arcsec', '90arcsec', '300arcsec', '1800arcsec' atmospheric CRF, the lower resolution '60arcmin'
 348 oceanic CRF, and the '1955-riverine-input' oceanic CRF for the sensitivity experiments. The listed set of DHFs
 349 defines the 'histsoc' set-up.

Forcing	Status	Source, description
Climate-Related Forcings ('obsclim')		
Atmospheric forcings		
Standard observation-based atmospheric climate forcing	mandatory	GSWP3-W5E5, 20CRv3-W5E5, 20CRv3-ERA5, 20CRv3, see section 3.1
Local atmospheric climate forcing for lake locations	mandatory	Atmospheric data extracted from the data sets above for 72 lakes that have been identified within the <i>lake</i> sector as locations (grid cells of the ISIMIP 0.5° grid) where models can be calibrated based on observed temperature profiles

		and hypsometry (Golub et al., 2022, https://www.isimip.org/gettingstarted/input-data-bias-adjustment/isimip3-local-lake-sites/).
Tropical cyclone tracks, as well as wind and precipitation fields	mandatory	Tracks from IBTrACS database (period 1950-2021; (Knapp et al., 2010). Wind and precipitation fields calculated by Holland (Holland, 1980, 2008), see section 3.2
Lightning	mandatory	Satellite-based (1995-2014) climatology of monthly flash rates (number of strokes km ⁻² d ⁻¹ on 0.5° grid (Cecil, 2006)
Oceanic forcings		
Standard observation-based oceanic forcing data	mandatory	GFDL MOM6/COBALTv2 simulations driven by reanalysis-based atmospheric forcing (Liu et al., 2021) see section 3.4
Regional oceanic climate forcing for regional <i>marine ecosystems</i> and <i>fisheries</i> sector	mandatory	Extraction from data set above for 21 regional marine ecosystems associated with the interests identified by the modelling groups (https://www.isimip.org/gettingstarted/input-data-bias-adjustment/isimip3-ocean-regions/). The extraction has been done for individual layers (ocean surface or bottom) and a subset of the variables that have been integrated along the ocean column (see Table 8).
Coastal water levels		
Coastal water levels	mandatory	Hourly coastal water levels with long-term trends, see section 3.3
Atmospheric composition		
Atmospheric CO ₂ concentration	mandatory	1850-2005: (Meinshausen et al., 2011); 2006-2021: Global annual CO ₂ from NOAA Global Monthly Mean CO ₂ ; (Lan et al., 2023; Büchner and Reyer, 2022)
Atmospheric CH ₄ concentration	mandatory	1850-2014: (Meinshausen et al., 2017); 2015-2021: (Büchner and Reyer, 2022; Lan et al., 2023)
Climate-Related Forcings for sensitivity experiments (30arcsec, 90arcsec, 300arcsec, 1800arcsec,		

60arcmin, and 1955-riverine-input), identical to 'obsclim' except for:		
Atmospheric forcings (30arcsec, 90arcsec, 300arcsec, 1800arcsec)		
High resolution observation-based atmospheric forcing data	mandatory	see section 3.1 for a description of the CHELSA method applied to downscale the W5E5 observation-based atmospheric data to 30". The data is then upscaled to 90" (~3 km), 300" (~10 km) and 1800" = 0.5° (~60 km) to provide the forcings for additional sensitivity experiments.
Oceanic forcings (60arcmin)		
Low resolution observation-based oceanic forcing data	mandatory	GFDL MOM6/COBALTv2 simulations (1961 - 2010) driven by reanalysis-based atmospheric forcing (Liu et al., 2021) upscaled to 1°, see section 3.4
Oceanic forcings (1955-riverine-input)		
Observation-based oceanic forcing data but assuming climatological 1951 to 1958 levels of riverine input	mandatory	GFDL MOM6/COBALTv2 simulations (1961 - 2010) driven by reanalysis-based atmospheric forcing (Liu et al., 2021), but fixed climatological 1951 to 1958 levels of freshwater and nutrients inputs, see section 3.4
Direct Human Forcing ('histsoc')		
Population data	mandatory	see section 4.1
GDP data	mandatory	see section 4.2
Land use and irrigation	mandatory	HYDE-based irrigated and rainfed cropland downscaled to up to 15 crops, managed pasture and grassland, and urban areas, see section 4.3
N-fertiliser inputs	mandatory	see section 4.4
Wood harvest	optional	Historical annual country-level wood harvesting data based on the LUH v2 Harmonization Data Set (del Valle et al., 2022; Hurtt et al., 2011, 2020, Land use harmonization, 2023), see section 4.5
Land transformation	mandatory	Historical annual land-use transformation data, based on the LUH v2 Harmonization Data Set (Hurtt et al., 2011, 2020,

		Land use harmonization, 2023), see section 4.5
N-deposition	optional	(Yang and Tian, 2020; Tian et al., 2018)
Crop calendar	optional	Observation-based representation of recent average planting and maturity dates not accounting for changes over time (Jägermeyr et al., 2021a), see section 4.7
Dams and reservoirs	optional	see section 4.8
Lake and reservoir surface area	optional	Total lake and reservoir area fractions (percentage of grid cell) calculated from the HydroLAKES v1.0 (Messenger et al., 2016) and GRanDv1.3 databases (Lehner et al., 2011b) mapped to 0.5 degrees resolution. Areas increase with time because of the increasing number of reservoirs documented in GRanDv1.3. Reservoirs from 2017 onwards are kept constant. This data set differs from the lake surface areas provided as static geographic forcing (see below) which describe the surface area of one representative lake per grid cell and does not change over time.
Water abstraction	optional	For modelling groups that do not have their own representation, we provide files containing the multi-model mean of domestic and industrial water withdrawal and consumption generated by the WaterGAP, PCR-GLOBWB, and H08 models (1850-2021). This data is based on ISIMIP2a ‘varsoc’ simulations for 1901-2005 and extended by SSP2-based simulations from the Water Futures and Solutions project up to 2021 (Wada et al., 2016b). Years before 1901 have been filled with the value for year 1901.
Marine fishing effort	mandatory	Observation-based reconstruction of fishing effort spanning 1841-2010 (Rousseau et al., 2022) based on (Rousseau et al., submitted 2023); see section 4.9 The climate-related forcing for the <i>marine ecosystems and fisheries</i> sector is only available for 1961-2010, but the spin-up procedure also requires fishing efforts for the earlier years (see description of the procedure for the ‘obsclim + histsoc; default’ scenario above).
Forest management	mandatory	Observed stem numbers, thinning type, planting numbers from and common management practices for 9 forest sites

		in Europe (Reyer et al., 2020b),(Reyer et al., 2023), see section 4.10
Static geographic forcing		
Lake volume at different depths	optional	The gridded data set describes the volume at different depths of one hypothetical lake representing the typical characteristics of all real lakes in the grid cell according to the GLOBathy (Khazaei et al., 2022; Messenger et al., 2016) and HydroLAKES v1.0 (Khazaei et al., 2022; Messenger et al., 2016) datasets (Golub et al., 2022). Each hypsographic curve consists of 11 data pairs. Level refers to the depth of the lake taking the lake bottom as the reference. Volume is the volume at the corresponding level.
Lake area at different depths	optional	The gridded data set describes the lake area at different depths of one hypothetical lake representing the typical characteristics of all real lakes in the grid cell according to the GLOBathy (Khazaei et al., 2022; Messenger et al., 2016)and HydroLAKES (Khazaei et al., 2022; Messenger et al., 2016) datasets (Golub et al., 2022). Each hypsographic curve consists of 11 data pairs. Level refers to the depth of the lake taking the lake bottom as the reference.
Lake elevation	optional	The gridded data set provides the elevation above sea level for the representative lakes described above. The information is derived from HydroLAKES v1.0 (Messenger et al., 2016).
Maximum lake depth	optional	Gridded data set that provides the maximum depth for the representative lakes described above and derived from GLOBathy (Khazaei et al., 2022). We recommend using the area or volume hypsographic curves described above as inputs for your lake model. Use this file only if your lake model does not accept a full hypsographic curve as an input.
Lake depth	optional	Gridded data set that provides the mean depth for the representative lakes as calculated from GLOBathy and HydroLAKES v1.0 (Khazaei et al., 2022; Messenger et al., 2016). We recommend using the area or volume

		hypographic curves described above as inputs for your lake model. Use this file only if your lake model does not accept a full hypographic curve as an input.
Lake volume	optional	Gridded data set of volume (km ³) for representative lakes described above as calculated from GLOBathy and HydroLAKES v1.0 (Khazaei et al., 2022; Messenger et al., 2016). We recommend using the area or volume hypographic curves described above as inputs for your lake model. Use this file only if your lake model does not accept a full hypographic curve as an input.
Lake surface area	optional	Gridded data set of surface area for the representative lakes described above as calculated from GLOBathy and HydroLAKES v1.0 (Khazaei et al., 2022; Messenger et al., 2016). As opposed to the “Lake and reservoir surface area” listed above under “Direct human forcing”, this data set refers to one specific lake associated with each grid cell, and the corresponding surface area does not change over time. We recommend using the area or volume hypographic curves described above as inputs for your lake model. Use this file only if your lake model does not accept a full hypographic curve as an input.
HydroLAKES ID	optional	HydroLAKES reference to relate HydroLAKES and GLOBathy database fields to the representative lakes described above. This dataset contains IDs of the 41449 representative lakes used in ISIMIP, which are a subset of the about 1.4 million lakes contained in the HydroLAKES and GLOBathy database.
HydroLAKES IDs for big lakes	optional	This dataset is analogous to the one above, but only contains IDs of 93 large lakes. It can be used to produce global plots with conspicuous large lakes. To be used together with the file storing the big lakes mask.
Big lakes mask	optional	This dataset indicates the 0.5° grid cells actually occupied by each of the 93 large lakes, which can be larger than a single grid cell. It can be used to produce global plots with conspicuous large lakes. To be used together with the big

		lakes IDs in the dataset above.
Drainage direction map for river routing	optional	Includes for each grid cell a basin number, flow direction, and slope. Source: ISIMIPddm30 (Müller Schmied, 2022) based on DDM30 (Döll and Lehner, 2002)
Soil data	optional	<p>Gridded soil characteristics have been generated within the Global Soil Wetness Project (GSWP3) (Dirmeyer et al., 2006; van den Hurk et al., 2016, Global soil wetness project phase 3 — GSWP3 documentation, 2023) and have already been provided within ISIMIP2a.</p> <p>Alternatively, we also provide maps of the dominant soil types (i.e., the type covering the largest fraction of the cell of the topmost soil layer) within each ISIMIP grid cell and the dominant soil types on the agricultural land within each ISIMIP grid cell. Both maps were derived from the Harmonized World Soil Database (HWSD Version 1.1, 2009) assuming that soil types are evenly distributed within the ISIMIP grid cells. We have used version 1.12 of the HWSD data at high resolution (30 arcsec). Information about the fraction of agricultural land within each ISIMIP 0.5°×0.5° grid cell was taken from MIRCA2000 (Portmann et al., 2010). If there is no soil information for an ISIMIP grid cell, e.g. due to differing land-sea-masks, the information from neighbouring cells is used. For further details please see GGCM-HWSD (2023).</p>
Land-sea mask	optional	We provide the binary land-sea mask of the W5E5 dataset. It is a conservative land mask where grid cells that in reality cover both land and ocean are counted as ocean. Thus, climate conditions over the land grid cells of this land-sea mask can be safely assumed to represent climate conditions over land rather than a mix of climate conditions over land and ocean. This refers to all climate datasets based on W5E5, i.e. GSWP3-W5E5 and 20CRv3-W5E5 of ISIMIP3a and the ISIMIP3b climate forcing that has been bias-adjusted using W5E5. The mask is also provided in a version without Antarctica. In addition, the generic land-sea mask from ISIMIP2b is provided to be used for global water

		simulations in ISIMIP3. It marks more grid cells as land than the main mask described above (Lange and Büchner, 2020).
Sea floor depth	optional	Grid cell level ocean depth in metres of GFDL-MOM6-COBALT2 data in 0.25 and 1° horizontal resolution
Binary country mask	optional	Binary country map on a 0.5° x 0.5° latitude-longitude grid
Fractional country mask	optional	Fractional country map on the ISIMIP 0.5° x 0.5° grid. This is the map that has been used to calculate the national data for ISIPedia (isipedia.org) and to e.g. prepare the national population and GDP data provided within ISIMIP3 (see sections 4.1 and 4.2).
Large Marine Ecosystem masks	mandatory	Binary masks available at 0.25°, 0.5°, and 1° resolution (Sherman, 2017).
Regional Marine Ecosystem masks	optional	Binary masks describing the 21 ocean regions for the regional modelling activities in the fisheries and marine ecosystems available at 0.25° and 1° resolution. These masks have been used for the ocean forcing data extractions (see CRF part of this table).

350

351 **Fixed 2015 direct human forcing (obsclim + 2015soc; default).** To allow for the quantification of the
352 effect of historical changes in direct human forcings, ISIMIP3a also contains an experiment where all
353 direct human forcings are held constant at year 2015 levels. The difference between the evaluation run
354 described above and this baseline simulation can be considered the impact of changes in direct human
355 forcings. In this sense the experiment allows for the attribution of observed changes in the natural,
356 human, and managed systems to changes in DHF after 2015. In addition, the simulated changes in
357 models' output variables can be considered the 'pure effects of climate-related forcings', conditional on
358 present-day socio-economic conditions. The experiment is also introduced because not all impact
359 models can account for varying direct human forcings but rather assume fixed 'present day' conditions.
360 All modelling teams are asked to do this experiment even if they are able to account for varying direct
361 human forcings to generate one set of impact simulations that can be integrated across all participating
362 models from different sectors or where all simulations from one sector can be compared. If a spin-up is
363 required, it should be based on the 'spinclim' data as described above but fixed 2015 direct human
364 forcings.

365

366 **Fixed 1901 direct human forcing baseline (obsclim + 1901soc; default).** Fixing direct human
367 forcings at 1901 levels is an alternative approach to quantify i) the effects of direct human forcings when

368 comparing these baseline simulations to the evaluation run and ii) the ‘pure effect of observed change
369 in climate-related systems’, conditional on socio-economic conditions observed before the onset of this
370 change. As such the experiment is the counterfactual baseline when aiming for the attribution of
371 observed changes in natural, human, and managed systems to observed changes in direct human
372 forcings instead of the attribution to observed changes in the climate-related systems based on the
373 analogous ‘counterfactual + histsoc, default’ experiment described in section 2.2. Both experiments
374 consider changes in direct human forcings or climate-related systems from 1901 levels, respectively.
375 Because of the low levels of direct human forcings in 1901, this experiment is similar to the sector-
376 specific ‘nat’ experiment that includes no direct human forcings whatsoever (see below). However,
377 while the fully naturalised ‘nat’ run is suitable for the dynamic vegetation models from the *biomes* sector
378 that simulate land cover by vegetation on their own, models in other sectors need land cover as an
379 input. As this information is not available for pristine conditions, we introduce the 1901soc scenario
380 such that models in the *water* sector can use land cover data approximately representative of 1901
381 conditions to describe a situation with minor human influences. If a spin-up is required, it should be
382 based on the ‘spinclim’ data as described above but fixed 1901 direct human forcings.

383

384 **No direct human forcing baseline (obsclim + nat; default).** To estimate the full effect of 2015 levels
385 of DHF we also introduce a baseline ‘nat’ experiment that does not consider any DHFs but a natural
386 state of the world. Then the difference to the ‘obsclim + 2015soc, default’ experiment can be considered
387 the effect of 2015 levels of DHF. The comparison to the ‘obsclim + histsoc, default’ experiment allows
388 for the attribution of observed changes in the natural, human, and managed systems to historical
389 changes in the DHF. Trends in the ‘obsclim + nat; default’ run only represent the impacts historical
390 changes in the climate-related forcings would have had on an otherwise natural state of the world.
391 While the ‘1901soc’ conditions may be similar to ‘nat’ conditions, trends in the ‘obsclim + 1901soc;
392 default’ run may not only be induced by historical changes in the CRFs but could also represent lagged
393 responses to changes in DHFs during the transition period. The ‘nat’ experiment can also be used to
394 quantify the natural carbon sequestration potential of natural vegetation without any management or
395 land-use as an important counterfactual baseline to assess the additionality of carbon sequestration
396 measures. The ‘nat’ experiment is sector-specific for the *biomes*, *peat* and *marine ecosystems and*
397 *fisheries* sectors. If a spin-up is required in the *biomes* and *peat* sector, it should be based on the
398 ‘spinclim’ data as described above but assuming no direct human forcings. In the *marine ecosystems*
399 *and fisheries* sector the spin-up should be based on the ‘1955 riverine input’ CRF as described for
400 ‘obsclim + histsoc, default’ section but assuming no DHF, i.e. no fishing efforts.

401

402 **2.1.2 Sensitivity experiments based on observed CRFs (‘obsclim’)**

403 This second part of section 2.1 is dedicated to the different sensitivity experiments described as
404 deviations from the default cases described in section 2.1.1. Instead of the ‘default’ specifier, all
405 experiments described here are labelled by a sensitivity specifiers indicating their deviation from the
406 default cases. The experiments listed here are not explicitly depicted in **Figure 1**.

407

408 **High and low resolution sensitivity experiments (obsclim + histsoc; 30arcsec, 90arcsec,**
409 **300arcsec, 1800arcsec, and 60arcmin).** To test whether high resolution atmospheric climate data
410 improve the climate impact model simulations, we also provide observational atmospheric forcing data
411 at 30" ('30arcsec'), 90" ('90arcsec'), and 300" ('300arcsec') resolution as well as atmospheric forcings
412 at the original 1800" resolution but derived from the 30" (~1 km) data ('1800arcsec'). In addition, the
413 oceanic data (original resolution of 0.25°) is upscaled to 1° to also test the sensitivity of the impact
414 simulations to this modification ('60arcmin').

415 The 30" atmospheric data (1979-2016) is derived from a topographic downscaling of the observational
416 W5E5 data (resolution of 0.5°) that particularly corrects for systematic effects induced by orographic
417 details not represented in global reanalyses (CHELSA-W5E5, see section 3.1). The data set comprises
418 daily mean precipitation, daily mean surface downwelling shortwave radiation, daily mean near-surface
419 air temperature, daily maximum near surface air temperature, daily minimum near surface air
420 temperature (see **Table 5**). We additionally provide simple approaches to downscale surface
421 downwelling longwave radiation, near-surface relative humidity, air pressure and near-surface wind
422 speed (see section 3.1). Given the considerable storage capacities required by daily 1 km x 1 km data
423 and constraints on data handling and download, we also aggregate the CHELSA-W5E5 data to 90" (~3
424 km), 300" (~10 km) and 1800" = 0.5° (~60 km) to determine which resolution is required to improve the
425 impact model simulations compared to observed impact indicators. The evaluation of these historical
426 sensitivity experiments will inform future downscaling activities for the GCM climate forcing data
427 including future projections. The '1800arcsec' experiment is included as a reference, as the aggregated
428 CHELSA-W5E5 data differ from the standard W5E5 data at the same resolution (see section 3.1). So
429 far the experiments have been added to the agriculture, lakes, global and regional water, regional
430 forests, terrestrial biodiversity, and labour protocol. However, they may be added to other sectors, too.
431 The inclusion of the experiment is only constrained by the restricted set of variables included in
432 CHELSA-W5E5. We do not provide spin-up data for the experiments. This means that models requiring
433 a spin-up currently cannot perform the experiments. We will work on a solution on demand.

434 In contrast to the experiment testing the sensitivity of the impact simulations to a higher resolution of
435 the atmospheric CRFs, the associated sensitivity experiment for the *marine ecosystems and fisheries*
436 sector is not based on higher but on lower resolution oceanic data. While the default 'obsclim' oceanic
437 forcing data is derived by interpolating the observation-based historical ocean simulations from a tri-
438 polar 0.25° grid to a regular 0.25° grid (see section 3.4), the CRFs for the sensitivity experiment are
439 derived by aggregating the default 'obsclim' data to a regular 1.0° grid ('60arcmin'). Evaluating the 1.0°
440 resolution is of interest because this is the resolution of the oceanic forcing data in ISIMIP3b. The low
441 resolution simulations could either start from the end of the simulations of the transition period of the
442 associated higher resolution runs ('obsclim + histsoc; default') or starting conditions could be newly
443 generated by following the 'spin-up + transition' procedure of 'obsclim + histsoc; default' experiment but
444 using the low-resolution '1955-riverine-input' CRF from the years 1961-1980.

445

446 **Low resolution sensitivity experiment (obsclim + nat; 60arcmin).** This sensitivity experiment for
447 the *marine ecosystems and fisheries* sector is analogous to the 'obsclim + nat; default' experiment

448 described further above, but using the lower-resolution oceanic CRF ('60arcmin'). The difference
449 between this experiment and the 'obsclim + histsoc; 60arcmin' sensitivity experiment can be considered
450 the effect of the historical changes in DHF as estimated using lower-resolution CRF, and comparison
451 with the same difference in the default experiments then indicates how the estimate of this effect
452 depends on the resolution of the oceanic forcing. The simulations could either start from the end of the
453 simulations of the transition period of the associated higher resolution runs ('obsclim + nat; default') or
454 starting conditions could be newly generated by following the 'spin-up + transition' procedure of 'obsclim
455 + nat, default' experiment but using the low-resolution '1955-riverine-input' CRF from the years 1961-
456 1980.

457

458 **CO₂ sensitivity experiments (obsclim + histsoc, obsclim + 2015soc, or obsclim + 1901soc;**
459 **1901co2).** To quantify the pure effect of the historical increase in atmospheric CO₂ concentrations on
460 vegetation leaf gas exchange and follow-on effects on carbon stocks, water use efficiency, vegetation
461 distribution etc., we introduced three sensitivity experiments where atmospheric CO₂ concentrations
462 are held constant at 1901 levels (= 296.13 ppm) in contrast to the default 'obsclim + histsoc', 'obsclim
463 + 2015soc', or 'obsclim + 1901soc' experiments, respectively, where atmospheric CO₂ concentrations
464 are assumed to increase according to observations. The effect is known as CO₂ fertilisation through an
465 increase of the photosynthesis rate of plants and limited leaf transpiration (increase in water use
466 efficiency) enabling a more efficient uptake of carbon by the plants. Comparing the 'obsclim + histsoc,
467 default' experiment to the 'obsclim + histsoc, 1901soc' experiment can be considered as attributing
468 historical changes in natural, human, and managed systems to historical changes in CO₂
469 concentrations as a single component of the changes in climate-related systems. The experiment is
470 included into the protocols of the *agriculture, terrestrial biodiversity, biomes, fire, lakes (global and*
471 *local), permafrost, peat and water (global and regional)* sector. A potentially required spin-up should be
472 identical to the spin-up for the associated default experiments using the transition period 1850-1900 to
473 reach the 1901 CO₂ level.

474

475 **Water management sensitivity experiment (obsclim + histsoc, obsclim + 2015soc; nowatermgt).**
476 In this "no water management" experiment, models are run assuming no irrigation, no human water
477 abstraction, no dams or reservoirs, and no seawater desalination, while other direct human forcings
478 such as land use changes are considered according to 'histsoc' or '2015soc'. By comparison to the
479 default experiments, the simulations allow for a quantification of the pure effects of dedicated water
480 management measures on, e.g., discharge. When comparing 'obsclim + histsoc, nowatermgt' to
481 'obsclim + histsoc, default' this can be considered attributing observed changes in natural, human, or
482 managed systems to (changes in) water management. The sensitivity experiment has been introduced
483 into the *global and regional water* sector protocols. If a spin-up is required, it should be done similar to
484 the spin-up for the associated default experiments but assuming "no water management".

485

486 **Irrigation sensitivity experiment (obsclim + histsoc, 1901irr).** In this "no irrigation expansion"
487 experiment, models are run assuming irrigation extent and irrigation water use efficiencies fixed at the

488 year 1901, while other direct human forcings such as land use changes and water management
489 categories are considered according to 'histsoc' or '2015soc'. By comparison to the default experiments,
490 the simulations allow for a quantification of the pure effects of historical irrigation expansion (i.e. the
491 attribution of historical changes in natural, human, or managed systems to changes in irrigation
492 compared to 1091). The sensitivity experiment has been introduced into the *global water and biome*
493 sector protocols. If a spin-up is required, it should be done similar to the spin-up for the associated
494 default experiments but assuming "no irrigation expansion". This experiment is designed such that its
495 outcomes are comparable to those of the Irrigation Impacts Model Intercomparison Project (IRRMIIP;
496 <https://hydr.vub.be/projects/irrmip>), in which Earth System Models simulate irrigation influences on the
497 Earth system.

498

499 **No-fire sensitivity experiment (obsclim + histsoc; nofire).** In this 'nofire' experiment, fire is switched
500 off in the model simulations. In comparison to the default 'obsclim + histsoc' simulations, the historical
501 effects of fires on, e.g., carbon fluxes and vegetation distributions can be determined. The sensitivity
502 experiment has been introduced into the *fire, biomes, permafrost, and peat* protocols. The required
503 spin-up should be done similar to the spin-up for the associated default experiments but assuming no
504 fire activities.

505

506 **Fixed 1955 riverine input into the ocean sensitivity experiment (obsclim + histsoc; obsclim +**
507 **nat; 1955-riverine-input).** In this '1955-riverine-input' experiment, riverine input into the ocean (amount
508 of freshwater and nutrients) is held constant at 1955 levels. In comparison to the default 'obsclim +
509 histsoc' simulation, the experiment allows for the quantification of the impacts of historical climate-
510 induced variations in freshwater influx in combination with the climate and directly human induced
511 changes in nutrient inputs (attribution of observed changes in marine ecosystems and fisheries to long
512 term changes in riverine freshwater and nutrient inputs). The riverine inputs in the 'obsclim + nat; 1955-
513 riverine-input' experiment are identical to the ones in the 'obsclim + histsoc; 1955-riverine-input', i.e.
514 the riverine inputs also account for the human contribution to the nutrient influx due to land use changes
515 and fertiliser inputs and are not 'naturalized'. Instead the 'nat' specifier in the marine ecosystems and
516 fisheries sector only means 'no fishing efforts'. Thus, the comparison to the naturalised default
517 experiment (obsclim + nat; default) not accounting for any fishing efforts to the 'obsclim + nat; 1955-
518 riverine-input' experiment allows for a quantification of the contribution of climate-induced changes in
519 freshwater-influx to the overall impacts of climate change in combination with the contribution of the
520 effect of the human contribution to nutrient inputs at 1955 levels. The sensitivity experiment has been
521 introduced into the marine ecosystems and fisheries protocol. A potentially required spin-up should be
522 done similar to the spin-up for the associated default experiments but assuming riverine inputs fixed at
523 1955 levels.

524

525 **Table 2: ISIMIP3a evaluation and sensitivity experiments**

Experiment	Short description	Period: Historical 1901-2019
model evaluation histsoc	CRF: Observed climate change, CO ₂ and CH ₄ levels, and coastal water levels	obsclim
1st priority	DHF: Varying direct human influences according to observations	histsoc
model evaluation 2015soc	CRF: Observed climate change, CO ₂ and CH ₄ levels, and coastal water levels	obsclim
1st priority	DHF: Fixed 2015 levels of direct human forcing for the entire time period	2015soc
model evaluation 1901soc	CRF: Observed climate change, CO ₂ and CH ₄ levels, and coastal water levels	obsclim
2nd priority	DHF: Fixed 1901 levels of direct human forcing for the entire time period	1901soc
model evaluation nat	CRF: Observed climate change, CO ₂ and CH ₄ levels, and coastal water levels	obsclim
2nd priority	DHF: No direct human influences	nat
CO₂ sensitivity histsoc	CRF: Observed climate change, CH ₄ concentrations and coastal water levels, fixed CO ₂ concentration at 1901 level	obsclim Sensitivity experiment: 1901co2
2nd priority	DHF: Varying direct human influences according to observations	histsoc
CO₂ sensitivity 2015soc	CF: Observed climate change, CH ₄ concentrations and coastal water levels, fixed CO ₂ concentration at 1901 level	obsclim Sensitivity experiment: 1901co2

2nd priority	DHF: Fixed 2015 levels of direct human forcing for the entire time period	2015soc
CO₂ sensitivity 1901soc 2nd priority	CRF: Observed climate change, CH ₄ concentrations and coastal water levels, fixed CO ₂ concentration at 1901 level	obsclim Sensitivity experiment: 1901co2
	DHF: Fixed 1901 levels of direct human forcing for the entire time period	1901soc
Water management sensitivity histsoc 2nd priority	CRF: Observed climate change, coastal water levels, and CO ₂ and CH ₄ concentrations	obsclim
	DHF: No accounting for water management but representation of other direct human influences such as land use changes according to "histsoc"	histsoc Sensitivity experiment: nowatermgt
Water management sensitivity 2015soc 2nd priority	CRF: Observed climate change, coastal water levels, and CO ₂ and CH ₄ concentrations	obsclim
	DHF: No accounting for water management but representation of other direct human influences such as land use patterns according to "2015soc"	2015soc Sensitivity experiment: nowatermgt
Irrigation sensitivity histsoc 2nd priority	CRF: Observed climate change, coastal water levels, and CO ₂ and CH ₄ concentrations	obsclim
	DHF: Fixed year-1901 irrigation areas and water use efficiencies but representation of other direct human influences such as land use changes according to "histsoc"	histsoc Sensitivity experiment: 1901irr
No-fire sensitivity	CRF: Observed climate change, coastal water levels, CO ₂ and CH ₄ concentrations	obsclim

histsoc 2nd priority	DHF: Varying direct human influences according to observations	histsoc Sensitivity experiment: nofire
Riverine influx sensitivity histsoc 2nd priority	CRF: Observation-based oceanic forcing data, but with constant riverine nutrient and freshwater influx. DHF: Varying direct human influences according to observations	obsclim Sensitivity experiment: 1955-riverine-input histsoc
Riverine influx sensitivity nat 2nd priority	CRF: Observation-based oceanic forcing data, but with constant riverine nutrient and freshwater influx. DHF: No direct human influences	obsclim Sensitivity experiment: 1955-riverine-input nat
High-resolution sensitivity, 1km histsoc 2nd priority	CRF: Observed high-resolution climate forcing (30"), coastal water levels, and CO ₂ and CH ₄ concentrations. For this experiment only 1979-2016 is covered DHF: Varying direct human influences according to observations	obsclim Sensitivity experiment: 30arcsec histsoc
High-resolution sensitivity, 3km histsoc 2nd priority	CRF: Observed high-resolution climate forcing (90"), coastal water levels, and CO ₂ and CH ₄ concentrations. For this experiment only 1979-2016 is covered DHF: Varying direct human influences according to observations	obsclim Sensitivity experiment: 90arcsec histsoc
High-resolution sensitivity, 12km	CRF: Observed high-resolution climate forcing (360"), coastal water levels, and CO ₂ and CH ₄ concentrations. For this experiment only 1979-	obsclim Sensitivity

histsoc 2nd priority	2016 is covered	experiment: 360arcsec
	DHF: Varying direct human influences according to observations	histsoc
High-resolution sensitivity, 60km histsoc 2nd priority	CRF: Observed climate forcings aggregated from high-resolution data, coastal water levels, CO ₂ and CH ₄ concentrations. For this experiment only 1979-2016 is covered	obsclim Sensitivity experiment: 1800arcsec
	DHF: Varying direct human influences according to observations	histsoc
Low-resolution sensitivity, 1° in the ocean histsoc 2nd priority	CRF: Observation-based oceanic forcing data	obsclim Sensitivity experiment: 60arcmin
	DHF: Varying direct human influences according to observations	histsoc
Low-resolution sensitivity, 1° in the ocean nat 2nd priority	CRF: Observation-based oceanic forcing data	obsclim Sensitivity experiment: 60arcmin
	DHF: No direct human influences	nat

526

527 **2.2 Counterfactual baseline simulations for impact attribution ('counterclim')**

528

529 The second set of impact model simulations within ISIMIP3a is dedicated to the attribution of historical
 530 changes in natural, managed, and human systems to long-term changes in climate-related systems,
 531 i.e. the atmosphere, ocean and cryosphere as physical or chemical systems (see section 1). In
 532 ISIMIP3a, we address attribution to changes in the climate system itself, e.g., trends in atmospheric
 533 temperature and precipitation, and changes in coastal water levels, and atmospheric CO₂
 534 concentrations. The provided counterfactual forcing data comprises daily atmospheric climate derived
 535 from the ISIMIP observational climate datasets (see section 3.1); daily counterfactual coastal water

536 levels derived from the ISIMIP historical coastal water level dataset (see section 3.3); and constant
 537 1901 atmospheric CO₂ and CH₄ concentrations (see **Table 3**). So far, we do not address attribution to
 538 long-term changes in i) the ocean (e.g. temperature or ocean acidification changes), ii) the cryosphere
 539 (e.g. glacier mass loss), and iii) tropical cyclone characteristics (e.g. trends in associated heavy
 540 precipitation or wind speeds) other than the effects mediated through sea level rise. **Table 3** lists the
 541 climate-related forcings defining the ‘counterclim’ experiments. The ‘counterclim’ climate-related
 542 forcings are combined with the observed direct human forcing to facilitate the attribution experiments
 543 listed in **Table 4** and explained below.

544

545

Table 3: ISIMIP3a counterfactual climate-related forcings (‘counterclim’)

Forcing	Status	Source, description
Climate-related forcings (counterclim)		
Atmospheric forcings		
Counterfactual ‘no-climate change’ atmospheric climate forcing	mandatory	Detrended versions of the GSWP3-W5E5, 20CRv3-W5E5, 20CRv3-ERA5, 20CRv3 data sets derived by the Attrici method, see section 3.1
Local atmospheric climate forcing for lake location	mandatory	Atmospheric data extracted from the data sets above for 72 lakes that have been identified within the <i>lake</i> sector as locations (grid cells of the ISIMIP 0.5° grid) where models can be calibrated based on observed temperature profiles and hypsometry (depth and area).
Tropical cyclone tracks and windfields	mandatory	We do not provide ‘no climate change’ TC tracks and windfields but the original tracks from the IBTrACS database (Knapp et al., 2010); period 1841-2021) windfields calculated by Holland model (Holland, 2008, 1980) should be used in combination with the counterfactual water levels to estimate the impacts of sea level rise on TC induced damages, losses or replacement, see section 3.2
Lightning	mandatory	We do not provide ‘no climate change’ lightning data. Instead the original Flash Rate Monthly Climatology (Cecil, 2006) should be used in the

		'counterclim' set-up.
Oceanic forcings		
Oceanic forcing data	-	We do not provide any counterfactual oceanic forcings, i.e. there is no 'no climate change' experiment proposed for the <i>marine ecosystems and fisheries</i> sector.
Coastal water levels		
Coastal water levels	mandatory	Counterfactual monthly (1901 - 1978) and hourly (1979 - 2015) coastal water levels where long-term trends have been removed, see section 3.3
Atmospheric composition or fluxes		
Atmospheric CO ₂ concentration	mandatory	1901 levels ([CO ₂] = 296.13 ppm) of observed atmospheric CO ₂ concentrations according to (Meinshausen et al., 2011)
Atmospheric CH ₄ concentration	mandatory	1901 levels of atmospheric CH ₄ concentrations ([CH ₄] = 928.80 ppb), according to (Meinshausen et al., 2017)

546

547 **Standard attribution experiment using counterfactual climate-related forcings and observed**
548 **variations of direct human forcings (counterclim + histsoc; default).** This is the twin experiment to
549 the default 'obsclim+histsoc' evaluation experiment. It uses the 'counterclim' climate-related forcings
550 as described in **Table 3** while all direct human forcings are the same as the ones used in the evaluation
551 experiment ('histsoc'). As the corresponding evaluation experiment aims to ensure that impact models
552 can fully capture the historical variations including its long-term trends, this experiment is best suited
553 for impact attribution. It is therefore the standard impact attribution experiment that each sector should
554 strive to follow.

555

556 **Fixed 2015 direct human forcing attribution experiment (counterclim + 2015soc; default).** This
557 is the twin experiment to the 'obsclim+2015soc' experiment. It uses the 'counterclim' climate-related
558 forcings as described in **Table 3** and constant direct human forcings at 2015 levels ('2015soc'). Impact
559 attribution using this experiment has caveats because the twin 'obsclim+2015soc' experiment is not
560 built to fully explain the historical observations including its trends. Impact attribution building on this
561 experiment therefore needs to find other means to ensure that the impact model correctly captures the

562 response to changes in the climate-related systems. It may e.g. build on the assumption that fixed direct
 563 human forcings do not change the models' sensitivity to historical climate change. The impact models
 564 that cannot account for varying historical direct human forcings can take up the attribution task through
 565 this experiment.

566
 567 **Fixed 1901 direct human forcing attribution experiment (counterclim + 1901soc; default).** This is
 568 the twin experiment to the 'obsclim+1901soc' experiment. It allows for a quantification of the combined
 569 effect of changes in all forcings (climate-related and direct human) during the historical period when
 570 compared to the default evaluation experiment ('obsclim+histsoc'). It also allows for a quantification of
 571 the effect of varying direct human drivers when compared to the 'counterclim+histsoc' experiment and
 572 the effect of the 2015 to 1901 difference in direct human forcing if compared to the
 573 'counterclim+2015soc' experiment, conditional on counterclim climate-related forcings.

574
 575 **No direct human forcing attribution experiment (counterclim + nat; default)** This is the twin
 576 experiment to the default 'obsclim+nat' experiment. It allows for a quantification of the effect of climate
 577 change under conditions of absent direct human forcings but a natural state of the world. The 'nat'
 578 experiment is included in the *biomes* sector protocol.

579

580 **Table 4: ISIMIP3a attribution experiments**

Experiment	Short description	Period: Historical 1901-2019
counterfactual climate histsoc 1st priority	CRF: Detrended observational atmospheric climate forcing, detrended observed coastal water level forcings, and other CRF as listed in Table 3	counterclim
	DHF: Varying direct human influences according to observations	histsoc
counterfactual climate 2015soc 1st priority	CRF: Detrended observational atmospheric climate forcing, detrended observed coastal water level forcings, and other CRF as listed in Table 3	counterclim
	DHF: Fixed 2015 levels of direct human forcing for the entire time period	2015soc

counterfactual climate 1901soc 2nd priority	CRF: Detrended observational atmospheric climate forcing, detrended observed coastal water level forcings, and other CRF as listed in Table 3	counterclim
	DHF: Fixed 1901 levels of direct human forcing for the entire time period	1901soc
counterfactual climate nat 2nd priority	CRF: Detrended observational atmospheric climate forcing, detrended observed coastal water level forcings, and other CRF as listed in Table 3	counterclim
	DHF: No direct human influences	nat

581

582 3 Climate-related forcing data

583

584 3.1 Observational atmospheric climate forcing data (factual + counterfactual)

585

586 The data sets described in this section all contain the variables listed in **Table 5** at the resolution
587 indicated there. While section **3.1.1** described the standard atmospheric climate forcing as one
588 component of the default ‘obsclim’ CRF used within the evaluation experiments (see section **2.1.1**),
589 section **3.1.2** describes the derivation of the high resolution data used within the ‘obsclim’-based
590 sensitivity experiments (see section **2.1.2**), and section **3.1.3** provides a description of the basic
591 approach and the references for the derivation of the counterfactual atmospheric climate forcings
592 used for the ‘counterclim’ experiments described in section **2.2**.

593

594

Table 5: Atmospheric climate variables provided as part of the climate-related forcing

Variable	Variable specifier	Unit	Resolution	Datasets
Near-Surface Relative Humidity	hurs	%	0.5° grid, daily	GSWP3-W5E5 (factual and counterfactual, 1901-2019), 20CRv3-W5E5 (factual and counterfactual, 1901-2019), 20CRv3-ERA5 (factual and counterfactual, 1901-2021), 20CRv3 (factual and counterfactual, 1901-2015)
Near-Surface Specific Humidity	huss	kg kg ⁻¹	0.5° grid, daily	GSWP3-W5E5 (factual and counterfactual, 1901-2019), 20CRv3-W5E5 (factual and counterfactual, 1901-2019), 20CRv3-ERA5

				(factual and counterfactual, 1901-2021), 20CRv3 (factual and counterfactual, 1901-2015)
Precipitation (including snowfall)	pr	kg m-2 s-1	0.5° grid, daily	GSWP3-W5E5 (factual and counterfactual, 1901-2019), 20CRv3-W5E5 (factual and counterfactual, 1901-2019), 20CRv3-ERA5 (factual and counterfactual, 1901-2021), 20CRv3 (factual and counterfactual, 1901- 2015)
			30" grid, 90" grid, 300" grid, 1800" grid; daily	CHELSA-W5E5 (factual, 1979-2016)
Snowfall	prsn	kg m-2 s-1	0.5° grid, daily	GSWP3-W5E5 (factual only, 1901-2019, 0.5°)
Surface Air Pressure	ps	Pa	0.5° grid, daily	GSWP3-W5E5 (factual and counterfactual, 1901-2019), 20CRv3-W5E5 (factual and counterfactual, 1901-2019), 20CRv3-ERA5 (factual and counterfactual, 1901-2021), 20CRv3 (factual and counterfactual, 1901- 2015)
Surface Downwelling Longwave Radiation	rlds	W m-2	0.5° grid, daily	GSWP3-W5E5 (factual and counterfactual, 1901-2019), 20CRv3-W5E5 (factual and counterfactual, 1901-2019), 20CRv3-ERA5 (factual and counterfactual, 1901-2021), 20CRv3 (factual and counterfactual, 1901- 2015)
Surface Downwelling Shortwave Radiation	rsds	W m-2	0.5° grid, daily	GSWP3-W5E5 (factual and counterfactual, 1901-2019), 20CRv3-W5E5 (factual and counterfactual, 1901-2019), 20CRv3-ERA5 (factual and counterfactual, 1901-2021), 20CRv3 (factual and counterfactual, 1901- 2015)

			30" grid, 90" grid, 300" grid, 1800" grid; daily	CHELSA-W5E5 (1979-2016)
Near-Surface Wind Speed	sfcwind	m s-1	0.5° grid, daily	GSWP3-W5E5 (factual and counterfactual, 1901-2019), 20CRv3-W5E5 (factual and counterfactual, 1901-2019), 20CRv3-ERA5 (factual and counterfactual, 1901-2021), 20CRv3 (factual and counterfactual, 1901-2015)
Near-Surface Air Temperature	tas	K	0.5° grid, daily	GSWP3-W5E5 (factual and counterfactual, 1901-2019), 20CRv3-W5E5 (factual and counterfactual, 1901-2019), 20CRv3-ERA5 (factual and counterfactual, 1901-2021), 20CRv3 (factual and counterfactual, 1901-2015)
			30" grid, 90" grid, 300" grid, 1800" grid; daily	CHELSA-W5E5 (1979-2016)
Daily Maximum Near-Surface Air Temperature	tasmax	K	0.5° grid, daily	GSWP3-W5E5 (factual and counterfactual, 1901-2019), 20CRv3-W5E5 (factual and counterfactual, 1901-2019), 20CRv3-ERA5 (factual and counterfactual, 1901-2021), 20CRv3 (factual and counterfactual, 1901-2015)
			30" grid, 90" grid, 300" grid, 1800" grid; daily	CHELSA-W5E5 (factual and counterfactual, 1979-2016)
Daily Minimum Near-Surface Air	tasmin	K	0.5° grid, daily	GSWP3-W5E5 (factual and counterfactual, 1901-2019), 20CRv3-W5E5 (factual and counterfactual, 1901-2019), 20CRv3-ERA5

Temperature				(factual and counterfactual, 1901-2021), 20CRv3 (factual and counterfactual, 1901-2015)
			30" grid, 90" grid, 300" grid, 1800" grid; daily	CHELSA-W5E5 (1979-2016)

595

596 3.1.1 Default factual data

597 As one component of the default ‘obsclim’ CRFs, we provide four observational datasets specifically
598 generated for the evaluation experiments of ISIMIP3a: GSWP3-W5E5, 20CRv3-W5E5, 20CRv3-ERA5,
599 and 20CRv3. All four datasets have daily temporal and 0.5° spatial resolution and cover the variables
600 listed in **Table 5**. Their temporal coverage varies, with GSWP3-W5E5 and 20CRv3-W5E5 covering
601 1901-2019, while 20CRv3-ERA5 covers 1901-2021 and 20CRv3 covers 1901-2015. Instead of
602 excluding datasets that do not cover the most recent years, we focused on including datasets that start
603 in 1901, to allow for a common spin-up procedure (described in section 2.1 for the ‘obsclim + histsoc;
604 default’ experiment), in order to support models that need to spin up, e.g., their carbon pools under
605 stable climate-related and direct human forcings before they can do the actual experiments.

606

607 The GSWP3-W5E5 dataset is based on W5E5 v2.0 (Lange et al., 2021), which is also used as the
608 observational reference dataset for the bias adjustment of climate input data for ISIMIP3b that will be
609 described in an ISIMIP3b protocol paper (Frieler, submitted 2023). W5E5 v2.0 combines WFDE5 v2.0
610 ((Cucchi et al., 2020) with data from the latest version of the European Reanalysis (ERA5; (Hersbach
611 et al., 2020) over the ocean. WFDE5 v2.0 is generated with the WATCH Forcing Data methodology
612 that includes bias adjustment of all variables (Cucchi et al., 2020). Since W5E5 v2.0 only covers the
613 years 1979 to 2019, it was extended backward in time to the year 1901. For this extension, we used
614 version 1.09 of the Global Soil Wetness Project phase 3 (GSWP3) dataset (Kim, 2017), bias-adjusted
615 to W5E5 v2.0 in order to reduce discontinuities at the 1978–1979 transition. The method used for this
616 bias adjustment was ISIMIP3BASD v2.5 (Lange, 2019, 2021). The GSWP3 dataset is a dynamically
617 downscaled and bias-adjusted version of the Twentieth Century Reanalysis version 2 (20CRv2; (Compo
618 et al., 2011)). For a detailed description of the GSWP3-W5E5 dataset and its constituents, see (Mengel
619 et al., 2021).

620

621 Unfortunately, for some variables, GSWP3 shows discontinuities at every turn of the month. The month-
622 by-month bias adjustment applied in its creation is responsible for this artefact (Rust et al., 2015). In
623 order to overcome this issue, which also affects GSWP3-W5E5, we additionally provide 20CRv3-
624 W5E5, a dataset where W5E5 v2.0 is backward-extended using ensemble member 1 of the Twentieth
625 Century Reanalysis version 3 (20CRv3; (Slivinski et al., 2019, 2021), interpolated to 0.5° and then bias-

626 adjusted to W5E5 v2.0 using ISIMIP3BASD v2.5. The 20CRv3-W5E5 data are continuous at every turn
627 of the month thanks to the application of ISIMIP3BASD v2.5 in running-window mode (see section 3.1).
628 Since GSWP3 is based on 20CRv2, the 20CRv3-W5E5 dataset can be considered an update of
629 GSWP3-W5E5.

630

631 Two more climate input datasets are provided in ISIMIP3a in order to facilitate climate input data-related
632 quantifications of uncertainty in the associated impact assessments. Those datasets are not based on
633 W5E5 to account for trend and variability artefacts in W5E5 that are related to the climatological infilling
634 procedures used to deal with gaps in the station observations employed for the bias adjustment of
635 ERA5 for the production of WFDE5 (for a detailed description of this caveat see
636 <https://data.isimip.org/caveats/20/>). The first of the additional ISIMIP3a climate input datasets is
637 20CRv3-ERA5, which was created in the same way as 20CRv3-W5E5, but using ERA5 instead of
638 W5E5 for the time period 1979-2021, and also as the bias adjustment target for the time period 1901-
639 1978. Finally, we also provide the ‘raw’ 20CRv3 data, i.e., ensemble member 1 of 20CRv3, interpolated
640 to 0.5° but not bias-adjusted to any other dataset. This dataset is included since it was generated with
641 only one method and did not need to be combined with another dataset to fully cover the 20th century.

642

643 3.1.2 High resolution atmospheric factual data (CHELSA-W5E5)

644 This dataset is provided to facilitate the high resolution sensitivity experiment described in section 2.1.2.
645 It covers the global land area at 30" (~1 km) horizontal and daily temporal resolution from 1979 to 2016
646 for the variables precipitation (pr), surface downwelling shortwave radiation (rsds), and daily mean,
647 minimum and maximum near-surface air temperature (tas, tasmin, tasmax). CHELSA-W5E5 v1.0
648 (Karger et al., 2022b) is a downscaled version of the W5E5 v1.0 dataset, where the downscaling is
649 done with the Climatologies at High resolution for the Earth’s Land Surface Areas (CHELSA) v2.0
650 algorithm (Karger et al., 2017, 2021, 2022a).

651

652 This algorithm applies topographic adjustments based on surface altitude (orog) information from the
653 Global Multi-resolution Terrain Elevation Data 2010 (GMTED2010; (Danielson and Gesch, 2011)). The
654 algorithm is applied day by day. CHELSA-W5E5 tas is obtained by applying a lapse rate adjustment to
655 W5E5 tas, using differences between CHELSA-W5E5 orog and W5E5 orog in combination with
656 temperature lapse rates from ERA5. Those lapse rates are calculated based on atmospheric
657 temperature, T , at 950 hPa and 850 hPa, and the geopotential height, z , of those pressure levels. The
658 lapse rate used for the adjustment is calculated as the daily mean of hourly values of $(T_{850} - T_{950}) /$
659 $(z_{850} - z_{950})$. The variables tasmax and tasmin are downscaled in the same way, using the same
660 lapse rate value.

661 Precipitation downscaling uses daily mean zonal and meridional wind components from ERA5 to
662 approximate the orographic wind effect on small-scale precipitation patterns (differences between
663 windward and leeward precipitation rates) and combines that with the height of the planetary boundary
664 layer to estimate the total orographic effect on precipitation intensity. Using that, precipitation from

665 W5E5 is downscaled such that precipitation fluxes are preserved at the original 0.5° resolution of W5E5.
666 More details are given in (Karger et al., 2021).

667 Surface downwelling shortwave radiation, $rsds$, at 30 arcsec resolution is strongly influenced by
668 topographic features such as aspect or terrain shadows, which are less pronounced at 0.5° resolution.
669 The downscaling algorithm combines such geometric effects with orographic effects on cloud cover for
670 an orographic adjustment of $rsds$. Geometric effects are considered by computing 30" clear-sky
671 radiation estimates using the method described in (Karger et al., 2022a) and a simplified, uniform
672 atmospheric transmittance of 80%. These effects include shadowing from surrounding terrain, diffuse
673 radiation, and terrain aspect. To include how orographic effects on cloud cover influence $rsds$, the clear-
674 sky radiation estimates are adjusted using downscaled ERA5 total cloud cover. The cloud cover
675 downscaling uses ERA5 cloud cover at all pressure levels and the orographic wind field following the
676 methods described in (Brun et al., 2022b). Finally, the clear-sky radiation estimates adjusted for cloud
677 cover are rescaled such that they match W5E5 $rsds$, B-spline interpolated to 30".

678 We provide the original CHELSA-W5E5 data with a horizontal resolution of 30" = $0.5'$ (~ 1 km) as well
679 as spatially aggregated versions with resolutions of $1.5'$ (~ 3 km, aggregation factor 3), $5.0'$ (~ 10 km,
680 aggregation factor 10) and $30.0' = 0.5^\circ$ (~ 60 km, aggregation factor 60). The aggregation to 0.5° is
681 necessary since the aggregated CHELSA-W5E5 data differ from the default GSWP3-W5E5 and
682 20CRv3-W5E5 data provided in the 'obsclim' set-up for 1979-2016. This has two reasons. First, the
683 downscaled data are based on W5E5 v1.0 whereas GSWP3-W5E5 and 20CRv3-W5E5 are based on
684 W5E5 v2.0. Secondly, for all variables except pr , the CHELSA downscaling algorithm produces data
685 that differs from the original data when it is upscaled (spatially aggregated) back to the original
686 resolution.

687
688 We do not provide a counterfactual version of the high resolution climate forcing.
689

690 The CHELSA method is not yet available for all variables included in the standard forcing data. Relative
691 humidity, surface wind, air pressure, and longwave radiation can not yet be downscaled by the
692 approach. To allow modellers to start the sensitivity experiments already now, we provide an alternative
693 downscaling approach as described below. We use observational data with the required higher spatial
694 resolution but lower temporal resolution to generate the high resolution daily relative humidity and
695 surface wind speeds. Air pressure is derived by on orographic correction of the linearly interpolated sea
696 level pressure and surface downwelling longwave radiation is derived from high-resolution
697 temperatures derived by CHELSA and relative humidity. The code required to generate the data is
698 freely available (Malle, 2023).

699
700 For daily mean near-surface relative humidity ($hurs$) the provided downscaling algorithm combines
701 monthly 30" CHELSA-BIOCLIM+ data (Brun et al., 2022b, a) with daily W5E5 data. In a first step we
702 regrid daily 0.5° W5E5 $hurs$ to the target grid (30") by bilinear interpolation. We assume relative humidity
703 to follow a beta-distribution and logit-transform both regridded monthly-averaged W5E5 ($hurs_{mon}^{W5E5}$) and

704 monthly CHELSA-BIOCLIM+ ($hurs_{mon}^{CHELSA}$) relative humidity data. The difference ($\Delta hurs_{mon}$) is then
 705 added to daily regrided and logit-transformed W5E5 hurs of the respective month, and the final raster
 706 is obtained by back-transforming the sum:

$$707 \quad hurs_{dly} = \frac{1}{(1+exp^{-h})}, \quad (1)$$

708 where

$$709 \quad h = \log\left(\frac{hurs_{dly}^{W5E5}}{1-hurs_{dly}^{W5E5}}\right) + \Delta hurs_{mon}, \quad (2)$$

$$710 \quad \Delta hurs_{mon} = \log\left(\frac{hurs_{mon}^{CHELSA}}{1-hurs_{mon}^{CHELSA}}\right) - \log\left(\frac{hurs_{mon}^{W5E5}}{1-hurs_{mon}^{W5E5}}\right). \quad (3)$$

711 To include orographic effects into daily mean near-surface wind speed ($sfcwind$) we follow the approach
 712 of (Brun et al., 2022b), and use an aggregation of the Global Wind Atlas 3.0 data (Badger et al.,
 713 n.d.) Technical University of Denmark (Badger et al., n.d.) in combination with daily 0.5° sfcwind from
 714 W5E5. We first regrid both the Global Wind Atlas data and the W5E5 sfcwind data to the target grid of
 715 30" using bilinear interpolation. The Global Wind Atlas data product ($sfcWind_{cli}^{GWA}$) represents average
 716 wind speeds for 2008 to 2017. We therefore average daily regrided W5E5 data over this time period
 717 ($sfcWind_{cli}^{W5E5}$). We assume surface wind speeds follows a Weibull distribution and log-transform both
 718 datasets before computing the difference $\Delta sfcWind_{cli}$, whereby a small positive constant (c) was added
 719 to all data points before applying the transformation to avoid the problem that $\log(0)$ is undefined. We
 720 add this difference layer ($\Delta sfcWind_{cli}$) to each log-transformed daily W5E5 raster, and back-transform
 721 the sum to obtain the final daily mean near-surface wind speed raster:

$$722 \quad sfcWind_{dly} = exp^{(\log(sfcWind_{dly}^{W5E5} + c) + \Delta sfcWind_{cli})} - c, \quad (4)$$

723 where

$$724 \quad \Delta sfcWind_{cli} = \log(sfcWind_{cli}^{GWA} + c) - \log(sfcWind_{cli}^{W5E5} + c). \quad (5)$$

725

726 Daily mean surface air pressure (ps) is calculated using the barometric formula:

$$727 \quad ps_{dly} = psl_{dly}^{W5E5} \times exp^{-(g \times orog \times M)/(T_0 \times R)}, \quad (6)$$

728 with psl_{dly}^{W5E5} being the regrided 0.5° W5E5 daily mean sea-level pressure (bilinear interpolation to 30"),
 729 g the gravitational acceleration constant (9.80665 m/s²), $orog$ the altitude at which air pressure is
 730 calculated (CHELSA-W5E5 orog, m), M the molar mass of dry air (0.02896968 kg/mol), R the universal
 731 gas constant (8.314462618 J/(mol K)) and T_0 the sea level standard temperature (288.16 K).

732

733 For Surface Downwelling Longwave Radiation (*rlds*) we follow (Fiddes and Gruber, 2014) as well as
 734 (Konzelmann et al., 1994), and account for orographic effects by reducing the clear-sky component of
 735 all-sky emissivity with elevation. We assume cloud emissivity remains unchanged when moving from
 736 coarse to fine resolution. First, we compute clear-sky emissivity components both for the 0.5° W5E5
 737 grid and the target 30" grid (ϵ_{clear}^{W5E5} , $\epsilon_{clear}^{highres}$ respectively):

$$738 \epsilon_{clear}^{highres/W5E5} = 0.23 + x1(pV_{dly}^{highres/W5E5} / tas_{dly}^{highres/W5E5})^{1/x2}, (7)$$

739 where $x1 = 0.43$ and $x2 = 5.7$ and $pV_{dly}^{highres/W5E5}$ is water vapour pressure as a function of relative
 740 humidity at the respective resolution (see (Fiddes and Gruber, 2014)). By using 0.5° W5E5 *rlds* and *tas*
 741 data and inverting the Stefan-Boltzmann equation we obtain all-sky emissivity:

$$742 \epsilon_{allsky}^{W5E5} = rlds_{dly}^{W5E5} / (\sigma \times (tas_{dly}^{W5E5})^4), (8)$$

743 with σ being the Stefan-Boltzmann constant ($5.67 \times 10^{-8} \text{ Js}^{-1} \text{ m}^{-2} \text{ K}^{-4}$). In a next step, the cloud-based
 744 component of emissivity ($\Delta\epsilon_{dly}^{W5E5}$) can be estimated as the difference between all-sky and clear-sky
 745 emissivity, which is then regridded to the target grid via bilinear interpolation.

$$746 \Delta\epsilon_{dly}^{W5E5} = \epsilon_{allsky}^{W5E5} - \epsilon_{clear}^{W5E5} (9)$$

747 In a last step we obtain elevation-corrected longwave radiation ($rlds_{dly}$) by adding $\Delta\epsilon_{dly}^{W5E5}$ to the high-
 748 resolution clear-sky emissivity ($\epsilon_{clear}^{highres}$) and applying the Stefan-Boltzmann law again:

$$749 rlds_{dly} = (\epsilon_{clear}^{highres} + \Delta\epsilon_{dly}^{W5E5}) \times \sigma \times (tas_{dly}^{highres})^4 (10)$$

750 As soon as the CHELSA approach is extended to also cover the missing variable we plan to also provide
 751 these data and test for the sensitivity of the impact simulations to these two alternative downscaling
 752 methods.

753

754 3.1.3 Default counterfactual data.

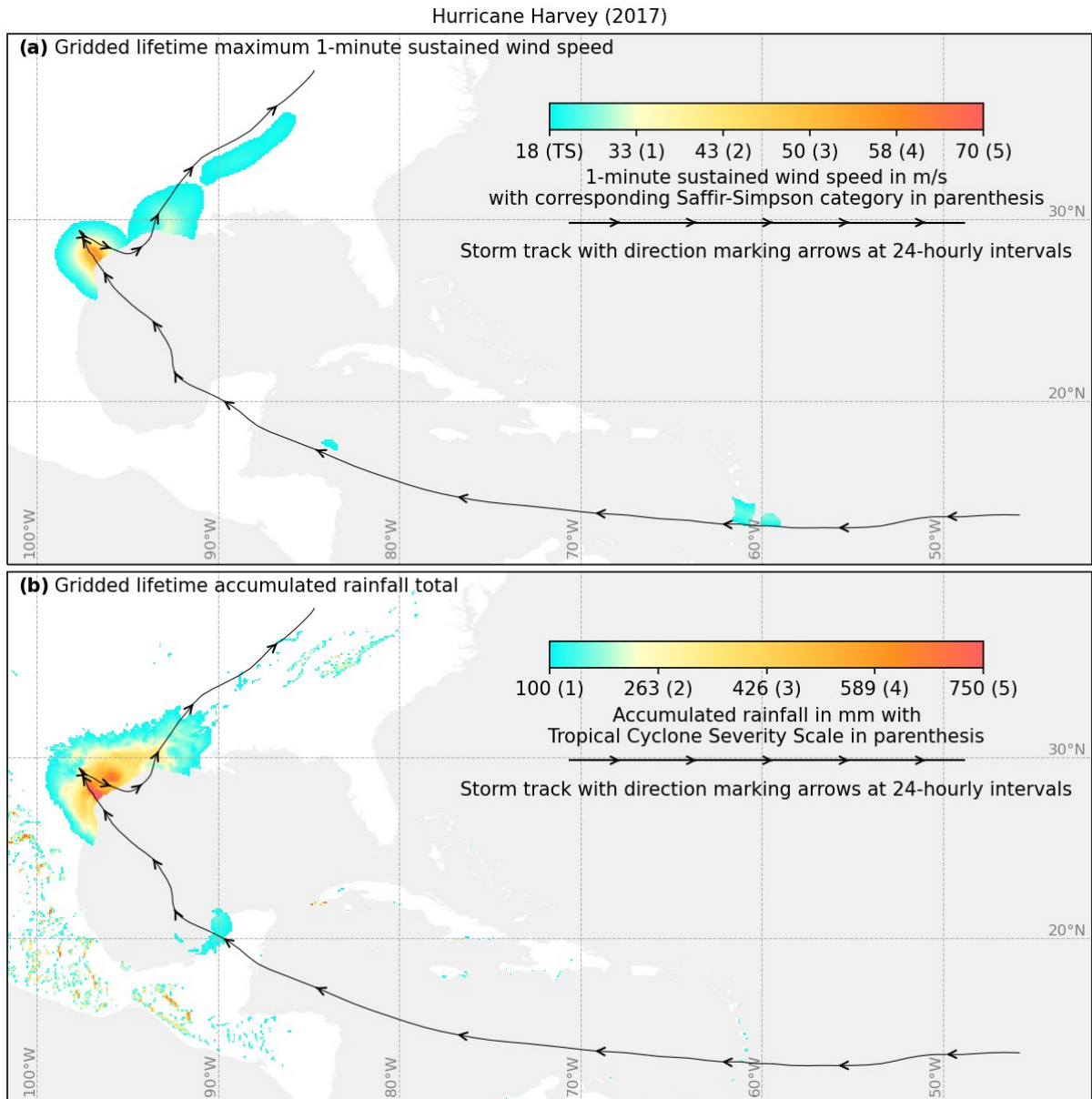
755 To simulate the baseline ‘no climate change’ state of a human or natural system that is required for
 756 impact attribution, we provide a detrended version of the observational factual forcing data using the
 757 ATTRICI approach (ATTRIButing Climate Impacts, Mengel et al., 2021). The method identifies the long-
 758 term shifts in the factual daily climate variables that are correlated to global mean temperature change
 759 assuming a smooth annual cycle of the associated scaling coefficients for each day of the year. The
 760 observed trends since 1901 are then removed from the observational data by projecting the observed
 761 data onto the estimated distributions assuming a fixed 1901 level of global warming. The projection is
 762 done through quantile mapping, a method borrowed from the bias adjustment literature. In this way we
 763 preserve the internal variability of the observed data in the sense that factual and counterfactual data

764 for a given day have the same rank in their respective statistical distributions. The impact model
 765 simulations forced by the counterfactual climate inputs therefore allow for quantifying the contribution
 766 of the observed climate change (no matter from where the trends originate) to observed long-term
 767 changes in impact indicators but also for quantifying the contribution of the observed trend in climate to
 768 the magnitude of individual impact events.

769

770 **3.2 Tropical cyclone (TC) data (factual)**

771



772

773 **Figure 2: Tropical cyclone storm track (a and b, line with arrows), derived maximum wind speeds (a,**
 774 **coloured shades) and accumulated rainfall totals (b, coloured shades) of Hurrican Harvey that made landfall**
 775 **in Texas (USA) in August 2017. The wind speeds are according to the Holland wind profile (Holland, 1980, 2008),**
 776 **and the rainfall is according to the TCR model (Zhu et al., 2013). The colouring in (b) follows the “Tropical Cyclone**
 777 **Severity Scale” (Bloemendaal et al., 2021).**

778

779 **Table 6: Tropical cyclone information provided as part of the ISIMIP3a climate-related forcing**

Variable	Variable specifier	Unit	Resolution	Datasets
Time associated with a given location of the storm centre	time	hours since 1950-01-01 00:00	along-track, at least 3-hourly	IBTrACS (1950-2021, postprocessed)
Latitudinal coordinate of storm centre (as defined by the reporting agencies)	lat	degrees north	along-track, at least 3-hourly	IBTrACS (1950-2021, postprocessed)
Longitudinal coordinate of storm centre (as defined by the reporting agencies)	lon	degrees east	along-track, at least 3-hourly	IBTrACS (1950-2021, postprocessed)
Ocean basin: NA/SA (North/South Atlantic), EP/WP/SP (East/West/South Pacific), NI/SI (North/South Indian Ocean)	basin	two-letter abbreviation	along-track, at least 3-hourly	IBTrACS (1950-2021, postprocessed)
Central pressure	pres	hPa	along-track, at least 3-hourly	IBTrACS (1950-2021, postprocessed)
Environmental pressure (pressure of the outermost closed isobar)	penv	mbar	along-track, at least 3-hourly	IBTrACS (1950-2021, postprocessed)
Maximum 1-minute sustained wind speed	windspatial max	knots	along-track, at least 3-hourly	IBTrACS (1950-2021, postprocessed)
Radius of maximum wind speeds	rmw	nautical miles	along-track, at least 3-hourly	IBTrACS (1950-2021, postprocessed)
Radius of the outermost closed isobar	roci	nautical miles	along-track, at least 3-hourly	IBTrACS (1950-2021, postprocessed)

Wind speed on the 850 hPa pressure level	u850 v850	ms ⁻¹	along-track, at least 3-hourly	IBTrACS (1950-2021, postprocessed)
Temperature on the 600 hPa pressure level	t600	K	along-track, at least 3-hourly	IBTrACS (1950-2021, postprocessed)
1-minute sustained wind speed	wind	ms ⁻¹	hourly on a 300 arc-seconds (~10 km) grid	according to the Holland wind profile (Holland, 1980, 2008) and the Emanuel-Rotunno wind profile (Emanuel and Rotunno, 2011)
Gridded lifetime maximum 1-minute sustained wind speed	windlifetime max	ms ⁻¹	per storm on a 300 arc-seconds (~10 km) grid	according to the Holland wind profile (Holland, 1980, 2008) and the Emanuel-Rotunno wind profile (Emanuel and Rotunno, 2011)
National territory exposed to wind speeds of at least 34, 48, 64, 96 knots	34knarea 48knarea 64knarea 96knarea	km ²	per storm and country	according to the Holland wind profile (Holland, 1980, 2008) and to the Emanuel-Rotunno wind profile (Emanuel and Rotunno, 2011)
Number of people exposed to wind speeds of at least 34, 48, 64, 96 knots	34knpop 48knpop 64knpop 96knpop	count	per storm and country	according to the Holland wind profile (Holland, 1980, 2008) and to the Emanuel-Rotunno wind profile (Emanuel and Rotunno, 2011) and assuming temporally varying (histsoc) or fixed 2015 (2015soc) population distributions

				(see section 4.1).
Economic assets exposed to wind speeds of at least 34, 48, 64, 96 knots	34knassets 48knassets 64knassets 96knassets	Int\$ PPP 2005	per storm and country	Windfields according to the Holland wind profile (Holland, 1980, 2008) and Emanuel-Rotunno wind profile (Emanuel and Rotunno, 2011) and assuming temporally varying (histsoc) or fixed 2015 (2015soc) asset distributions (see section 4.2).
Total rainfall	rain	mm	hourly on a 300 arc-seconds (~10 km) grid	according to the Holland wind profile (Holland, 1980, 2008) and to the Emanuel-Rotunno wind profile (Emanuel and Rotunno, 2011)
Maximum 24-hourly rainfall total during the whole storm duration	max_rain	mm	per storm on a 300 arc-seconds (~10 km) grid	according to the Holland wind profile (Holland, 1980, 2008) and to the Emanuel-Rotunno wind profile (Emanuel and Rotunno, 2011)

780 As additional CRF, we provide historical TC tracks (information about the observed location of minimal
781 pressure), with associated gridded wind and rain fields (see variable names and units in **Table 6** and
782 the maps of maximum wind speed and accumulated rainfall totals for the example of hurricane Harvey
783 in **Figure 2**). In addition to this purely CRF, we also provide wind exposure in terms of i) shares of
784 national territory affected by extreme winds speeds, ii) national shares of people exposed to extreme
785 winds speeds, and iii) national shares of economic assets affected by extreme winds speeds as derived
786 from the estimated wind fields and historical population and GDP distributions (see below). **Table 6**
787 provides a comprehensive list of all variables, their meaning and resolution as well as their source.

789 **TC Tracks (position of storm centre, central pressure, environmental pressure, radius of**
790 **maximum wind speed and the outermost closed isobar).** We provide processed track information
791 of historical TCs from 1950 to 2021. The information is derived from IBTrACS, the most comprehensive
792 global dataset of historical TC activity (Knapp et al., 2010) that provides information about the location
793 of the storm centre, the pressure at the centre and at the outermost closed isobar as well as the
794 maximum 1-minute sustained wind speed as reported by the WMO Regional Specialised Meteorological
795 Centers (RSMCs) and by agencies in Shanghai and Hong Kong. For recent events and most reporting
796 agencies, IBTrACS also contains observational information about the radius from the centre where
797 maximum wind speed is attained and the radius of the outermost closed isobar. Information is provided
798 in at least 6-hourly time steps. Usually temporal resolution reaches three hours or even less. The latest
799 version (v04r00) of IBTrACS is continuously updated with near real time data taken from regional
800 meteorological agencies. The data is marked as provisional before it is replaced by so-called best track
801 data up to two years after the events. IBTrACS contains data from 1842 to present, but coverage by
802 the WMO RSMCs starts much later for some of the basins (around 1850 for the North Atlantic and
803 South Indian, in 1905 for the South Pacific, in 1950 for the North Pacific, and in 1990 for the Northern
804 Indian basin). Data quality is globally consistent starting from the mid 1970s when satellite observations
805 became available.

806 The data set we provide uses best track data from 1950 to 2021. For each TC in IBTrACS, we merge
807 the data of different reporting agencies into a single track data set with information about the following
808 variables: time, location of the storm centre, ocean basin, central pressure, maximum 1-minute
809 sustained wind speed, environmental pressure, radius of maximum wind speeds, and radius of the
810 outermost closed isobar (see Table 8). Several processing steps are applied to ensure consistency and
811 completeness of the data: For each storm, the variables that are not reported by the officially responsible
812 WMO RSMC for this storm are taken from the next agency in the following list that did report this variable
813 for this storm: the US agencies (NHC, JTWC, CPHC), Japanese Meteorological Agency, Indian
814 Meteorological Department, MeteoFrance (La Reunion), Bureau of Meteorology (Australia), Fiji
815 Meteorological Service, New Zealand MetService, Chinese Meteorological Administration, Hong Kong
816 Observatory. Thus, for different storms, the same variable might be taken from different agencies. As
817 sustained wind speeds are reported at different averaging intervals by different agencies, we use
818 multiplicative factors to rescale all wind speeds to 1-minute sustained winds (Knapp and Kruk, 2010).
819 All variables are extracted at the highest temporal resolution where time and location information is
820 available in IBTrACS. Temporal reporting gaps within a variable are linearly interpolated so that the
821 temporal resolution is at least 3-hourly. After interpolation, time steps where neither central pressure
822 nor maximum wind speeds are available, are discarded. Tracks with less than two valid time steps are
823 discarded. If at least one of central pressure or maximum wind speed is available, one variable is
824 estimated from the other using statistical wind-pressure relationships. Missing RMW and ROCI values
825 are estimated from the central pressure using statistical relationships. Finally, missing environmental

826 pressure values are filled with basin-specific defaults (1010 hPa for the Atlantic and Eastern Pacific,
827 1005 hPa for the Indian Ocean and Western Pacific, and 1004 hPa for the South Pacific).

828 We provide two additional along-track variables that are taken from the European Reanalysis (ERA5;
829 (Hersbach et al., 2020), and that are needed for the computation of precipitation (see below): The
830 temperature at the storm centre on the 600 hPa pressure level, and the wind speed on the 850 hPa
831 pressure level, averaged over the 200-500 km annulus around the storm centre.

832 **Gridded maps of (maximum) wind speeds.** We derive two different gridded wind field products from
833 an extrapolation of the observed TC track information to gridded estimates of surface wind speeds (1-
834 minute sustained winds at 10 metres above ground), at a spatial resolution of 300 arc-seconds
835 (approximately 10 km). The two products are based on circular wind fields from different radial wind
836 profiles. The first is a semiempirical model that estimates the full wind profile from the central pressure
837 variable based on the gradient wind balance assumption (Holland, 1980, 2008). The second, more
838 physics-based model uses the less-reliable maximum wind speed variable to derive the wind profile
839 from the boundary layer angular momentum balance (Emanuel and Rotunno, 2011). This wind profile
840 represents the storm's inner core very well, but tails off too sharply in the outer region (Chavas and Lin,
841 2016). However, for high-impact events, the core is the most relevant storm region, and outer wind
842 profiles are not analytically solvable, incurring considerable computational expense when applied to a
843 large track set.

844 In both cases, the circular wind fields are combined with translational wind vectors that arise from the
845 TC movement, assuming that the influence of translational wind decreases with distance from the TC
846 centre (Cyclone Database Manager, 2023). We use the highest available temporal resolution (up to 3-
847 hourly) provided in IBTrACS and interpolate it to 1-hourly resolution before applying the parametric
848 wind field models. In a postprocessing step, we also calculate the maximum value of wind speeds over
849 the duration of the TC event ('max_wind').

850 The approach by Holland has been successfully applied in socioeconomic risk and impact analyses
851 (Peduzzi et al., 2012; Geiger et al., 2018; Eberenz et al., 2021). The Emanuel-Rotunno approach has
852 been used for storm surge simulations (Krien et al., 2017; Marsooli et al., 2019; Gori et al., 2020; Yang
853 et al., 2021), and as the basis for the rain field model that we describe below (Feldmann et al., 2019).

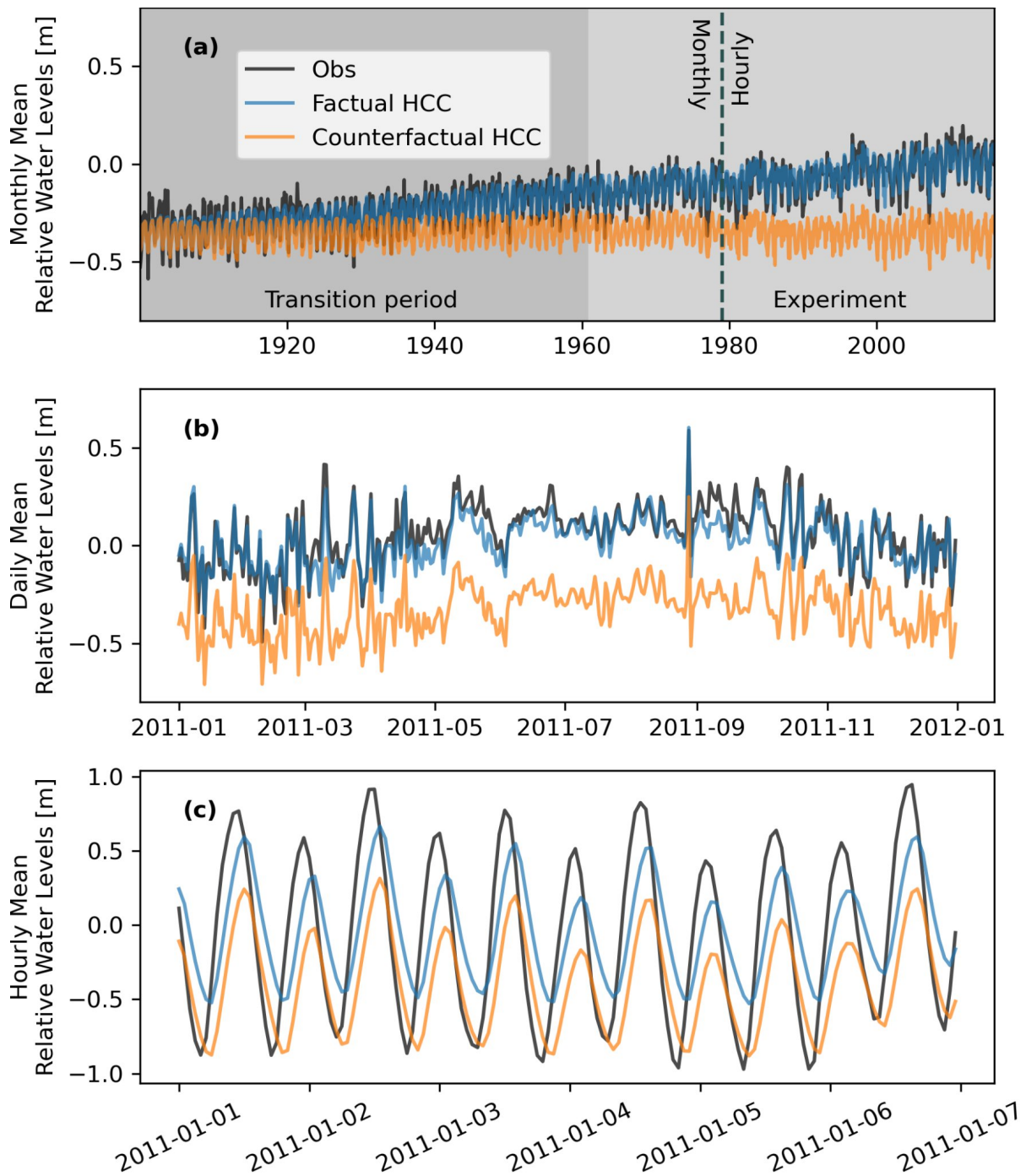
854 **Wind Exposure.** As an extension of the tropical cyclone exposure data set TCE-DAT (Geiger et al.,
855 2018), we provide national shares of people and economic assets exposed to 1-minute sustained winds
856 above 34, 48, 64, and 96 knots for each storm. In addition to that, shares of national territory affected
857 by 1-minute sustained winds above 34, 48, 64, and 96 knots are provided. To estimate the exposed
858 population and assets we use the 'histsoc' population and GDP distributions described in section 4.1
859 and section 4.2, respectively. The GDP values are converted to assets by applying the decadal (2010-
860 2019) mean of national capital stock to GDP ratios from the Penn World Table version 10.0 (Feenstra
861 et al., 2015). We also provide exposed population and assets assuming fixed 2015 population and
862 asset distributions.

863 **Precipitation.** We are also planning to provide rainfall fields, following a physics-based model that
864 simulates convective TC rainfall by relating the precipitation rate to the total upward velocity within the
865 TC vortex (Zhu et al., 2013). The approach has been successfully applied in rainfall risk assessments
866 in the US (Feldmann et al., 2019; Gori et al., 2022). The rain rate will be simulated for all events in the
867 IBTrACS database at 0.5-hourly temporal and 300 arc-seconds (approximately 10 km) spatial resolution
868 within a 1500 km radius around the storm centre. We provide the derived rainfall totals at hourly
869 resolution as well as the maximum 24-hourly rainfall total during the entire storm duration since this
870 variable is frequently used for rainfall risk assessment studies (Fagnant et al., 2020).

871 Different TC wind profiles can be used as an input for the rain field model (Lu et al., 2018; Xi et al.,
872 2020). We will provide the rainfall fields for the two wind profile models by Holland and Emanuel-
873 Rotunno that we also use for the wind fields described above.

875 **3.3 Coastal water levels (factual + counterfactual)**

876



877

878

879 **Figure 3: Observed and reconstructed coastal relative water levels** at New York, USA. The counterfactual
 880 baseline represents water levels without long-term trend since 1900. Water levels are aggregated to monthly
 881 means in panel (a) and daily means in the year 2011 in panel (b) while panel c shows part of the data in hourly
 882 resolution. The reconstructed water levels are available as monthly mean values from 1901 to 1978 and as hourly
 883 mean values from 1979 to 2015.

884

885

Table 7: Information about coastal water levels provided as ISIMIP3a climate-related forcing.

Variable	Variable specifier	Unit	Resolution	Datasets
Coastal water levels	cwl	m	custom coastal grid; monthly from 1901 to 1978 and hourly from 1979 to 2015	HCC obsclim and counterclim (Treu et al.2023)

886

887 To enable the quantification of impacts of historical relative sea level rise on coastal systems we provide
888 observation-based coastal water levels building on the HCC dataset (Hourly Coastal water levels with
889 Counterfactual; Treu et al.2023). In contrast to absolute sea levels, relative sea levels are measured
890 against a land-based reference frame (tide gauge measurements). This means that they are not only
891 determined by thermal expansion, loss of land ice, or dynamical processes influenced by climate
892 change, but also by vertical land movements (Wöppelmann and Marcos, 2016) induced by, e.g., glacial
893 isostatic adjustments (Caron et al., 2018; Whitehouse, 2018) or human interventions such as ground
894 water abstraction (Wada et al., 2016a). HCC encompasses factual and counterfactual coastal water
895 levels along global coastlines from 1901 to 1978 on monthly resolution and from 1979 to 2015 on hourly
896 resolution (see **Figure 3**). The counterfactual coastal water levels are derived from the factual dataset
897 by removing the trend in relative sea level since 1900. The detrending preserves the timing of historical
898 extreme sea-level events similar to the counterfactual atmospheric climate forcing described in section
899 **3.1** (see **Figure 3**, panel B). Hence, the data can be used for an event-based attribution of, e.g.,
900 observed flooding to observed relative sea-level rise with pairs of impact simulations driven with the
901 factual and counterfactual datasets. It is important to highlight that ‘attribution to observed changes in
902 relative water levels’ does not imply attribution to anthropogenic climate forcing because such observed
903 changes may include trends that are not driven by human greenhouse gas emissions. Important
904 sources for such trends are the ongoing adjustments of ice sheets, glaciers and the earth crust to
905 climate conditions before industrialization (Slangen et al. 2016) and the land subsidence due to water,
906 gas and oil extraction (Nicholls et al. 2021). In the following the derivation of the data is described in
907 more detail.

908

909 **Default factual data.** To capture the impacts of extreme water levels we provide hourly observation-
910 based coastal water levels as forcing data. To this end we combine the Coastal Dataset for the
911 Evaluation of Climate Impact (CoDEC) dataset (Muis et al., 2020) that describes high frequency
912 variation of sea level along global coastlines with a recent reconstruction of observed long-term sea-
913 level rise (Dangendorf et al., 2019). The CoDEC hourly data builds on a shallow-water model with fixed
914 ocean density driven by ERA5 wind and atmospheric pressure fields. The CoDEC data thus starts only
915 in the year 1979 and does not include variations due to ocean density changes and multi-year trends
916 from observed sea-level rise or vertical land movement. In contrast, the hybrid reconstructions (HR)
917 dataset from (Dangendorf et al., 2019) represents sea-level change since 1900 on a monthly timescale,
918 including density variations and multi-year trends. Long term sea-level change in HR is based on fitting
919 theoretically known and modelled spatial-temporal fields of individual contributing factors of sea level

920 change to a set of observations of sea level change from tide gauges. The individual contributing factors
921 are theoretically known cryospheric fingerprints from two ice sheets, 18 major glacier regions, glacial
922 isostatic adjustment from 161 Earth rheological models and dynamic changes of sea surface height
923 modelled by six global climate models. Short term sea-level variations are represented in HR by
924 extending the spatio-temporal patterns from satellite altimetry back to the year 1900 using tide gauge
925 records. We create the HCC dataset by low-pass filtering the HR dataset and high-pass filtering the
926 CoDEC dataset before summing them. Vertical land motion is subsequently added to yield relative
927 changes of water levels along global coastlines. HCC shows improved agreement with tide gauge
928 records on hourly to monthly time scales when compared to CoDEC due to the inclusion of density
929 variations. This is most apparent for lower latitudes. The performance on interannual time scales is
930 equal to (Dangendorf et al., 2019).

931

932 **Default counterfactual data.** To estimate the effects of historical sea-level rise on coastal systems,
933 we provide a counterfactual sea-level dataset as forcing for coastal impact models (Treu et al. 2023).
934 To this end the long term trend in the HCC data (1900-2015) was identified by a simple quadratic model
935 in time and subtracted from the factual HCC data. The quadratic model assumes a constant
936 acceleration of sea-level rise over time. Analysis of sea level rise acceleration shows variation
937 throughout the last century with an acceleration phase in the early century followed by a deceleration
938 and then again acceleration until today (Dangendorf et al., 2019). By design, this variation is not
939 included in our quadratic trend estimate. In general, we expect our trend estimation to largely exclude
940 natural variability from the trend due to the low dimensionality of the trend model and the long data
941 period. This is a desired outcome and preserves the natural variability in the counterfactual. Extreme
942 sea-level events have the same timing in the counterfactual and the factual dataset, facilitating event-
943 based impact attribution.

944

945 **3.4 Ocean data (factual)**

946

947 **Default factual data.** For the fisheries and marine ecosystem models, we provide a number of physical
948 and biogeochemical variables for the period 1961 to 2010 at different depth levels in the ocean (see
949 **Table 8**). Since direct measurements of these variables are very scarce (Sarmiento and Gruber, 2006,
950 WOCE Atlas, 2023), the only way to obtain a globally (or even regionally) complete and consistent
951 forcing dataset is to use numerical models. Global ocean models, which also serve as oceanic
952 components of Earth System models, often simulate many or all of the required variables. To let
953 observations at least indirectly enter the oceanic forcing data for ISIMIP3a, we provide outputs from an
954 ocean model run that is forced by an observation-based reanalysis product of atmospheric forcing (Liu
955 et al., 2021). Compared to the oceanic forcing (Stock et al., 2014) provided to generate the ISIMIP2a
956 simulations for the *marine ecosystems and fisheries* sector (Tittensor et al., 2018), this new dataset is
957 based on the latest GFDL-MOM6 and COBALTv2 physical and biogeochemical ocean models running
958 on a tripolar 0.25° grid and using the JRA-55 reanalysis (Tsujino et al., 2018) as the surface forcing, in
959 contrast to the inter-annual forcing dataset of (Large and Yeager, 2009), which was previously used to

960 drive GFDL-MOM4. The simulations also account for dynamic, time-varying river freshwater and
 961 nitrogen inputs that were simulated based on GFDL's land-watershed model LM3-TAN (Land Model
 962 version 3 with Terrestrial and Aquatic Nitrogen; (Lee et al., 2019), adjusted using observations from the
 963 Global Nutrient Export from WaterSheds (NEWS) database (Seitzinger et al., 2006). To create the
 964 default 'obsclim' climate-related forcings for the fisheries and marine ecosystem models these ocean
 965 model simulation data have been interpolated to a regular 0.25° grid while vertical resolution is
 966 preserved. In contrast to the atmospheric data, oceanic CRF are provided at monthly temporal
 967 resolution.

968

969 **Low resolution factual data.** To test to what degree a lower spatial resolution of the climate-related
 970 forcings affects the impact model simulations, the oceanic climate-related forcings have also been
 971 aggregated to one degree resolution as input for the 'obsclim + histsoc, 60arcmin' sensitivity
 972 experiment.

973

974 **CRF for the '1955-riverine-input' sensitivity experiment.** The '1955-riverine-inputs' sensitivity
 975 experiment builds on 0.25 degree GFDL-COBALT2 simulation forced by the JRA-55 reanalysis, but
 976 without time-varying riverine inputs. Instead the influx of freshwater and nutrients are fixed at mean
 977 1951 to 1958 levels as described in the "control run" introduced by (Liu et al., 2021). The data is
 978 interpolated to a regular 0.25 degree grid in the same way as the default 'obsclim' CRFs.

979

980 We currently do not provide counterfactual versions of the ocean data forcing, though options are being
 981 explored.

982

983 **Table 8: ISIMIP3a oceanic climate-related forcing.** Variables with suffixes -bot, -surf, and -vint were obtained
 984 from the seafloor, the top layer of the ocean, and vertical integration, respectively.

Variable	Variable specifier	Unit	Resolution	Datasets
Mass concentration of total phytoplankton expressed as chlorophyll	chl	kg m-3	0.25° and 1° grid, 35 levels (m from the surface), monthly	GFDL-COBALT2 simulation forced by the JRA-55 reanalysis, accounting for climate-driven changes in riverine inputs ('default') or assuming fixed levels of riverine inputs ('1955-riverine-input'). Standard salt water density of 1035 kg m-3 applied when converting from mass to volumetric unit, i.e. µg kg-1 to kg m-3

Downward flux of organic particles expressed as organic carbon at ocean bottom	expc-bot	mol m-2 s-1	0.25° and 1° grid, monthly	<p>GFDL-COBALT2 simulation forced by the JRA-55 reanalysis, accounting for climate-driven changes in riverine inputs ('default') or assuming fixed levels of riverine inputs ('1955-riverine-input'). Derived from nitrogen detritus flux at ocean bottom (fndet_btm) by multiplying with fixed N-C ratio of 6.625.</p> <p>Extractions for individual grid cells available in ASCII format for regional models (see Table 1).</p>
Particulate organic carbon content in the upper 100 m	intpoc	kg m-2	0.25° and 1° grid, monthly	<p>GFDL-COBALT2 simulation forced by the JRA-55 reanalysis, accounting for climate-driven changes in riverine inputs ('default') or assuming fixed levels of riverine inputs ('1955-riverine-input'). Derived by aggregating bacterial, detritus, diazotroph, large+small phytoplankton, large+medium+small zooplankton nitrogen biomass and multiplying by a fixed N-C ratio of 6.625.</p> <p>Extractions for individual grid cells available in ASCII format for regional models (see Table 1).</p>
Net primary organic carbon production by all types of phytoplankton in grid cell column	intpp	mol m-2 s-1	0.25° and 1° grid, monthly	<p>GFDL-COBALT2 simulation forced by the JRA-55 reanalysis, both accounting for climate-driven changes in riverine inputs ('default') or assuming fixed levels of riverine inputs ('1955-riverine-input'). Derived by aggregating net primary productions by diatoms,</p>

				<p>diazotrophs and pico-phytoplankton and under the assumption of a fixed N-C ratio of 6.625.</p> <p>Extractions for individual grid cells available in ASCII format for regional models (see Table 1).</p>
Net primary organic carbon production by diatoms in grid cell column	intppdiat	mol m-2 s-1	0.25° and 1° grid, monthly	<p>GFDL-COBALT2 simulation forced by the JRA-55 reanalysis, both accounting for climate-driven changes in riverine inputs ('default') or assuming fixed levels of riverine inputs ('1955-riverine-input'). Derived under the assumption of a fixed N-C ratio of 6.625.</p> <p>Extractions for individual grid cells available in ASCII format for regional models (see Table 1).</p>
Net primary organic carbon production of carbon by diazotrophs in grid cell column	intppdiaz	mol m-2 s-1	0.25° and 1° grid, monthly	<p>GFDL-COBALT2 simulation forced by the JRA-55 reanalysis, both accounting for climate-driven changes in riverine inputs ('default') or assuming fixed levels of riverine inputs ('1955-riverine-input'). Derived under the assumption of a fixed N-C ratio of 6.625.</p> <p>Extractions for individual grid cells available in ASCII format for regional models (see Table 1).</p>

Net Primary Mole Productivity of Carbon by Picophytoplankton in grid cell column	intppico	mol m ⁻² s ⁻¹	0.25° and 1° grid, monthly	GFDL-COBALT2 simulation forced by the JRA-55 reanalysis, both accounting for climate-driven changes in riverine inputs ('default') or assuming fixed levels of riverine inputs ('1955-riverine-input'). Derived under the assumption of a fixed N-C ratio of 6.625.
Mixed Layer Ocean Thickness defined by a Sigma Theta difference (= density difference) of 0.125 kg m ⁻³ compared to the surface	mlotst-0125	m	0.25° and 1° grid, monthly	GFDL-COBALT2 simulation forced by the JRA-55 reanalysis, both accounting for climate-driven changes in riverine inputs ('default') or assuming fixed levels of riverine inputs ('1955-riverine-input')
Dissolved oxygen concentration; vertically resolved, at the bottom or at the surface, respectively	o2, o2-bot, o2-surf	mol m ⁻³	0.25° and 1° grid, 35 levels (m from the surface), monthly	GFDL-COBALT2 simulation forced by the JRA-55 reanalysis, both accounting for climate-driven changes in riverine inputs ('default') or assuming fixed levels of riverine inputs ('1955-riverine-input'). Extractions for individual grid cells of the bottom and surface layer available in ASCII format for regional models (see Table 1).
pH; vertically resolved, at the bottom or at the surface, respectively	ph, ph-bot, ph-surf	1	0.25° and 1° grid, 35 levels (m from the surface), ocean bottom and surface fields, monthly	GFDL-COBALT2 simulation forced by the JRA-55 reanalysis, both accounting for climate-driven changes in riverine inputs ('default') or assuming fixed levels of riverine inputs ('1955-riverine-input') where pH is derived from ion concentrations H ⁺ as $\text{pH} = -\log_{10}(\text{H}^+)$.

				Extractions for individual grid cells of the bottom and surface layer available in ASCII format for regional models (see Table 1).
Total phytoplankton carbon concentration; vertically resolved or integrated over the grid cell column, respectively	phyc, phyc-vint	mol m-3	0.25° and 1° grid, 35 levels (m from the surface) and vertically integrated, monthly	GFDL-COBALT2 simulation forced by the JRA-55 reanalysis, both accounting for climate-driven changes in riverine inputs ('default') or assuming fixed levels of riverine inputs ('1955-riverine-input'). Aggregated from diatom, diazotroph and pico-phytoplankton. Standard salt water density of 1035 kg m-3 and fixed N-C ratio of 6.625 applied when converting from mass to volumetric unit, i.e. mol kg-1 to mol m-3. Extractions for individual grid cells of the vertically integrated data set are available in ASCII format for regional models (see Table 1).
Concentration of diatoms expressed as carbon in sea water; vertically resolved or integrated over the grid cell column, respectively	phydiat, phydiat-vint	mol m-3	0.25° and 1° grid, 35 levels (m from the surface) and vertically integrated, monthly	GFDL-COBALT2 simulation forced by the JRA-55 reanalysis, both accounting for climate-driven changes in riverine inputs ('default') or assuming fixed levels of riverine inputs ('1955-riverine-input'). Standard salt water density of 1035 kg m-3 and fixed N-C ratio of 6.625 applied when converting from mass to volumetric unit, i.e. mol kg-1 to mol m-3. Extractions for individual grid cells of the vertically integrated data set are available in ASCII format for regional models (see Table 1).

				regional models (see Table 1).
Concentration of diazotrophs expressed as carbon in sea water; vertically resolved or integrated over the grid cell column, respectively	phydiaz, phydiaz-vint	mol m-3	0.25° and 1° grid, 35 levels (m from the surface) and vertically integrated, monthly	GFDL-COBALT2 simulation forced by the JRA-55 reanalysis, both accounting for climate-driven changes in riverine inputs ('default') or assuming fixed levels of riverine inputs ('1955-riverine-input'). Standard salt water density of 1035 kg m-3 and fixed N-C ratio of 6.625 applied when converting from mass to volumetric unit, i.e. mol kg-1 to mol m-3.
Mole concentration of picophytoplankton expressed as carbon in sea water; vertically resolved or integrated over the grid cell column, respectively	phypico, phypico-vint	mol m-3	0.25° and 1° grid, 35 levels (m from the surface) and vertically integrated, monthly	GFDL-COBALT2 simulation forced by the JRA-55 reanalysis, both accounting for climate-driven changes in riverine inputs ('default') or assuming fixed levels of riverine inputs ('1955-riverine-input'). Standard salt water density of 1035 kg m-3 and fixed N-C ratio of 6.625 applied when converting from mass to volumetric unit, i.e. mol kg-1 to mol m-3.
Net downward shortwave radiation at sea water surface	rsntds	W m-2	0.25° and 1° grid, monthly	From JRA-55 reanalysis
Sea ice area fraction	siconc	%	0.25° and 1° grid, monthly	From JRA-55 reanalysis

Sea water salinity; vertically resolved, at the bottom, or at the surface, respectively	so, so-bot, so-surf	0.001	0.25° and 1° grid, 35 levels (m from the surface), ocean bottom and surface fields, monthly	GFDL-COBALT2 simulation forced by the JRA-55 reanalysis, both accounting for climate-driven changes in riverine inputs ('default') or assuming fixed levels of riverine inputs ('1955-riverine-input'). Extractions for individual grid cells of the surface and bottom layer are available in ASCII format for regional models (see Table 1).
Sea water potential temperature	thetao	°C	0.25° and 1° grid, 35 levels (m from the surface), monthly	GFDL-COBALT2 simulation forced by the JRA-55 reanalysis, both accounting for climate-driven changes in riverine inputs ('default') or assuming fixed levels of riverine inputs ('1955-riverine-input')
Ocean model cell thickness	thkcello	m	0.25° and 1° grid, 35 levels (m from the surface), constant	GFDL-COBALT2 simulation forced by the JRA-55 reanalysis, both accounting for climate-driven changes in riverine inputs ('default') or assuming fixed levels of riverine inputs ('1955-riverine-input')
Sea water potential temperature at sea floor (bottom)	tob	°C	0.25° and 1° grid, monthly	GFDL-COBALT2 simulation forced by the JRA-55 reanalysis, both accounting for climate-driven changes in riverine inputs ('default') or assuming fixed levels of riverine inputs ('1955-riverine-input'). Extractions for individual grid cells are available in ASCII format for regional models (see Table 1).

Sea surface temperature	tos	°C	0.25° and 1° grid, monthly	GFDL-COBALT2 simulation forced by the JRA-55 reanalysis, both accounting for climate-driven changes in riverine inputs ('default') or assuming fixed levels of riverine inputs ('1955-riverine-input'). Extracted from uppermost ocean layers potential temperatures. Extractions for individual grid cells are available in ASCII format for regional models (see Table 1).
Sea water zonal velocity	uo	m s-1	0.25° and 1° grid, 35 levels (m from the surface), monthly	GFDL-COBALT2 simulation forced by the JRA-55 reanalysis, both accounting for climate-driven changes in riverine inputs ('default') or assuming fixed levels of riverine inputs ('1955-riverine-input')
Sea water meridional velocity	vo	m s-1	0.25° and 1° grid, 35 levels (m from the surface), monthly	GFDL-COBALT2 simulation forced by the JRA-55 reanalysis, both accounting for climate-driven changes in riverine inputs ('default') or assuming fixed levels of riverine inputs ('1955-riverine-input')
Concentration of zooplankton of meso size expressed as carbon in seawater; vertically resolved or integrated over the grid cell column, respectively	zmeso, zmeso-vint	mol m-3	0.25° and 1° grid, 35 levels (m from the surface) and vertically integrated, monthly	GFDL-COBALT2 simulation forced by the JRA-55 reanalysis, both accounting for climate-driven changes in riverine inputs ('default') or assuming fixed levels of riverine inputs ('1955-riverine-input'). Aggregated from large and medium zooplankton. Standard salt water density of 1035 kg m-3 and fixed N-C ratio of 6.625 applied when converting from

				<p>mass to volumetric unit, i.e. mol kg⁻¹ to mol m⁻³.</p> <p>Extractions for individual grid cells of the vertically integrated data set are available in ASCII format for regional models (see Table 1).</p>
<p>Concentration of zooplankton of micro scale expressed as carbon in seawater; vertically resolved or integrated over the grid cell column, respectively.</p>	<p>zmicro, zmicro-vint</p>	<p>mol m⁻³</p>	<p>0.25° and 1° grid, 35 levels (m from the surface) and vertically integrated, monthly</p>	<p>GFDL-COBALT2 simulation forced by the JRA-55 reanalysis, both accounting for climate-driven changes in riverine inputs ('default') or assuming fixed levels of riverine inputs ('1955-riverine-input'). Standard salt water density of 1035 kg m⁻³ and fixed N-C ratio of 6.625 applied when converting from mass to volumetric unit, i.e. mol kg⁻¹ to mol m⁻³.</p> <p>Extractions for individual grid cells of the vertically integrated data set are available in ASCII format for regional models (see Table 1).</p>
<p>Total Zooplankton Carbon Concentration; vertically resolved or integrated over the grid cell column, respectively</p>	<p>zooc, zooc-vint</p>	<p>mol m⁻³</p>	<p>0.25° and 1° grid, 35 levels (m from the surface) and vertically integrated, monthly</p>	<p>GFDL-COBALT2 simulation forced by the JRA-55 reanalysis, both accounting for climate-driven changes in riverine inputs ('default') or assuming fixed levels of riverine inputs ('1955-riverine-input'), aggregated from large, medium and micro zooplankton. Standard salt water density of 1035 kg m⁻³ and fixed N-C ratio of 6.625 applied when converting from mass to volumetric unit, i.e. mol kg⁻¹ to mol m⁻³.</p> <p>Extractions for individual grid cells</p>

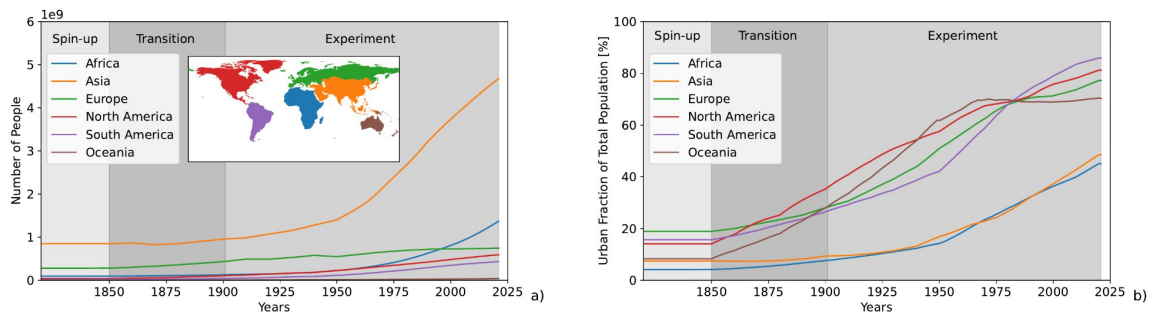
				of the vertically integrated data set are available in ASCII format for regional models (see Table 1).
--	--	--	--	--

985

986 **4 Direct human forcings**

987

988 **4.1 Population data**



989

990 **Figure 4: Historical evaluation of population for different continents.** Total number of people living in the
 991 region (panel a) and urban population as a fraction of the total population per region (panel b).
 992
 993

Table 9: Population data provided as part of the ISIMIP3a direct human forcing.

Variable	Variable specifier	Unit	Resolution	Datasets
National population	pop	Number of people in millions	annual	UN 2019 WPP database (2023): census-based from 1950 to 2020 + “medium-variant” forecast provided for 2021
Gridded total population	total-population	Number of people	0.5°x 0.5°, annual	HYDE3.3 data for 1950-2020 constantly extended to 2021 and adjusted to match the national UN numbers described above (see text below)
Gridded rural population	rural-population	Number of people	0.5°x 0.5°, annual	HYDE3.3 data for 1950-2020 constantly extended to 2021 and rescaled by the same national scaling factors as the total population
Gridded urban population	urban-population	Number of people	0.5°x 0.5°, annual	HYDE3.3 data for 1950-2020 constantly extended to 2021 and rescaled by the same national scaling factors as the total population

994

995 For ISIMIP3a we provide consistent gridded and national population data (see **Table 9**) by rescaling
996 the gridded data to match the national aggregates. **Figure 4** shows the temporal evolution of total and
997 urban population for different continents.

998

999 **National data.** Annual national population data are taken from the 2019 UN World Population Prospects
1000 (WPP) database for the period from 1950 – 2021 (United Nations, 2019). The 2019 revision of the WPP
1001 provides census-based population numbers from 1950 through 2020. For the year 2021, we use the
1002 “medium-variant” of the probabilistic forecast also provided by the WPP. The forecast accounts the
1003 past experience of each country, while reflecting uncertainty about future changes based on the past
1004 experience of other countries under similar conditions (see United Nations, 2019 for details). For
1005 countries not covered in the database, estimates are taken from the MissingIslands dataset (Arujo et
1006 al., 2021) to finally provide population data for 249 countries.

1007

1008 **Gridded data.** We provide gridded population data that is based on HYDE v3.3 (Klein Goldewijk, 2022).
1009 Just like the original dataset we provide total, rural and urban population per grid cell. The original HYDE
1010 3.3 data was on a $1/12^\circ \times 1/12^\circ$ grid and has been interpolated to ISIMIP's $0.5^\circ \times 0.5^\circ$ grid. Furthermore,
1011 the land-sea distinction was modified to comply with the ISIMIP country mask (see **Table 1**). Before the
1012 year 1950 HYDE provides data every ten years, the intermediate years have been filled by linear
1013 interpolation. Also, the original HYDE data ends in 2020. So to cover the whole ISIMIP3a time frame
1014 the final year 2020 has been duplicated as 2021. In this way annual coverage of 1850 to 2021 has been
1015 achieved.

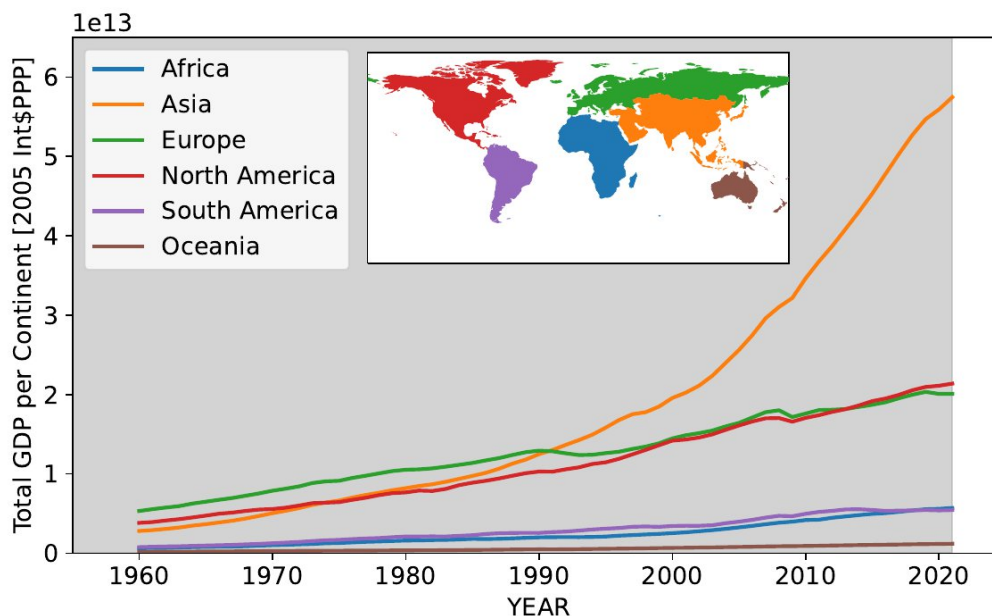
1016 Data for all grid cells of a country, as defined by the ISIMIP $0.5^\circ \times 0.5^\circ$ fractional country map (see **Table**
1017 **1**), have been rescaled such that the country's total population matches the numbers provided in the
1018 national population data. Since the national data only starts in 1950, all years prior to 1950 have been
1019 rescaled by the national scaling factors of 1950. The urban and rural populations have been rescaled
1020 by the same national scaling factors as the total population.

1021

1022

1023 **4.2 Gross Domestic Product (GDP)**

1024



1025

1026 **Figure 5: Aggregated GDP (Int\$ PPP 2005) for different continents.**

1027

1028

Table 10: GDP data provided as part of the ISIMIP3a direct human forcing.

Variable	Variable specifier	Unit	Resolution	Datasets
National Gross Domestic Product	gdp	Int\$ PPP 2005	annual	World Bank's World Development Indicator database (Anon, 2008)
Gridded Gross Domestic Product	gridded-gdp	Int\$ PPP 2005	annual	National GDP data downscaled to the 0.5° grid according to (Wang and Sun, 2022)

1029

1030 Similar to the population data we also provide gridded and national GDP data (see **Table 10**). The
 1031 downscaling of the national numbers is based on population and nightlight data (see below). In contrast
 1032 to ISIMIP2a the gridded GDP and population data are now consistent such that previous artefacts in
 1033 the derived GDP per capita could be eliminated (see below). **Figure 5** shows the historical increase in
 1034 GDP for different continents.

1035

1036 **National GDP data.** Time series of per-capita GDP for the time period 1960-2021 are taken from the
 1037 World Bank's World Development Indicator database (WDI) (Anon, 2008) and converted into constant
 1038 2005 Int\$PPP, using deflators and PPP conversion factors from WDI. For countries not covered in the

1039 WDI database, data from the MissingIslands dataset (Arujo et al., 2021) is used to allow covering 249
1040 countries. Following a method developed by (Koch and Leimbach, 2023); the values for the year 2021
1041 are derived from the IMF's World Economic Outlook short-term estimates of GDP per capita growth
1042 (International Monetary Fund, 2021) that comprise estimates of the growth impacts of the Covid-19
1043 shock.

1044

1045 **Gridded GDP data.** Gridded GDP data at 0.5 degree resolution are derived from the national GDP time
1046 series by applying the LitPop method (Zhao et al., 2017; Eberenz et al., 2019), which uses the ISIMIP3a
1047 gridded population based on HYDE v.3.3 and nighttime light (NTL) data to downscale national GDP
1048 data for the period 1960-2021 to the ISIMIP 0.5°×0.5° grid.

1049

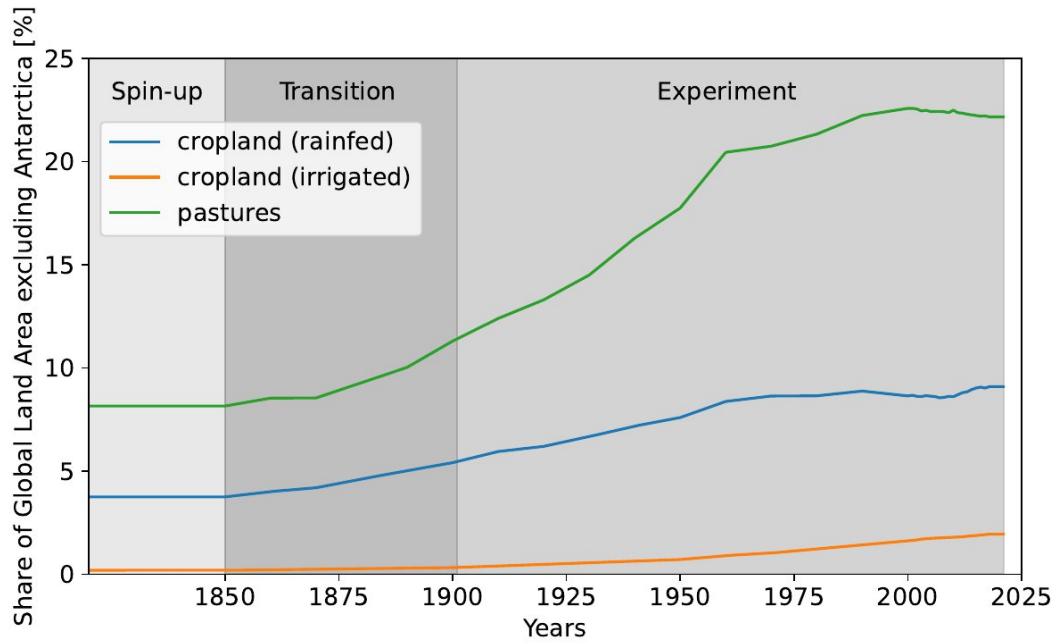
1050 As the disaggregation of GDP is not only based on population but also uses the NTL GDP per capita,
1051 it is not constant within different countries. Deriving the gridded GDP data from the gridded population
1052 data provided within ISIMIP3a ensures that the both data sets can be combined such that the associated
1053 GDP per capita does no longer show the artefacts that have been found in the ISIMIP2a GDP per capita
1054 (ISIMIP2a: suspicious gridded GDP per capita data; new functions in the isimip data repository; Forum
1055 on Scenarios for Climate and Societal Futures, 2023).

1056

1057

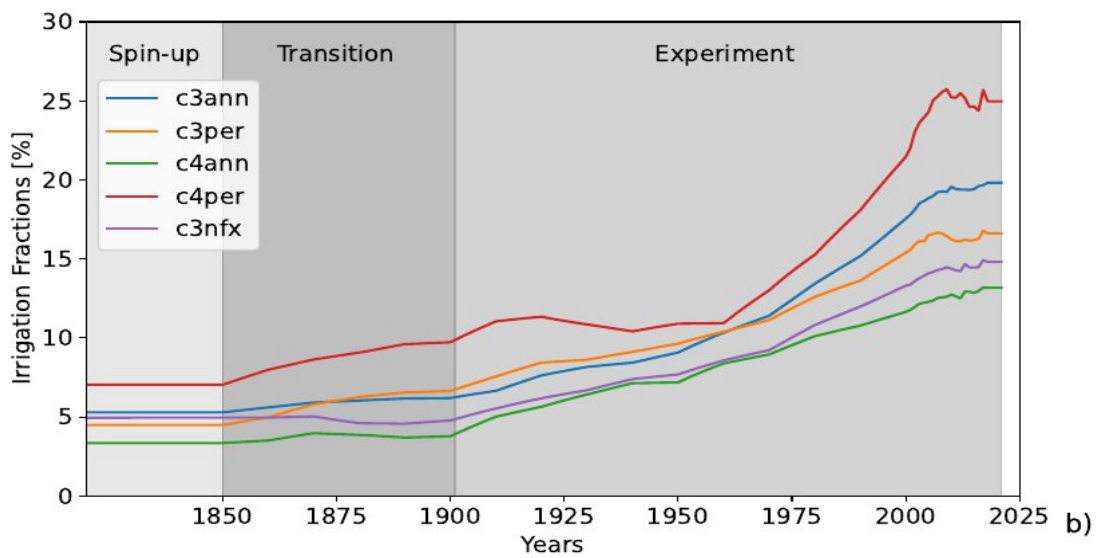
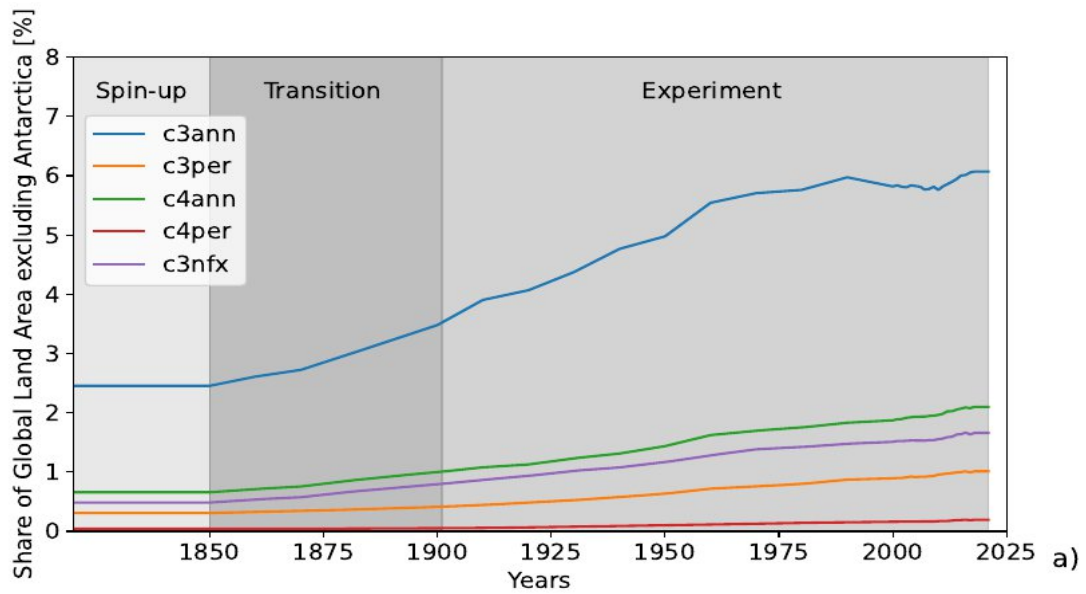
1058 **4.3 Land use and irrigation patterns**

1059



1060

1061 **Figure 6: Share of Global Land Area excluding Antarctica covered by rainfed cropland (green), irrigated**
1062 **cropland (blue), and pasture (orange) [%].** The information is from the LUH v2 data set provided as direct human
1063 forcing for ISIMIP3a (see details below).
1064



1065
1066
1067
1068
1069
1070
1071

Figure 7: Panel A: Share of Global Land Area excluding Antarctica covered by different groups of crops (C3 annual (blue), C3 perennial (orange), C4 annual (green), C4 perennial (red), C3 nitrogen fixing (purple)). Panel B: Fraction of irrigated land for the different groups of crops. The information is from the LUH v2 data set (see details on further disaggregation of the LUH v2 groups below).

Table 11: Historical land use and irrigation patterns provided as part of the ISIMIP3a direct human forcing.

Variable	Variable specifier	Unit	Resoluti on	Datasets

Total crop land, rainfed cropland, irrigated cropland	cropland_total, cropland_rainfed, cropland_irrigated	unitless (share of area in a grid cell)	0.5°×0.5°, annual	LUH2 v2 (Hurt et al., 2020, Land use harmonization, 2023)
pastures	pastures	unitless (share of area in a grid cell)	0.5°×0.5°, annual	sum of 'managed_pastures' and 'rangeland' from HYDE 3.2 (see below)
Managed pastures	managed_pastures	1 (share of area in a grid cell)	0.5°×0.5°, annual	first subcategory of 'pastures' from HYDE 3.2 (see above)
rangeland	rangeland	1 (share of area in a grid cell)	0.5°×0.5°, annual	second subcategory of 'pastures' from HYDE 3.2, more extensive management than 'managed pastures' (see above)
C3 annual rainfed cropland, C3 annual irrigated cropland	c3ann_irrigated, c3ann_rainfed	1 (share of area in a grid cell)	0.5°×0.5°, annual	LUH v2, for the disaggregation we consider C3 annual to be: rapeseed, rice, temperate cereals, temperate roots, tropical roots, sunflower, others C3 annual (see below)

C3 perennial cropland	c3per_irrigated, c3per_rainfed	1 (share of area in a grid cell)	0.5°×0.5°, annual	LUH v2 (this variable appears in the file only distinguishing 5 land use types and in the file with the downscaled 15 land use types. The provided values are identical)
C3 nitrogen-fixing rainfed cropland, C3 nitrogen-fixing irrigated cropland	c3nfx_irrigated, c3nfx_rainfed	1 (share of area in a grid cell)	0.5°×0.5°, annual	LUH v2 for the disaggregation we consider 'C3 nitrogen-fixing' to be: groundnut, pulses, soybean, others C3 nitrogen-fixing (see below)
C4 annual rainfed cropland, C4 annual irrigated cropland	c4ann_irrigated, c4ann_rainfed	1 (share of area in a grid cell)	0.5°×0.5°, annual	LUH v2, for the disaggregation we consider 'C4 annual' to be: maize, tropical cereals (see below)
C4 perennial rainfed cropland, C4 perennial irrigated cropland	c4per_irrigated, c4per_rainfed	1 (share of area in a grid cell)	0.5°×0.5°, annual	LUH v2 (this variable appears in the file only distinguishing 5 land use types and in the file with the downscaled 15 land use types. The provided values are identical), in the file with the 15 crops 'C4 perennial' is considered to be

				sugarcane
Fraction of grid cell where maize is grown (rainfed and irrigated)	maize_irrigated, maize_rainfed	1 (share of area in a grid cell)	0.5°×0.5° annual	downscaled from LUH v2 data based on the crop distribution from (Monfreda et al., 2008). The method is described in (Frieler et al., 2017)
Fraction of grid cell where groundnut is grown (rainfed and irrigated)	oil_crops_groundnut_irrigated, oil_crops_groundnut_rainfed,	1 (share of area in a grid cell)	0.5°×0.5° annual	downscaled from LUH v2 data based on the crop distribution from (Monfreda et al., 2008). The method is described in (Frieler et al., 2017)

Fraction of grid cell where rapeseed is grown (rainfed and irrigated)	oil_crops_rapeseed_irrigated, oil_crops_rapeseed_rainfed	1 (share of area in a grid cell)	0.5°×0.5°, annual	downscaled from LUH v2 data based on the crop distribution from (Monfreda et al., 2008). The method is described in (Frieler et al., 2017)
Fraction of grid cell where soybean is grown (rainfed and irrigated)	oil_crops_soybean_irrigated, oil_crops_soybean_rainfed	1 (share of area in a grid cell)	0.5°×0.5°, annual	downscaled from LUH v2 data based on the crop distribution from (Monfreda et al., 2008). The method is described in (Frieler et al., 2017)
Fraction of grid cell where sunflower is grown (rainfed and irrigated)	oil_crops_sunflower_irrigated, oil_crops_sunflower_rainfed	1 (share of area in a grid cell)	0.5°×0.5°, annual	downscaled from LUH v2 data based on the crop distribution from (Monfreda et al., 2008). The method is described in (Frieler et al., 2017)
Fraction of grid cell where pulses are grown (rainfed and irrigated)	pulses_irrigated, pulses_rainfed	1 (share of area in a grid cell)	0.5°×0.5°, annual	downscaled from LUH v2 data based on the crop distribution from (Monfreda et al., 2008). The method is described in (Frieler et al., 2017)
Fraction of grid cell where rice is grown (rainfed and irrigated)	rice_irrigated, rice_rainfed	1 (share of area in a grid cell)	0.5°×0.5°, annual	downscaled from LUH v2 data based on the crop distribution from

		grid cell)		(Monfreda et al., 2008). The method is described in (Frieler et al., 2017)
Fraction of grid cell where temperate cereals are grown (rainfed and irrigated)	temperate_cereals_irrigated, temperate_cereals_rainfed	1 (share of area in a grid cell)	0.5°×0.5°, annual	downscaled from LUH v2 data based on the crop distribution from (Monfreda et al., 2008). The method is described in (Frieler et al., 2017)
Fraction of grid cell where temperate roots are grown (rainfed and irrigated)	temperate_roots_irrigated, temperate_roots_rainfed	1 (share of area in a grid cell)	0.5°×0.5°, annual	downscaled from LUH v2 data based on the crop distribution from (Monfreda et al., 2008). The method is described in (Frieler et al., 2017)
Fraction of grid cell where tropical cereals are grown (rainfed and irrigated)	tropical_cereals_irrigated, tropical_cereals_rainfed	1 (share of area in a grid cell)	0.5°×0.5°, annual	downscaled from LUH v2 data based on the crop distribution from (Monfreda et al., 2008). The method is described in (Frieler et al., 2017)
Fraction of grid cell where tropical roots are grown (rainfed and irrigated)	tropical_roots_irrigated, tropical_roots_rainfed	1 (share of area in a grid cell)	0.5°×0.5°, annual	downscaled from LUH v2 data based on the crop distribution from (Monfreda et al., 2008). The method is described in (Frieler et al., 2017)

Fraction of grid cell where C3 annual crops other than rapeseed, rice, temperate cereals, temperate roots, tropical roots, and sunflower are grown (rainfed and irrigated)	others_c3ann_irrigated, others_c3ann_rainfed	1 (share of area in a grid cell)	0.5°×0.5°, annual	downscaled from LUH v2 data based on the crop distribution from (Monfreda et al., 2008). The method is described in (Frieler et al., 2017)
Fraction of grid cell where nitrogen fixing C3 crops other than groundnut, pulses, and soybean are grown (rainfed and irrigated)	others_c3nfx_irrigated, others_c3nfx_rainfed	1 (share of area in a grid cell)	0.5°×0.5°, annual	downscaled from LUH v2 data based on the crop distribution from (Monfreda et al., 2008). The method is described in (Frieler et al., 2017)
Urban areas	urbanareas	1 (share of area in a grid cell)	0.5°×0.5°, annual	LUH v2

1072

1073 Historical land use and irrigation patterns for ISIMIP3a simulations are taken from LUH v2 (Hurtt et al.,
1074 2020, Land use harmonization, 2023). The data set is, up to 2018, identical to the data provided with
1075 ISIMIP2b. The data are based on the HYDE 3.2 land use data set (Klein Goldewijk et al., 2017) and
1076 have been constantly extended up to 2021, i.e., by copying the 2018 patterns into 2019, 2020, and
1077 2021.

1078 The original HYDE 3.2 data distinguishes four categories of land use: rainfed and irrigated cropland,
1079 managed pastures, and more extensively managed rangelands (see **Table 11**). The latter two
1080 categories are combined to grazing lands (ISIMIP variable 'pastures', see **Figure 6**). In LUH v2 the crop
1081 land information is further downscaled to five crop types: C3 annual plants, C3 perennial plants, C3

1082 nitrogen fixing plants, C4 annual plants and C4 perennial plants (see global aggregates in **Figure 7**). In
1083 the same vein as the HYDE case, the LUH v2 data set distinguishes between rainfed and irrigated
1084 croplands. For the purpose of driving the ISIMIP impact models, the LUH v2 data was interpolated from
1085 the original $0.25^\circ \times 0.25^\circ$ to the standard ISIMIP $0.5^\circ \times 0.5^\circ$ global grid. In a further downscaling step
1086 the 5 crops land use data has been downscaled even further to 15 crop types (see global aggregates
1087 in **Figure 7**). For this purpose the Monfreda land use dataset (Monfreda et al., 2008) has been used. It
1088 describes the crop land areas of 175 crops in the year 2000, and we use this to downscale the 5 crops
1089 categories into land use areas of 15 more specific crop types (maize, groundnut, rapeseed, soybeans,
1090 sunflower, rice, sugarcane, pulses, temperate cereals (including wheat), temperate roots, tropical
1091 cereals, tropical roots, others annual, others perennial, and others N-fixing). The ratios determined from
1092 the year 2000 numbers have then been applied to all years. For further details please refer to (Frieler
1093 et al., 2017).

1094

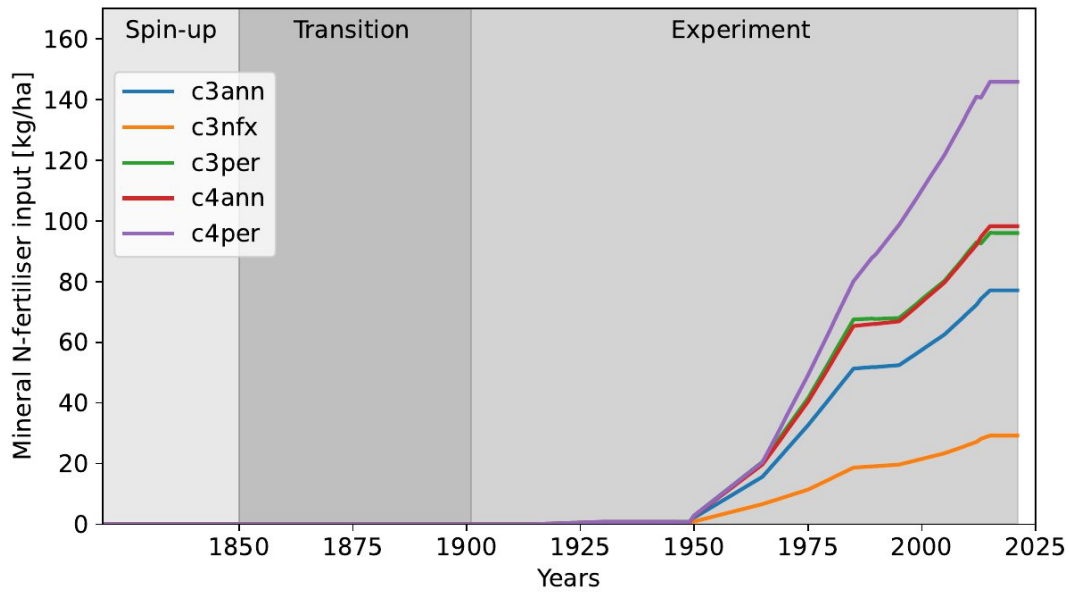
1095 The areas outside of the specified agricultural and urban land is considered 'natural vegetation' and not
1096 prescribed further to not constrain the dynamical vegetation models.

1097

1098

1099 **4.4 Fertiliser input**

1100



1101

1102

1103

1104

1105

Figure 8: Mean mineral N-fertiliser input averaged across the land areas where the considered crop groups are grown.

Table 12: Fertiliser inputs provided as part of the ISIMIP3a direct human forcing.

Variable	Variable specifier	Unit	Resolution	Datasets
Mineral N-fertiliser input for annual C3 crops (C4annual, C4 perennial, C3 nitrogen fixing)	ferti_c3ann,	kg ha-1 yr-1 (crop season)	0.5°×0.5°, annual	LUH v2 (Hurtt et al., 2020)
Mineral N-fertiliser input for perennial C3 crops	ferti_c3per	kg ha-1 yr-1 (crop season)	0.5°×0.5°, annual	LUH v2 (Hurtt et al., 2020)
Mineral N-fertiliser input for annual C4 crops	ferti_c4ann	kg ha-1 yr-1 (crop season)	0.5°×0.5°, annual	LUH v2 (Hurtt et al., 2020)

Mineral N-fertiliser input for perennial C4 crops	fertl_c4per	kg ha-1 yr-1 (crop season)	0.5°×0.5°, annual	LUH v2 (Hurtt et al., 2020)
Mineral N-fertiliser input for nitrogen-fixing C3 crops	fertl_c3nfx	kg ha-1 yr-1 (crop season)	0.5°×0.5°, annual	LUH v2 (Hurtt et al., 2020)

1106

1107 The LUH v2 data set also includes national application rates of industrial nitrogen fertiliser (Hurtt et al.,
1108 2020). This does not include manure. The fertiliser data is not based on HYDE but was derived from
1109 other sources. The data for the years 1915–1960 are based on (Smil, 2001), 1961–2011 are based on
1110 a compilation by (Zhang et al., 2015) which in turn is based on FAOSTAT (FAO, 2016), and 2012–2015
1111 are based on a projection by the International Fertilizer Association (IFASTAT, 2015). For the pure crop
1112 runs within ISIMIP, where the considered crops are assumed to be grown everywhere without a land
1113 use specification, the LUH v2 national fertiliser inputs are assumed to be applied everywhere within the
1114 country. To calculate crop production, the LUH2 v2 land use patterns are applied in post-processing,
1115 i.e. by multiplying the crop yields from the pure crop run with the land use patterns (fraction of the grid
1116 cell where the crop has been grown).

1117

1118 4.5 Land transformation

1119

1120 **Table 13: Land transformation and wood harvest provided as part of the ISIMIP3a direct human forcing.**

Variable	Variable specifier	Unit	Resolution	Datasets
Wood harvest area from primary forest land	primf-harv	Fraction of the national land area, kg in case of biomass	Annual, national sum	Based on LUH v2 v2h (Hurtt et al., 2011, 2020; del Valle et al., 2022, Land use harmonization, 2023)

Wood harvest area from primary non-forest land	primn-harv	Fraction of the national land area, kg in case of biomass	Annual , national sum	Based on LUH v2 v2h (Hurtt et al., 2011, 2020; del Valle et al., 2022)
Wood harvest area from secondary mature forest land	secmf-harv	Fraction of the national land area, kg in case of biomass	Annual , national sum	Based on LUH v2 v2h (Hurtt et al., 2011, 2020; del Valle et al., 2022)
Wood harvest area from secondary young forest land	secyf-harv	Fraction of the national land area, kg in case of biomass	Annual , national sum	Based on LUH v2 v2h (Hurtt et al., 2011, 2020; del Valle et al., 2022)
Wood harvest area from secondary non-forest land	secnf-harv	Fraction of the national land area, kg in case of biomass	Annual , national sum	Based on LUH v2 v2h (Hurtt et al., 2011, 2020; del Valle et al., 2022)
Wood harvest biomass carbon from primary forest land	primf-bioh	Fraction of the national land area, kg in case of biomass	Annual , national sum	Based on LUH v2 v2h (Hurtt et al., 2011, 2020; del Valle et al., 2022)
Wood harvest biomass carbon from primary non-forest land	primn-bioh	Fraction of the national land area, kg in case of biomass	Annual , national sum	Based on LUH v2 v2h (Hurtt et al., 2011, 2020; del Valle et al., 2022)

Wood harvest biomass carbon from secondary mature forest land	secmf-bioh	Fraction of the national land area, kg in case of biomass	Annual, national sum	Based on LUH v2 v2h (Hurtt et al., 2011, 2020; del Valle et al., 2022)
Wood harvest biomass carbon from secondary young forest land	secyf-bioh	Fraction of the national land area, kg in case of biomass	Annual, national sum	Based on LUH v2 v2h (Hurtt et al., 2011, 2020; del Valle et al., 2022)
Wood harvest biomass carbon from secondary non-forest land	secnf-bioh	Fraction of the national land area, kg in case of biomass	Annual, national sum	Based on LUH v2 v2h (Hurtt et al., 2011, 2020; del Valle et al., 2022)
Not forest-related land transformations All transitions from one type of land use to another	<type 1>_to_<type 2> With type 1 and type 2 from the following list: secdf (potentially forested secondary land), secdn (potentially non-forested secondary land), urban (urban land), c3ann (C3 annual crops), c4ann (C4 annual crops), c3per (C3 perennial crops), c4per (C4 perennial crops), c3nfx (C3 nitrogen-fixing crops), pastr (managed pasture) range (rangeland)	Fraction of the grid cell	Annual	Based on LUH v2h (Hurtt et al., 2011, 2020, Land use harmonization, 2023); Land is considered to be 'potentially forested' if the above ground biomass density (kg C m ⁻²) of the potential vegetation as estimated by the Miami-LU model accounting for changes in cropland and grazing land is > 2 kg C m ⁻²

				(Hurtt et al., 2020)
--	--	--	--	----------------------

1121

1122 These datasets are based on the LUH v2 Harmonization Data Set covering 850 to 2015 (Hurtt et al.,
 1123 2020, Land use harmonization, 2023). The wood harvest data were obtained by aggregating from the
 1124 original LUH v2 grid to the ISIMIP 0.5° × 0.5° grid (first-order conservative remapping) and then
 1125 aggregating to the national sums. Wood harvesting data are used in the vegetation models to mimic
 1126 wood removal as part of forest management and clearing, and has a strong influence on the carbon
 1127 balance. National data are provided so that models can use their internal routines to distribute the
 1128 harvesting within a country's forest area. The gridded land transformation data were obtained by
 1129 aggregating from the original LUH v2 grid to the ISIMIP 0.5° × 0.5° grid; these data always end a year
 1130 earlier than all other land use data, because a year in these data sets actually describes the changes
 1131 from the current to the next year. The data have been extended up to 2021 by copying the 2015 data
 1132 into the following years (files end in 2020).

1133

1134 **4.6 Nitrogen Deposition**

1135

1136

Table 14: Nitrogen deposition provided as part of the ISIMIP3a direct human forcing.

Variable	Variable specifier	Unit	Resolution	Datasets
Reduced nitrogen deposition	nhx	g N m ⁻² mon- 1	monthly	based on simulations from (Tian et al., 2018)

Oxidised nitrogen deposition	noy	g N m ⁻² mon-1	monthly	based on simulations from (Tian et al., 2018)
------------------------------	------------	---------------------------	---------	---

1137

1138

1139 Reduced and oxidised nitrogen deposition (NH_x, NO_y) are based on simulations by the NCAR
 1140 Chemistry-Climate Model Initiative during 1850-2014 (Tian et al., 2018). Nitrogen deposition data was
 1141 interpolated to 0.5° by 0.5° using the nearest grid point method. Data in 2015-2021 are assumed to be
 1142 the same as that in 2014.

1143

1144 4.7 Crop calendar

1145

1146 **Table 15:** Crop calendar provided as optional representation of agricultural management. The information is
 1147 given for 18 crop types.

Variable	Variable specifier	Unit	Resolution	Datasets
Planting day, separated for rainfed and irrigated crops where applicable	planting_day	day of year	0.5°, time average, no variation in time	(Jägermeyr et al., 2021b)
Maturity day, separated for rainfed and irrigated crops where applicable	maturity_day	day of year	0.5°, time average, no variation in time	(Jägermeyr et al., 2021b)

1148

1149 Unfortunately, there is no global data set describing changes in growing seasons across the historical
 1150 period. Instead we provide a static crop calendar that has been developed within the AgMIP Global
 1151 Gridded Crop Model Intercomparison GGCM and merges information from various observational data
 1152 sources (Jägermeyr et al., 2021b). It provides planting and maturity days for 18 different crops at the
 1153 ISIMIP standard 0.5° grid. Grid cells outside of currently cultivated areas are spatially extrapolated
 1154 (details below). For wheat and rice two growing seasons are provided while for all other crops the
 1155 calendar only specifies one main growing season. The reported growing seasons should not be
 1156 considered the growing seasons for one specific year but as 'representative growing season' across
 1157 the recent years. Within the crop models different crop varieties are represented by different heat units

1158 required to reach physiological maturity. The crop calendar should be implemented by adjusting the
 1159 required heat units to the average of the annual sums of heat units between the specified planting and
 1160 maturity date over all growing seasons between 1979 and 2010.

1161 If modellers use a temporal adjustment of cultivars by varying required heat units in response to socio-
 1162 economic development or historical climate change this is certainly allowed within the 'histsoc' set-up.
 1163 If cultivars are fixed according to the method described above this simulation will be considered a
 1164 '2015soc' simulation as long as other direct human drivers are also held constant at 2015 levels.
 1165 However, if, e.g., fertiliser inputs are varied over time according to provided forcing data (see section
 1166 **4.4**), the run will be considered a 'histsoc' run.

1167 GGCM is currently working on a temporally resolved global crop calendar at the same spatial resolution
 1168 based on various new data sources including agricultural ministries, census reports, phenological data
 1169 bases, experimental sites, etc. This data set will be published separately and could then be used to
 1170 inform 'histsoc' simulations.

1171

1172 **4.8 Dams and reservoirs**

1173

1174 **Table 16: Information about dams and reservoirs**

Variable	Variable specifier	Unit	Resolution	Datasets
Unique ID for each point representing a dam and its associated reservoir.	ID	unitless numbers: 1-7320 from GRanD and J3-J26 from GeoDAR v1.2	per dam	Global Reservoir and Dam Database (GRanDv1.3, data up to 2016; (Lehner et al., 2011a, b) and GeoDAR v1.2 (Wang et al., 2022) covering the period 2016-2020
Name of the dam structure	DAM_NAME	unitless	per dam	GRanDv1.3, GeoDARv1.2
Original longitudinal location of the dam	LON_ORIG	degree (°)	per dam	GRanDv1.3, GeoDARv1.2
Original longitudinal location of the dam	LAT_ORIG	degree (°)	per dam	GRanDv1.3, GeoDARv1.2

Longitude, adjusted to the ISIMIPddm30 0.5° grid cell centres	LON_DDM30	degree (°)	per dam	Adjustment of original GRanDv1.3, GeoDARv1.2 data
Latitude, adjusted to the ISIMIPddm30 0.5° grid cell centres	LAT_DDM30	degree (°)	per dam	Adjustment of original GRanDv1.3, GeoDARv1.2 data
Upstream area draining into the reservoir using ISIMIPddm30	CATCH_SKM_DDM30	km ²	per dam	Derived from dam location and the ISIMIPddm30 drainage map.
Upstream area draining into the reservoir acc. to GRanD [km ²]	CATCH_SKM_GRanD	km ²	per dam	GRanDv1.3
Representative maximum storage capacity of reservoir	CAP_MCM	10 ⁶ m ³	per dam	GRanDv1.3, GeoDARv1.2
Year of construction, completion, commissioning, etc. (not specified)	YEAR	year	per dam	GRanDv1.3, GeoDARv1.2 + complemented by internet research
Alternative year (may indicate multi-year construction, secondary dam, etc.)	ALT_YEAR	year	per dam	GRanD
Original, rounded location has been shifted with automatic mapping (FLAG_CORR=1)	FLAG_CORR	Unitless labels: 1 or 2	per dam	Introduced when adjusting the locations to the ISIMIPddm30

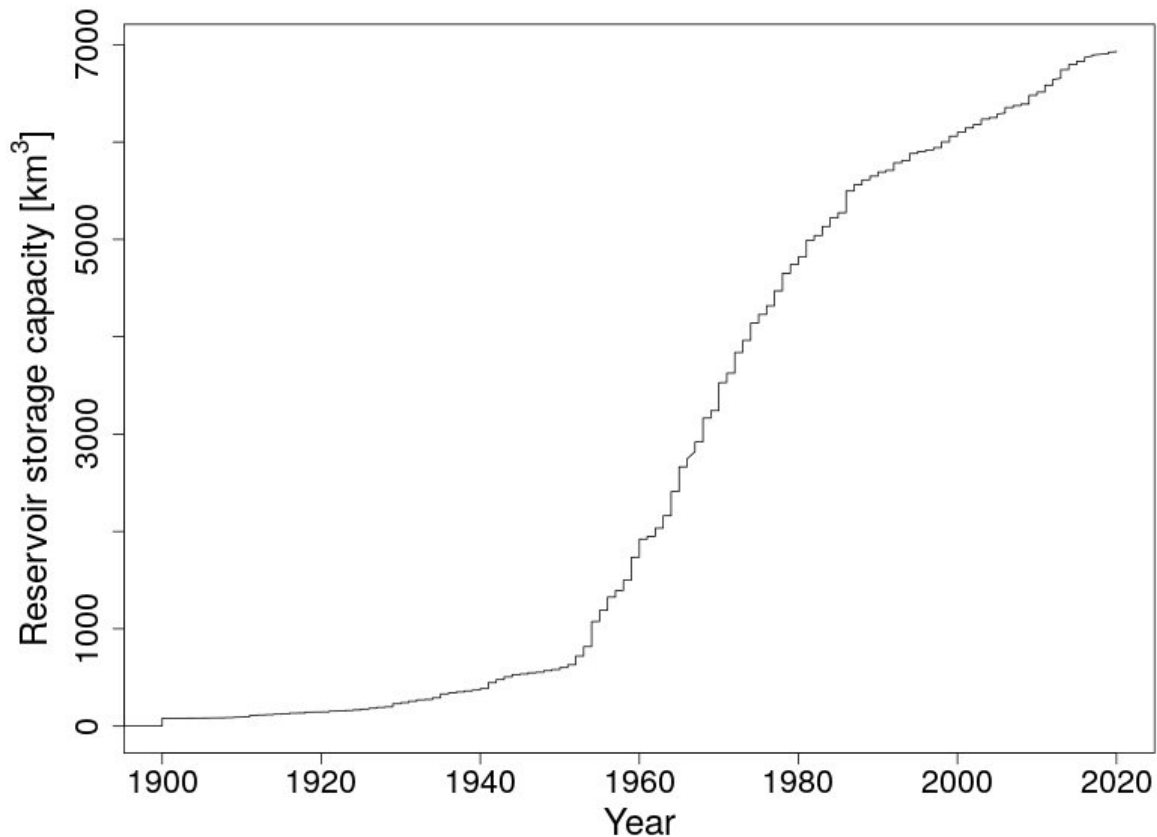
If visual check or manual re-location has been applied (FLAG_CORR=2)				0.5° grid
Name of the river which the dam impounds	RIVER	unitless	per dam	GeoDARv1.2. For GRanD records, it can be found in the GRanD database
Country where the dam is located	COUNTRY	unitless	per dam	GeoDARv1.2. For GRanD records, it can be found in the GRanD database
Height of the dam. If multiple heights are available, the foundation height was used.	D_Hght_m	m	per dam	GeoDARv1.2. For GRanD records, it can be found in the GRanD database
Maximum inundation area of the reservoir	R_Area_km2	km ²	per dam	GeoDARv1.2. For GRanD records, it can be found in the GRanD database
Maximum inundation length of the reservoir	R_Lgth_km	km	per dam	GeoDARv1.2. For GRanD records, it can be found in the GRanD database

				database
Main purpose(s) of the dam	PURPOSE	no units	per dam	GeoDARv1.2. For GRanD records, it can be found in the GRanD database
Sources used to collect this dam's information	SOURCE	no units	per dam	GeoDARv1.2. For GRanD records, it can be found in the GRanD database. If filled out for GeoDAR records, it corresponds to the source for the year of construction/ commissioning
Other notes related to the mapping or re-location of dams to ISIMIPddm30	COMMENTS	no units	per dam	

1175

1176 In order to offer a consistent and common source of information about reservoirs and associated dams
1177 for climate impact modellers (see **Table 16**), we joined the Global Reservoir and Dam Database of the
1178 Global Water System Project (GRanD v1.3; (Lehner et al., 2011a, b) with a subset of the Georeferenced
1179 global Dams And Reservoirs (GeoDAR v1.2) database (Wang et al., 2022), developed at Kansas State
1180 University (KSU), and provided by Jida Wang ahead of publication, so that it could be provided when
1181 launching ISIMIP3 in 2020. These additional dams have construction or projected finalisation dates
1182 between 2016 and 2025, while GRanD v1.3 includes dams constructed up until 2017. In total, the
1183 combined database now includes 7331 dams whose construction will be finished by 2025. It includes
1184 dams that were constructed before the simulation period, but still exist (the first reported dam was
1185 finished in the year 286). For the simulations described here, dams with (projected) construction dates

1186 after 2020 are not considered; these will become relevant in the ISIMIP3b simulations, with exception
1187 of the Grand Ethiopian Renaissance Dam, which we decided to include since its reservoir reached a
1188 first stage of filling of 4.9 km³ in July 2020 (BBC news: Nile dam row, 2020; Tractebel: Filling of the
1189 reservoir of the Grand Renaissance Dam, 2020).
1190



1191
1192 **Figure 9: Cumulative reservoir storage capacity between 1900 and 2020.** Reservoirs that are active before
1193 the year 1901 have been assigned to the year 1900. Horizontal axis shows year of construction, completion, or
1194 commissioning, reflecting ambiguity in available data.
1195

1196 The original GRanDv1.3 dam locations were mapped to the global 30-min drainage direction map
1197 (ISIMIPddm30, (Müller Schmied, 2022) based on DDM30 (Döll and Lehner, 2002), by applying the
1198 following algorithm:

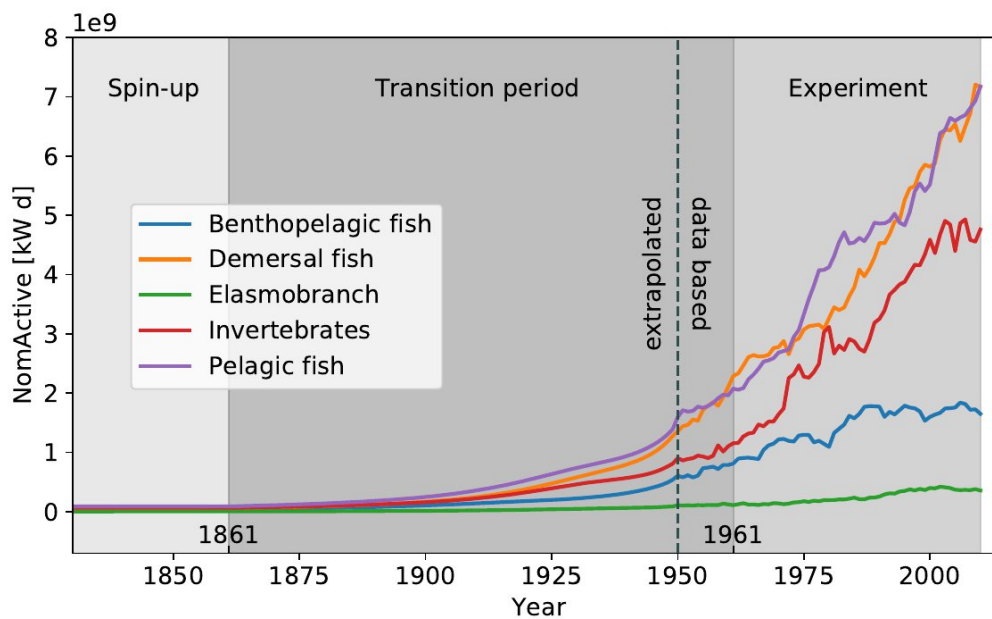
1199 Firstly, the locations have been rounded to the closest 0.5° grid cell centre. Then, the area of the
1200 upstream catchment draining into the GRanD reservoirs (previous version of GRanDv1.3) in the
1201 ISIMIPddm30 map have been calculated and compared against the ones reported in GRanD. All dams
1202 with an upstream area bigger than 10000 km² in GRanD and more than 50% deviation from the GRanD
1203 upstream area have been shifted to the 8 possible neighbouring cells. If any of these shifts resulted in
1204 a smaller deviation from the GRanD upstream areas, the dam was moved to the grid cell resulting in
1205 the smallest deviation in the upstream area.

1206 Additionally, a visual validation and, where appropriate, manual relocation were applied with the aim to
1207 find the best fitting grid cell from a hydrological perspective. Due to the low resolution of the model grid,

1208 reservoirs might get wrongly assigned to e.g. the main stream (either before or after the confluence of
 1209 two rivers), even though the dam is located in a particular tributary according to the database.
 1210 In those cases, and based on visual GIS inspection, the best location was searched, e.g. by moving the
 1211 dam location one cell upstream to preserve the routing order and to avoid a different or much deviating
 1212 river basin in the ISIMIPddm30 stream network. In case a dam is not assigned to any river basin in the
 1213 ISIMIPddm30 (which can happen due to the difference in spatial resolution), the most suited location
 1214 according to the observed upstream area was selected. Because of limited capacity, this visual
 1215 validation procedure was applied only for dams present in the earlier GranDv1.1 version that have a
 1216 maximum storage capacity greater than 0.5 km³ (1108 dams), as well as for all the 458 additional dams
 1217 in GRanDv1.3 and the 11 dams (excluding post-2020 dams) added from GeoDAR v1.2, and not for
 1218 several thousand smaller dams present in GranDv1.1. In total the reported dams have a global
 1219 cumulative storage capacity of approximately 6932 km³ (**Figure 9**).

1220

1221 **4.9 Fishing intensities**



1222

1223 **Figure 10: Evolution of historical nominal active fishing effort (NomActive) as provided for the spin-up,**
 1224 **transition period, and 'obsclim + histoc, default' ISIMIP3a experiment, separated by target functional group. The**
 1225 **groups represent an aggregation of 29 even finer categories covered by the data set (see Table 17).**

1226

1227 **Table 17: Information about historical fishing intensities provided as DHF within ISIMIP3a.** For the spin-up
 1228 + transition period required by models within the *marine ecosystems and fisheries* sector the forcing is provided
 1229 for 1841-2010 although the 'obsclim + histoc, default' experiment only starts in 1961.

Variable	Variable specifier	Unit	Resolution	Datasets
Total nominal active fishing effort (i.e., accounting for total)	NomActive	kW d (kilowatts of fleet)	annual data spatially grouped by Exclusive Economic Zones	Reconstruction based on historical yearbook and FAO

power of the fleet but not including changes in the efficiency of fishing technology) separated by fishing sector, fleet, and target functional groups.		power times days at sea)	(EEZ), (Sea Around Us Area Parameters and Definitions) and nested within Large Marine Ecosystems. Masks for the latter are provided as static geographic information (see Table 1).	compilations ((Rousseau et al., 2022) based on (Rousseau et al., submitted 2023). The reconstructions have been extended backwards to 1841 by constant 1861 values to cover the 120 years of spin-up required for the marine ecosystems and fisheries models
---	--	--------------------------	---	--

1230

1231 The data set of reconstructed historical fishing efforts (Rousseau et al., 2022) serves as the DHF for
 1232 the *marine ecosystems and fisheries* sector. The efforts are quantified for 'artisanal' and 'industrial'
 1233 fishing (sector), 66 Large Marine Ecosystems (LME), 187 national Exclusive Economic Zones (EEZ)
 1234 and 'high seas', 244 country identifiers from the Sea Around Us Project (SAUP), 16 different categories
 1235 of applied gears (e.g. bottom trawls, longlines and purse seines), 29 target functional groups (see
 1236 nominal active fishing effort for 5 aggregated categories in **Figure 10**), separately.

1237 The original annual time series spanning 1950-2015 were further extrapolated into the past to 1861
 1238 using generalised additive models (Rousseau et al., submitted 2023; see **Figure 10**). To cover the
 1239 'spin-up + transition' period from 1841-1960 the data set has been extended backwards by 1861 values.
 1240 Forcing with this dataset allows for a comparison of simulated catches against the congruent (Watson,
 1241 2019) reconstruction of historical fisheries catches (spanning the period 1869-2015; (Watson and Tidd,
 1242 2018). To permit integration into marine ecosystem models that capture different fishing sectors, fleets,
 1243 and functional groups these data include nominal active fishing effort disaggregated by location
 1244 (Exclusive Economic Zone/High Seas and Large Marine Ecosystem), fishing country, fishing gear,
 1245 targeted functional group, and fishing sector (coastal artisanal and industrial). Impact modellers are
 1246 allowed to distribute this effort across space, time, and target organisms in any method compatible with
 1247 their models' structure. The fishing effort data does not include any information about changes in the
 1248 efficiency of fishing technology over time (technological creep). Assumptions about these efficiencies
 1249 are left to the individual modellers and usually determined in model calibration.

1250

1251 **4.10 Forest management for *regional forest* sector**

1252

1253 **Table 18:** Information about historical forest management provided as DHF for the *regional forest* sector within
 1254 ISIMIP3a

Variable	Variable specifier	Unit	Resolution	Datasets
Silvicultural system	sysi	na	stand	(Reyer et al., 2023)
Tree species	species	na	stand	(Reyer et al., 2023)
Harvest type	harvtype	na	stand	(Reyer et al., 2023)
Thinning type	thintype	% of basal area	stand	(Reyer et al., 2023)
Rotation length	rotlength	year	stand	(Reyer et al., 2023)
Thinning frequency	thinfrequ	year	stand	(Reyer et al., 2023)
Year of Management intervention	manyear	year	stand	(Reyer et al., 2023)
Type of management intervention	mantype	na	stand	(Reyer et al., 2023)
Regeneration species	regen	na	stand	(Reyer et al., 2023)
Planting density	plantdens	na	stand	(Reyer et al., 2023)
Planting age	plantage	year	stand	(Reyer et al., 2023)
Planting seedling height	planthei	m	stand	(Reyer et al., 2023)
Planting diameter at breast height	plantdbh	cm	stand	(Reyer et al., 2023)
Age when diameter at breast height is	dbhage	year	stand	(Reyer et al., 2023)

reached				
Stem number	stemno	na	stand	(Reyer et al., 2020a) based on (Reyer et al., 2020b)

1255

1256 For the *regional forest* sector, forest management is defined for nine forest sites in Europe, four in
1257 Germany (Peitz, KROOF, Solling-beech, Solling-spruce) as well in Czech Republic (Bily Kriz), Denmark
1258 (Sorø), France (Le Bray), Italy (Collelongo) and Finland (Hyytiälä) (Reyer et al., 2020b). Additionally, a
1259 set of forest site-specific forest management rules and planting numbers based on historical standard
1260 management practices of the area where the forest sites are located are defined and spelled out in
1261 concrete management schedules to enable modellers to simulate ‘2015soc’ conditions (Reyer et al.,
1262 2023). The regional forest management data has not been harmonised to the global gridded wood
1263 harvest data provided for the biomes sector, because the data is very site-specific and the variation not
1264 resolved in the global data set.

1265

1266 **5 Conclusion**

1267 The first part of the third simulation round of the Inter-sectoral Impact Model Intercomparison Project
1268 ISIMIP (ISIMIP3a) is intended to facilitate impact model evaluation and impact attribution experiments
1269 to significantly move forward our understanding of observed changes in natural and human systems
1270 and their respective drivers. Impact models as participating in ISIMIP encode our process knowledge
1271 on how several drivers (climate-related ones as well as direct human influences) come together to
1272 generate observed changes. As such, they are ideal tools for this task. The new ISIMIP3a simulation
1273 framework including the provision of the relevant forcing data is intended to unleash the power of a wide
1274 range of models from different sectors to quantify the contribution of observed changes in climate-
1275 related systems to observed environmental or societal changes.

1276 As a first step towards impact attribution, the ISIMIP3a evaluation experiments will help to clarify how
1277 well the current generation of impact models can explain observed changes in impacted systems based
1278 on provided information about the different forcings. The performance of the models in reproducing
1279 observed variations and long-term changes in the impacted systems, certainly does not only depend
1280 on the models themselves but also on the availability and uncertainties associated with the climate-
1281 related and direct human forcings (see Table 1). We capture part of this uncertainty by providing four
1282 different observational atmospheric climate forcing data and associated counterfactual forcings (see
1283 section 2.1) and TC windfields derived from two different modelling approaches (see section 3.2).
1284 Uncertainties in the direct human forcings are represented to the degree that the forcing data sets
1285 considered as ‘optional’ vary from model to model. In addition, the multi-model framework of ISIMIP
1286 allows for testing to what degree different process-representations may be better suitable to explain the
1287 observations than others.

1288 High explanatory power is then a prerequisite for impact attribution through the ISIMIP3a attribution
1289 experiments based on counterfactual climate-related forcings following the IPCC definition (O'Neill et
1290 al., 2022).

1291

1292 The setup is the first that allows to easily and broadly address impact attribution across many impact
1293 categories. This will fill an important gap as only few process-based impact models have been used in
1294 this field despite their general suitability. The presented work can thus lay the ground for urgently
1295 necessary works to inform climate litigation (Burger et al., 2020; Burger and Tigre, 2023), the loss and
1296 damage debate (Mechler et al., 2018; Wyns, 2023), and last but not least also decisions about short
1297 term adaptation measures. It will ultimately help to carve out the sensitivity of our ecosystems and
1298 human societies to historical climate change, which is a precondition for robustly projecting future
1299 climate impacts.

1300 This paper aims to give an overview of the ISIMIP3a experiments and the provided climate-related and
1301 direct human forcing data sets. It is intended to work as a catalogue where modellers can find all
1302 relevant information about the data sets they need for the impact model simulations within ISIMIP3a.
1303 As a community-driven initiative across multiple disciplines the selection of the best available forcing
1304 data for ISIMIP builds on the expertise within the different sectoral communities.

1305 We would like to improve or complement these data sets in a continuous process wherever possible.
1306 So this paper can also be read as a call for contributing additional data that could i) be provided within
1307 the current round (ISIMIP3) as optional data (see explanation in the introduction) that is not harmonised
1308 within or across sectors or ii) as mandatory forcing for an upcoming simulation round. In particular, we
1309 aim for temporally resolved historical growing seasons that have been shown to be critical to reproduce
1310 observed crop yields (Jägermeyr and Frieler, 2018), counterfactual oceanic climate-related forcings,
1311 counterfactual TC-related precipitation (Risser and Wehner, 2017; van Oldenborgh et al., 2017; Wang
1312 et al., 2018; Patricola and Wehner, 2018), temporally resolved lightning data for the full set of considered
1313 climate model simulations, and temporally resolved human drainage and restoration activities in
1314 peatlands as one of the key controls over global peatland greenhouse gas emissions (Loisel et al.,
1315 2020).

1316

1317 **Author contribution:** KF lead the project and developed the concept with contributions from JS, MM,
1318 CO, CPOR, JLB, CSH, CMP, TDE, KOC, CN, RH, DT, OM, JJ, GL, SC, EB, AGS, NS, JC, SH, CB, AG,
1319 FL, SNG, HMS, FH, TH, RM, DP, WT, DMB, MB. JV supported the data generation and harmonisation
1320 of the protocol across all sectors. SL provided atmospheric climate forcing data. MM provided coastal
1321 water level data and atmospheric forcing data. MdRRL, JW and FY provided dam data. CO and IJS
1322 provided GDP data. CPOR provided forest management data. DNK and JTM provided high resolution
1323 climate forcing data. ST provided coastal water levels and counterfactual climate forcing data. YR
1324 provided data on fishing efforts. CS and XL provided ocean forcing data. TV provided TC data. TW and
1325 FS provided gridded GDP data. IV provided lake data. JJ provided growing seasons. CM provided soil
1326 data. KF prepared the manuscript with contributions from all co-authors.

1327

1328 **Code and data availability:** All input data described is available for participating modelers with a
1329 respective account at the DKRZ server. Data will be made publicly available, and most data is already
1330 publicly available at <https://data.isimip.org/>. Availability is documented on www.isimip.org where the
1331 way of accessing the data is described, as well. Model output is already partly available at
1332 <https://data.isimip.org/>.

1333 The ISIMIP Repository fulfills the Archive standards as stated in the "GMD code and data policy". The
1334 Repository is hosted and maintained by the Potsdam Institute for Climate Impact Research (PIK). Data
1335 can only be published or removed from the repository by the ISIMIP data team, that is monitored by the
1336 ISIMIP steering committee according to the organisational structure of ISIMIP (ISIMIP organigram,
1337 2020). DOI are used to refer to datasets in a persistent way. Whenever a dataset is replaced for any
1338 reason a copy is kept on tape, and a new DOI is issued, while the old DOI is kept online with information
1339 on how to retrieve the archived data. Detailed information can be found in the ISIMIP terms of use
1340 (ISIMIP terms of use, 2023).

1341
1342 **Competing interests:** At least one of the (co-)authors is a member of the editorial board of
1343 Geoscientific Model Development.

1344 1345 **Acknowledgements**

1346 This article is based upon work from COST Action CA19139 PROCLIAS (PROcess-based models for
1347 CLimate Impact Attribution across Sectors), supported by COST (European Cooperation in Science
1348 and Technology; <https://www.cost.eu>). Funding from the EU Horizon 2020 research and innovation
1349 program under grant agreement 821010 (CASCADES) supported the work of C.P.O.R., J.V. and
1350 I.D.VdV., and the provisioning of the high resolution climate data, and supported the work of ST under
1351 grant agreement No 820712 (RECEIPT). SL received funding from the German Research Foundation
1352 (DFG, project number 427397136). The German Federal Ministry Ministry of Education and Research
1353 (BMBF) supported the work under the research projects ISIAccess (16QK05), SLICE (01LA1829A),
1354 QUIDIC (01LP1907A), CHIPS (01LS1904A), ISlpedia (01LS1711A). FL received funding from the
1355 National Key Research and Development Program of China (project number 2022YFE0106500). JC
1356 received funding from the National Key Research and Development Program of China (project number
1357 2022YFF0801904). MB acknowledges funding from the Research Foundation—Flanders (FWO,
1358 G095720N). SC and NS were supported by the National Environmental Research Council (NERC)
1359 grant NE/R015791/1. SC, AGS, MB and NS acknowledge funding through NERC NE/V01854X/1
1360 (MOTHERSHIP). CB was supported by the Newton Fund through the Met Office. The research by DNK
1361 was funded through the 2019-2020 BiodivERsA joint call for research proposals, under the BiodivClim
1362 ERA-Net COFUND program, and with the funding organisations Swiss National Science Foundation
1363 SNF (project: FeedBaCks, 193907), and the Swiss National Science Foundation SNF (project: Adohris,
1364 205530). RM was supported by the Alter-C project (PID2020-114024GB-C32/AEI
1365 /10.13039/501100011033). CSH was supported by Open Philanthropy, NSF award 2218777, and
1366 NOAA CPO.

1367

1368 **References**

- 1369 Anon: World development indicators, World Bank Publications, Washington, D.C., DC, 2008.
- 1370 Land use harmonization: <https://luh.umd.edu>, last access: 9 January 2023.
- 1371 Outcomes of the ISIMIP Strategy Group Meeting: <https://www.isimip.org/news/outcome-isimip-strategy-group-meeting-2018/>, last access: 14 January 2023.
- 1372
- 1373 Protocol - TRENDY: <https://blogs.exeter.ac.uk/trendy/protocol/>, last access: 18 October 2023.
- 1374 ISIMIP2a: suspicious gridded GDP per capita data; new functions in the isimip data repository; Forum
1375 on Scenarios for Climate and Societal Futures: <https://www.isimip.org/newsletter/simip2a-suspicious-gridded-gdp-capita-data-new-functions-isimip-data-repository-forum-scenarios-climate-and-societal-futures/>, last access: 10 February 2023.
- 1376
- 1377
- 1378 ISIMIP Output Data Table: <https://www.isimip.org/outputdata/>, last access: 19 October 2023.
- 1379 ISIMIP terms of use: <https://www.isimip.org/gettingstarted/terms-of-use/>, last access: 14 January
1380 2023.
- 1381 ISIMIP3 simulation protocol: <https://protocol.isimip.org/>, last access: 14 January 2023.
- 1382 WOCE Atlas: <http://woceatlas.ucsd.edu>, last access: 11 January 2023.
- 1383 Arujo, E., Bodirsky, B. L., Crawford, M. S., Leip, D., and Dietrich, J.: MissingIslands dataset for filling
1384 in data gaps from the WDI datasets, <https://doi.org/10.5281/zenodo.4421504>, 2021.
- 1385 Badger, J., Bauwens, I., Casso, P., Davis, N., Hahmann, A., Hansen, S. B. K., Hansen, B. O.,
1386 Heathfield, D., Knight, O. J., Lacave, O., Lizcano, G., Mas, A. B. i., Mortensen, N. G., Olsen, B. T.,
1387 Onninen, M., Van Loon, A. P., and Volker, P.: Global Wind Atlas, n.d.
- 1388 Bloemendaal, N., de Moel, H., Mol, J. M., Bosma, P. R. M., Polen, A. N., and Collins, J. M.:
1389 Adequately reflecting the severity of tropical cyclones using the new Tropical Cyclone Severity Scale,
1390 *Environ. Res. Lett.*, 16, 014048, 2021.
- 1391 Brun, P., Zimmermann, N. E., Hari, C., Pellissier, L., and Karger, D. N.: CHELSA-BIOCLIM+ A novel
1392 set of global climate-related predictors at kilometre-resolution, <https://doi.org/10.16904/envidat.332>,
1393 2022a.
- 1394 Brun, P., Zimmermann, N. E., Hari, C., Pellissier, L., and Karger, D. N.: Global climate-related
1395 predictors at kilometre resolution for the past and future, , <https://doi.org/10.5194/essd-2022-212>,
1396 2022b.
- 1397 Büchner, M. and Reyer, C.: ISIMIP3a atmospheric composition input data,
1398 <https://doi.org/10.48364/ISIMIP.664235.2>, 2022.
- 1399 Burger, M. and Tigre, M. A.: Global Climate Litigation Report: 2023 Status Review, 2023.
- 1400 Burger, M., Wentz, J., and Horton, R.: The Law and Science of Climate Change Attribution, 1, 45,
1401 <https://doi.org/10.7916/cjel.v45i1.4730>, 2020.
- 1402 Caron, L., Ivins, E. R., Larour, E., Adhikari, S., Nilsson, J., and Blewitt, G.: GIA model statistics for
1403 GRACE hydrology, cryosphere, and ocean science, *Geophys. Res. Lett.*, 45, 2203–2212, 2018.
- 1404 Cecil, D.: LIS/OTD 0.5 Degree High Resolution Monthly Climatology (HRMC),
1405 <https://doi.org/10.5067/LIS/LIS-OTD/DATA303>, 2006.
- 1406 Chavas, D. R. and Lin, N.: A Model for the Complete Radial Structure of the Tropical Cyclone Wind
1407 Field. Part II: Wind Field Variability, *J. Atmos. Sci.*, 73, 3093–3113, 2016.
- 1408 Compo, G. P., Whitaker, J. S., Sardeshmukh, P. D., Matsui, N., Allan, R. J., Yin, X., Gleason, B. E.,
1409 Vose, R. S., Rutledge, G., Bessemoulin, P., Brönnimann, S., Brunet, M., Crouthamel, R. I., Grant, A.

- 1410 N., Groisman, P. Y., Jones, P. D., Kruk, M. C., Kruger, A. C., Marshall, G. J., Maugeri, M., Mok, H. Y.,
 1411 Nordli, Ø., Ross, T. F., Trigo, R. M., Wang, X. L., Woodruff, S. D., and Worley, S. J.: The twentieth
 1412 century reanalysis project, *Quart. J. Roy. Meteor. Soc.*, 137, 1–28, 2011.
- 1413 Cramer, W., Yohe, G. W., Auffhammer, M., Huggel, C., Molau, U., da Silva Dias, M. A. F., Solow, A.,
 1414 Stone, D. A., and Tibig, L.: Detection and Attribution of Observed Impacts: Climate Change 2014:
 1415 Impacts Adaptation and Vulnerability, Contribution of Working Group II to the Fifth Assessment Report
 1416 of the Intergovernmental Panel on Climate Change, in: *Climate Change 2014: Impacts Adaptation and*
 1417 *Vulnerability, Contribution of Working Group II to the Fifth Assessment Report of the*
 1418 *Intergovernmental Panel on Climate Change*, Cambridge University Press, 2014.
- 1419 Cucchi, M., Weedon, G. P., Amici, A., Bellouin, N., Lange, S., Müller Schmied, H., Hersbach, H., and
 1420 Buontempo, C.: WFDE5: bias-adjusted ERA5 reanalysis data for impact studies, *Earth Syst. Sci.*
 1421 *Data*, 12, 2097–2120, 2020.
- 1422 Dangendorf, S., Hay, C., Calafat, F. M., Marcos, M., Piecuch, C. G., Berk, K., and Jensen, J.:
 1423 Persistent acceleration in global sea-level rise since the 1960s, *Nat. Clim. Chang.*, 9, 705–710, 2019.
- 1424 Danielson, J. J. and Gesch, D. B.: Global multi-resolution terrain elevation data 2010 (GMTED2010),
 1425 U.S. Geological Survey, <https://doi.org/10.3133/ofr20111073>, 2011.
- 1426 Dirmeyer, P. A., Gao, X., Zhao, M., Guo, Z., Oki, T., and Hanasaki, N.: GSWP-2: Multimodel Analysis
 1427 and Implications for Our Perception of the Land Surface, *Bull. Am. Meteorol. Soc.*, 87, 1381–1398,
 1428 2006.
- 1429 Döll, P. and Lehner, B.: Validation of a new global 30-min drainage direction map, *J. Hydrol.*, 258,
 1430 214–231, 2002.
- 1431 Eberenz, S., Stocker, D., Rösli, T., and Bresch, D. N.: LitPop: Global Exposure Data for Disaster
 1432 Risk Assessment, 2019.
- 1433 Eberenz, S., Lüthi, S., and Bresch, D. N.: Regional tropical cyclone impact functions for globally
 1434 consistent risk assessments, *Nat. Hazards Earth Syst. Sci.*, 21, 393–415, 2021.
- 1435 Elvidge, C. D., Baugh, K., Zhizhin, M., Hsu, F. C., and Ghosh, T.: VIIRS night-time lights, *Int. J.*
 1436 *Remote Sens.*, 38, 5860–5879, 2017.
- 1437 Emanuel, K. and Rotunno, R.: Self-Stratification of Tropical Cyclone Outflow. Part I: Implications for
 1438 Storm Structure, *J. Atmos. Sci.*, 68, 2236–2249, 2011.
- 1439 Fagnant, C., Gori, A., Sebastian, A., Bedient, P. B., and Ensor, K. B.: Characterizing spatiotemporal
 1440 trends in extreme precipitation in Southeast Texas, *Nat. Hazards*, 104, 1597–1621, 2020.
- 1441 FAO: Faostat: FAO Statistical Databases, 2016.
- 1442 Feenstra, R. C., Inklaar, R., Timmer, M., and Woltjer, P.: Penn World Table 10.0,
 1443 <https://doi.org/10.15141/S5Q94M>, 2015.
- 1444 Feldmann, M., Emanuel, K., Zhu, L., and Lohmann, U.: Estimation of Atlantic Tropical Cyclone
 1445 Rainfall Frequency in the United States, *J. Appl. Meteorol. Climatol.*, 58, 1853–1866, 2019.
- 1446 Fiddes, J. and Gruber, S.: TopoSCALE v.1.0: downscaling gridded climate data in complex terrain,
 1447 *Geosci. Model Dev.*, 7, 387–405, 2014.
- 1448 Friedlingstein, P., O'Sullivan, M., Jones, M. W., Andrew, R. M., Gregor, L., Hauck, J., Le Quéré, C.,
 1449 Lujikx, I. T., Olsen, A., Peters, G. P., Peters, W., Pongratz, J., Schwingshackl, C., Sitch, S., Canadell,
 1450 J. G., Ciais, P., Jackson, R. B., Alin, S. R., Alkama, R., Arneeth, A., Arora, V. K., Bates, N. R., Becker,
 1451 M., Bellouin, N., Bittig, H. C., Bopp, L., Chevallier, F., Chini, L. P., Cronin, M., Evans, W., Falk, S.,
 1452 Feely, R. A., Gasser, T., Gehlen, M., Gkritzalis, T., Gloege, L., Grassi, G., Gruber, N., Gürses, Ö.,
 1453 Harris, I., Hefner, M., Houghton, R. A., Hurtt, G. C., Iida, Y., Ilyina, T., Jain, A. K., Jersild, A., Kadono,
 1454 K., Kato, E., Kennedy, D., Klein Goldewijk, K., Knauer, J., Korsbakken, J. I., Landschützer, P.,
 1455 Lefèvre, N., Lindsay, K., Liu, J., Liu, Z., Marland, G., Mayot, N., McGrath, M. J., Metz, N., Monacci, N.

- 1456 M., Munro, D. R., Nakaoka, S.-I., Niwa, Y., O'Brien, K., Ono, T., Palmer, P. I., Pan, N., Pierrot, D.,
 1457 Pocock, K., Poulter, B., Resplandy, L., Robertson, E., Rödenbeck, C., Rodriguez, C., Rosan, T. M.,
 1458 Schwinger, J., Séférian, R., Shutler, J. D., Skjelvan, I., Steinhoff, T., Sun, Q., Sutton, A. J., Sweeney,
 1459 C., Takao, S., Tanhua, T., Tans, P. P., Tian, X., Tian, H., Tilbrook, B., Tsujino, H., Tubiello, F., van der
 1460 Werf, G. R., Walker, A. P., Wanninkhof, R., Whitehead, C., Willstrand Wranne, A., et al.: Global
 1461 carbon budget 2022, *Earth Syst. Sci. Data*, 14, 4811–4900, 2022.
- 1462 Frieler, K.: Scenario Set-up and the new CMIP6-based climate-related forcings provided within the
 1463 third round of the Inter-Sectoral Model Intercomparison Project (ISIMIP3b, group I and II),
 1464 Geoscientific Model Development, submitted 2023.
- 1465 Frieler, K., Lange, S., Piontek, F., Reyer, C. P. O., Schewe, J., Warszawski, L., Zhao, F., Chini, L.,
 1466 Denvil, S., Emanuel, K., Geiger, T., Halladay, K., Hurtt, G., Mengel, M., Murakami, D., Ostberg, S.,
 1467 Popp, A., Riva, R., Stevanovic, M., Suzuki, T., Volkholz, J., Burke, E., Ciais, P., Ebi, K., Eddy, T. D.,
 1468 Elliott, J., Galbraith, E., Gosling, S. N., Hattermann, F., Hickler, T., Hinkel, J., Hof, C., Huber, V.,
 1469 Jägermeyr, J., Krysanova, V., Marcé, R., Müller Schmied, H., Mouratiadou, I., Pierson, D., Tittensor,
 1470 D. P., Vautard, R., van Vliet, M., Biber, M. F., Betts, R. A., Bodirsky, B. L., Deryng, D., Frohking, S.,
 1471 Jones, C. D., Lotze, H. K., Lotze-Campen, H., Sahajpal, R., Thonicke, K., Tian, H., and Yamagata, Y.:
 1472 Assessing the impacts of 1.5 °C global warming – simulation protocol of the Inter-Sectoral Impact
 1473 Model Intercomparison Project (ISIMIP2b), *Geosci. Model Dev.*, 10, 4321–4345, 2017.
- 1474 Geiger, T., Frieler, K., and Bresch, D. N.: A global historical data set of tropical cyclone exposure
 1475 (TCE-DAT), *Earth System Science Data*, 10, 185–194, 2018.
- 1476 Gillett, N. P., Shiogama, H., Funke, B., Hegerl, G., Knutti, R., Matthes, K., Santer, B. D., Stone, D.,
 1477 and Tebaldi, C.: The Detection and Attribution Model Intercomparison Project (DAMIP v1.0)
 1478 contribution to CMIP6, *Geoscientific Model Development*, 9, 3685–3697, 2016.
- 1479 Golub, M., Thiery, W., Marcé, R., Pierson, D., Vanderkelen, I., Mercado-Bettin, D., Woolway, R. I.,
 1480 Grant, L., Jennings, E., Kraemer, B. M., Schewe, J., Zhao, F., Frieler, K., Mengel, M., Bogomolov, V.
 1481 Y., Bouffard, D., Côté, M., Couture, R.-M., Debolskiy, A. V., Droppers, B., Gal, G., Guo, M., Janssen,
 1482 A. B. G., Kirillin, G., Ladwig, R., Magee, M., Moore, T., Perroud, M., Piccolroaz, S., Raaman Vinnua,
 1483 L., Schmid, M., Shatwell, T., Stepanenko, V. M., Tan, Z., Woodward, B., Yao, H., Adrian, R., Allan, M.,
 1484 Anneville, O., Arvola, L., Atkins, K., Boegman, L., Carey, C., Christianson, K., de Eyto, E., DeGasperi,
 1485 C., Grechushnikova, M., Hejzlar, J., Joehnk, K., Jones, I. D., Laas, A., Mackay, E. B., Mammarella, I.,
 1486 Markensten, H., McBride, C., Özkundakci, D., Potes, M., Rinke, K., Robertson, D., Rusak, J. A.,
 1487 Salgado, R., van der Linden, L., Verburg, P., Wain, D., Ward, N. K., Wollrab, S., and Zdrovennova,
 1488 G.: A framework for ensemble modelling of climate change impacts on lakes worldwide: the ISIMIP
 1489 Lake Sector, *Geosci. Model Dev.*, 15, 4597–4623, 2022.
- 1490 Gori, A., Lin, N., and Smith, J.: Assessing compound flooding from landfalling tropical cyclones on the
 1491 North Carolina coast, *Water Resour. Res.*, 56, <https://doi.org/10.1029/2019wr026788>, 2020.
- 1492 Gori, A., Lin, N., Xi, D., and Emanuel, K.: Tropical cyclone climatology change greatly exacerbates US
 1493 extreme rainfall–surge hazard, *Nat. Clim. Chang.*, 12, 171–178, 2022.
- 1494 Hansen, G., Stone, D., Auffhammer, M., Huggel, C., and Cramer, W.: Linking local impacts to
 1495 changes in climate: a guide to attribution, *Regional Environ. Change*, 16, 527–541, 2016.
- 1496 Hersbach, H., Bell, B., Berrisford, P., Hirahara, S., Horányi, A., Muñoz-Sabater, J., Nicolas, J.,
 1497 Peubey, C., Radu, R., Schepers, D., Simmons, A., Soci, C., Abdalla, S., Abellan, X., Balsamo, G.,
 1498 Bechtold, P., Biavati, G., Bidlot, J., Bonavita, M., Chiara, G., Dahlgren, P., Dee, D., Diamantakis, M.,
 1499 Dragani, R., Flemming, J., Forbes, R., Fuentes, M., Geer, A., Haimberger, L., Healy, S., Hogan, R. J.,
 1500 Hólm, E., Janisková, M., Keeley, S., Laloyaux, P., Lopez, P., Lupu, C., Radnoti, G., Rosnay, P.,
 1501 Rozum, I., Vamborg, F., Villaume, S., and Jean-Noël Thépaut: The ERA5 global reanalysis, *Quart. J.*
 1502 *Roy. Meteor. Soc.*, 146, 1999–2049, 2020.
- 1503 Holland, G.: A Revised Hurricane Pressure–Wind Model, *Mon. Weather Rev.*, 136, 3432–3445, 2008.
- 1504 Holland, G. J.: An Analytic Model of the Wind and Pressure Profiles in Hurricanes, *Mon. Weather*
 1505 *Rev.*, 108, 1212–1218, 1980.

- 1506 Hope, P., Cramer, W., van Aalst, M., Flato, G., Frieler, K., Gillett, N., Huggel, C., Minx, J., Otto, F.,
1507 Parmesan, C., Rogelj, J., Rojas, M., Seneviratne, S. I., Slangen, A., Stone, D., Terray, L., Vautard, R.,
1508 and Zhang, X.: Cross-Working Group Box CONTRIBUTION | Attribution in the IPCC Sixth Assessment
1509 Report, in: *Climate Change 2022 – Impacts, Adaptation and Vulnerability: Working Group II*
1510 *Contribution to the Sixth Assessment Report of the Intergovernmental Panel on Climate Change*,
1511 edited by: Pörtner, H.-O., Roberts, D. C., Tignor, M., Poloczanska, E. S., Mintenbeck, K., Alegría, A.,
1512 Craig, M., Langsdorf, S., Löschke, S., Möller, V., Okem, A., and Rama, B., Cambridge University
1513 Press, 121–196, 2022.
- 1514 van den Hurk, B., Kim, H., Krinner, G., Seneviratne, S. I., Derksen, C., Oki, T., Douville, H., Colin, J.,
1515 Ducharne, A., Cheruy, F., Viovy, N., Puma, M. J., Wada, Y., Li, W., Jia, B., Alessandri, A., Lawrence,
1516 D. M., Weedon, G. P., Ellis, R., Hagemann, S., Mao, J., Flanner, M. G., Zampieri, M., Matera, S.,
1517 Law, R. M., and Sheffield, J.: LS3MIP (v1.0) contribution to CMIP6: the Land Surface, Snow and Soil
1518 moisture Model Intercomparison Project – aims, setup and expected outcome, *Geosci. Model Dev.*, 9,
1519 2809–2832, 2016.
- 1520 Hurtt, G. C., Chini, L. P., Frohking, S., Betts, R. A., Feddema, J., Fischer, G., Fisk, J. P., Hibbard, K.,
1521 Houghton, R. A., Janetos, A., Jones, C. D., Kindermann, G., Kinoshita, T., Klein Goldewijk, K., Riahi,
1522 K., Shevliakova, E., Smith, S., Stehfest, E., Thomson, A., Thornton, P., van Vuuren, D. P., and Wang,
1523 Y. P.: Harmonization of land-use scenarios for the period 1500–2100: 600 years of global gridded
1524 annual land-use transitions, wood harvest, and resulting secondary lands, *Clim. Change*, 109, 117,
1525 2011.
- 1526 Hurtt, G. C., Chini, L., Sahajpal, R., Frohking, S., Bodirsky, B. L., Calvin, K., Doelman, J. C., Fisk, J.,
1527 Fujimori, S., Klein Goldewijk, K., Hasegawa, T., Havlik, P., Heinemann, A., Humpenöder, F.,
1528 Jungclaus, J., Kaplan, J. O., Kennedy, J., Krisztin, T., Lawrence, D., Lawrence, P., Ma, L., Mertz, O.,
1529 Pongratz, J., Popp, A., Poulter, B., Riahi, K., Shevliakova, E., Stehfest, E., Thornton, P., Tubiello, F.
1530 N., van Vuuren, D. P., and Zhang, X.: Harmonization of global land use change and management for
1531 the period 850–2100 (LUH2) for CMIP6, *Geosci. Model Dev.*, 13, 5425–5464, 2020.
- 1532 IFASTAT: <https://www.ifastat.org>, last access: 21 January 2015.
- 1533 International Monetary Fund: *World economic outlook*, 2021.
- 1534 IPCC: Annex II: Glossary [Mach, K.J., S. Planton and C. von Stechow (eds.)], in: *Climate Change*
1535 *2014: Synthesis Report. Contribution of Working Groups I, II and III to the Fifth Assessment Report of*
1536 *the Intergovernmental Panel on Climate Change*, edited by: Core Writing Team, R. K. Pachauri and L.
1537 A. Meyer, Geneva, Switzerland, 117–130, 2014.
- 1538 ISIMIP Coordination Team, Sectoral Coordinators, Scientific Advisory Board: *The Inter-Sectoral*
1539 *Impact Model Intercomparison Project (ISIMIP), Mission & Implementation Document*,
1540 https://www.isimip.org/documents/646/MissionAndImplementation_12Sep2018_5Hlvj2N.pdf, 2018.
- 1541 Jägermeyr, J. and Frieler, K.: Spatial variations in crop growing seasons pivotal to reproduce global
1542 fluctuations in maize and wheat yields, *Sci Adv*, 4, eaat4517, 2018.
- 1543 Jägermeyr, J., Müller, C., Ruane, A. C., Elliott, J., Balkovic, J., Castillo, O., Faye, B., Foster, I.,
1544 Folberth, C., Franke, J. A., Fuchs, K., Guarin, J. R., Heinke, J., Hoogenboom, G., Iizumi, T., Jain, A.
1545 K., Kelly, D., Khabarov, N., Lange, S., Lin, T.-S., Liu, W., Mialyk, O., Minoli, S., Moyer, E. J., Okada,
1546 M., Phillips, M., Porter, C., Rabin, S. S., Scheer, C., Schneider, J. M., Schyns, J. F., Skalsky, R.,
1547 Smerald, A., Stella, T., Stephens, H., Webber, H., Zabel, F., and Rosenzweig, C.: Climate impacts on
1548 global agriculture emerge earlier in new generation of climate and crop models, *Nature Food*, 2,
1549 873–885, 2021a.
- 1550 Jägermeyr, J., Müller, C., Minoli, S., Ray, D., and Siebert, S.: GGCM Phase 3 crop calendar,
1551 <https://doi.org/10.5281/ZENODO.5062513>, 2021b.
- 1552 Karger, D. N., Conrad, O., Böhner, J., Kawohl, T., Kreft, H., Soria-Auza, R. W., Zimmermann, N. E.,
1553 Linder, H. P., and Kessler, M.: Climatologies at high resolution for the earth's land surface areas, *Sci*
1554 *Data*, 4, 170122, 2017.
- 1555 Karger, D. N., Wilson, A. M., Mahony, C., Zimmermann, N. E., and Jetz, W.: Global daily 1 km land

- 1556 surface precipitation based on cloud cover-informed downscaling, *Sci Data*, 8, 307, 2021.
- 1557 Karger, D. N., Lange, S., Hari, C., Reyer, C. P. O., Conrad, O., Zimmermann, N. E., and Frieler, K.:
 1558 CHELSA-W5E5: Daily 1 km meteorological forcing data for climate impact studies, *Earth System*
 1559 *Science Data Discussions*, <https://doi.org/10.5194/essd-2022-367>, 2022a.
- 1560 Karger, D. N., Lange, S., Hari, C., Reyer, C. P. O., and Zimmermann, N. E.: CHELSA-W5E5 v1.0:
 1561 W5E5 v1.0 downscaled with CHELSA v2.0, <https://doi.org/10.48364/ISIMIP.836809.3>, 2022b.
- 1562 Khazaei, B., Read, L. K., Casali, M., Sampson, K. M., and Yates, D. N.: GLOBathy, the global lakes
 1563 bathymetry dataset, *Sci. Data*, 9, 36, 2022.
- 1564 Global soil wetness project phase 3 — GSWP3 documentation: <http://hydro.iis.u-tokyo.ac.jp/GSWP3/>,
 1565 last access: 9 January 2023.
- 1566 Kim, H.: Global Soil Wetness Project Phase 3 Atmospheric Boundary Conditions (Experiment 1),
 1567 <https://doi.org/10.20783/DIAS.501>, 2017.
- 1568 Klein Goldewijk, K.: 2022.
- 1569 Klein Goldewijk, K., Beusen, A., Doelman, J., and Stehfest, E.: Anthropogenic land use estimates for
 1570 the Holocene – HYDE 3.2, *Earth Syst. Sci. Data*, 9, 927–953, 2017.
- 1571 Knapp, K. R. and Kruk, M. C.: Quantifying Interagency Differences in Tropical Cyclone Best-Track
 1572 Wind Speed Estimates, *Mon. Weather Rev.*, 138, 1459–1473, 2010.
- 1573 Knapp, K. R., Kruk, M. C., Levinson, D. H., Diamond, H. J., and Neumann, C. J.: The International
 1574 Best Track Archive for Climate Stewardship (IBTrACS): Unifying Tropical Cyclone Data, *Bull. Am.*
 1575 *Meteorol. Soc.*, 91, 363–376, 2010.
- 1576 Koch, J. and Leimbach, M.: SSP economic growth projections: Major changes of key drivers in
 1577 integrated assessment modelling, *Ecol. Econ.*, 206, 107751, 2023.
- 1578 Konzelmann, T., van de Wal, R. S. W., Greuell, W., Bintanja, R., Henneken, E. A. C., and Abe-Ouchi,
 1579 A.: Parameterization of global and longwave incoming radiation for the Greenland Ice Sheet, *Glob.*
 1580 *Planet. Change*, 9, 143–164, 1994.
- 1581 Krien, Y., Dudon, B., Roger, J., Arnaud, G., and Zahibo, N.: Assessing storm surge hazard and impact
 1582 of sea level rise in the Lesser Antilles case study of Martinique, *Nat. Hazards Earth Syst. Sci.*, 17,
 1583 1559–1571, 2017.
- 1584 Lange, S.: Trend-preserving bias adjustment and statistical downscaling with ISIMIP3BASD (v1.0),
 1585 *Geosci. Model Dev.*, 12, 3055–3070, 2019.
- 1586 Lange, S.: ISIMIP3BASD, <https://doi.org/10.5281/zenodo.4686991>, 2021.
- 1587 Lange, S. and Büchner, M.: ISIMIP3 land-sea masks, <https://doi.org/10.48364/ISIMIP.822294>, 2020.
- 1588 Lange, S., Menz, C., Gleixner, S., Cucchi, M., Weedon, G. P., Amici, A., Bellouin, N., Schmied, H. M.,
 1589 Hersbach, H., Buontempo, C., and Cagnazzo, C.: WFDE5 over land merged with ERA5 over the
 1590 ocean (W5E5 v2.0), <https://doi.org/10.48364/ISIMIP.342217>, 2021.
- 1591 Lan, X., Tans, P., and Thoning, K. W.: Trends in globally-averaged CO₂ determined from NOAA
 1592 Global Monitoring Laboratory measurements. Version 2023-01 NOAA/GML, 2023.
- 1593 Large, W. G. and Yeager, S. G.: The global climatology of an interannually varying air–sea flux data
 1594 set, *Clim. Dyn.*, 33, 341–364, 2009.
- 1595 Lawrence, D. M., Hurtt, G. C., Arneth, A., Brovkin, V., Calvin, K. V., Jones, A. D., Jones, C. D.,
 1596 Lawrence, P. J., de Noblet-Ducoudré, N., Pongratz, J., Seneviratne, S. I., and Shevliakova, E.: The
 1597 Land Use Model Intercomparison Project (LUMIP) contribution to CMIP6: rationale and experimental
 1598 design, *Geosci. Model Dev.*, 9, 2973–2998, 2016.

- 1599 Lee, M., Shevliakova, E., Stock, C. A., Malyshev, S., and Milly, P. C. D.: Prominence of the tropics in
1600 the recent rise of global nitrogen pollution, *Nat. Commun.*, 10, 1437, 2019.
- 1601 Lehner, B., Reidy Liermann, C., Revenga, C., Vorosmarty, C., Fekete, B., Crouzet, P., Doll, P.,
1602 Endejan, M., Frenken, K., Magome, J., Nilsson, C., Robertson, J. C., Rodel, R., and Sindorf, N.:
1603 Global Reservoir and Dam Database, Version 1 (GRanDv1): Dams, Revision 01,
1604 <https://doi.org/10.7927/H4N877QK>, 2011a.
- 1605 Lehner, B., Liermann, C. R., Revenga, C., Vörösmarty, C., Fekete, B., Crouzet, P., Döll, P., Endejan,
1606 M., Frenken, K., Magome, J., Nilsson, C., Robertson, J. C., Rödel, R., Sindorf, N., and Wisser, D.:
1607 High-resolution mapping of the world's reservoirs and dams for sustainable river-flow management,
1608 *Front. Ecol. Environ.*, 9, 494–502, 2011b.
- 1609 Lejeune, Q., Maskell, G., Menke, I., and Pleeck, S.: Stakeholder Survey Report,
1610 https://www.isimip.org/documents/376/ISllopedia_survey_result_report_w47NU6L.pdf, 2018.
- 1611 Liu, X., Stock, C. A., Dunne, J. P., Lee, M., Shevliakova, E., Malyshev, S., and Milly, P. C. D.:
1612 Simulated global coastal ecosystem responses to a half-century increase in river nitrogen loads,
1613 *Geophys. Res. Lett.*, 48, <https://doi.org/10.1029/2021gl094367>, 2021.
- 1614 Loisel, J., Gallego-Sala, A. V., Amesbury, M. J., Magnan, G., Anshari, G., Beilman, D. W., Benavides,
1615 J. C., Blewett, J., Camill, P., Charman, D. J., Chawchai, S., Hedgpeth, A., Kleinen, T., Korhola, A.,
1616 Large, D., Mansilla, C. A., Müller, J., van Bellen, S., West, J. B., Yu, Z., Bubier, J. L., Garneau, M.,
1617 Moore, T., Sannel, A. B. K., Page, S., Väiliranta, M., Bechtold, M., Brovkin, V., Cole, L. E. S., Chanton,
1618 J. P., Christensen, T. R., Davies, M. A., De Vleeschouwer, F., Finkelstein, S. A., Frolking, S., Gałka,
1619 M., Gandois, L., Girkin, N., Harris, L. I., Heinemeyer, A., Hoyt, A. M., Jones, M. C., Joos, F., Juutinen,
1620 S., Kaiser, K., Lacourse, T., Lamentowicz, M., Larmola, T., Leifeld, J., Lohila, A., Milner, A. M.,
1621 Minkinen, K., Moss, P., Naafs, B. D. A., Nichols, J., O'Donnell, J., Payne, R., Philben, M., Piilo, S.,
1622 Quillet, A., Ratnayake, A. S., Roland, T. P., Sjögersten, S., Sonnentag, O., Swindles, G. T., Swinnen,
1623 W., Talbot, J., Treat, C., Valach, A. C., and Wu, J.: Expert assessment of future vulnerability of the
1624 global peatland carbon sink, *Nat. Clim. Chang.*, 11, 70–77, 2020.
- 1625 Lu, P., Lin, N., Emanuel, K., Chavas, D., and Smith, J.: Assessing Hurricane Rainfall Mechanisms
1626 Using a Physics-Based Model: Hurricanes Isabel (2003) and Irene (2011), *J. Atmos. Sci.*, 75,
1627 2337–2358, 2018.
- 1628 Marsooli, R., Lin, N., Emanuel, K., and Feng, K.: Climate change exacerbates hurricane flood hazards
1629 along US Atlantic and Gulf Coasts in spatially varying patterns, *Nat. Commun.*, 10, 3785, 2019.
- 1630 Matthews, J. B. R., Möller, V., van Diemen, R., Fuglestedt, J. S., Masson-Delmotte, V., Méndez, C.,
1631 Semenov, S., and Reisinger, A.: Annex VII: Glossary, in: *Climate Change 2021: The Physical Science
1632 Basis. Contribution of Working Group I to the Sixth Assessment Report of the Intergovernmental
1633 Panel on Climate Change*, edited by: Masson-Delmotte, V., Zhai, P., Pirani, A., Connors, S. L., Péan,
1634 C., Berger, S., Caud, N., Chen, Y., Goldfarb, L., Gomis, M. I., Huang, M., Leitzell, K., Lonnoy, E.,
1635 Matthews, J. B. R., Maycock, T. K., Waterfield, T., Yelekçi, O., Yu, R., and Zhou, B., Cambridge,
1636 United Kingdom and New York, NY, USA, 2215–2256, 2021.
- 1637 Mechler, R., Bouwer, L. M., Schinko, T., Surminski, S., and Linnerooth-Bayer, J.: Loss and damage
1638 from climate change: Concepts, methods and policy options, 1st ed., edited by: Mechler, R., Bouwer,
1639 L. M., Schinko, T., Surminski, S., and Linnerooth-Bayer, J., Springer International Publishing, Cham,
1640 Switzerland, 557 pp., 2018.
- 1641 Meinshausen, M., Smith, S. J., Calvin, K., Daniel, J. S., Kainuma, M. L. T., Lamarque, J.-F.,
1642 Matsumoto, K., Montzka, S. A., Raper, S. C. B., Riahi, K., Thomson, A., Velders, G. J. M., and van
1643 Vuuren, D. P. P.: The RCP greenhouse gas concentrations and their extensions from 1765 to 2300,
1644 *Clim. Change*, 109, 213, 2011.
- 1645 Meinshausen, M., Vogel, E., Nauels, A., Lorbacher, K., Meinshausen, N., Etheridge, D. M., Fraser, P.
1646 J., Montzka, S. A., Rayner, P. J., Trudinger, C. M., Krummel, P. B., Beyerle, U., Canadell, J. G.,
1647 Daniel, J. S., Enting, I. G., Law, R. M., Lunder, C. R., O'Doherty, S., Prinn, R. G., Reimann, S.,
1648 Rubino, M., Velders, G. J. M., Vollmer, M. K., Wang, R. H. J., and Weiss, R.: Historical greenhouse
1649 gas concentrations for climate modelling (CMIP6), *Geoscientific Model Development*, 10, 2057–2116,

- 1650 2017.
- 1651 Mengel, M., Treu, S., Lange, S., and Frieler, K.: ATTRICI v1.1 – counterfactual climate for impact
1652 attribution, *Geosci. Model Dev.*, 14, 5269–5284, 2021.
- 1653 Messenger, M. L., Lehner, B., Grill, G., Nedeva, I., and Schmitt, O.: Estimating the volume and age of
1654 water stored in global lakes using a geo-statistical approach, *Nat. Commun.*, 7, 13603, 2016.
- 1655 Monfreda, C., Ramankutty, N., and Foley, J. A.: Farming the planet: 2. Geographic distribution of crop
1656 areas, yields, physiological types, and net primary production in the year 2000, *Global Biogeochem.*
1657 *Cycles*, 22, <https://doi.org/10.1029/2007gb002947>, 2008.
- 1658 Cyclone Database Manager:
1659 [https://citeseerx.ist.psu.edu/document?repid=rep1&type=pdf&doi=b80049f3add16c6c4b8937c8f6b80](https://citeseerx.ist.psu.edu/document?repid=rep1&type=pdf&doi=b80049f3add16c6c4b8937c8f6b804071dd110b3)
1660 [4071dd110b3](https://citeseerx.ist.psu.edu/document?repid=rep1&type=pdf&doi=b80049f3add16c6c4b8937c8f6b804071dd110b3), last access: 18 October 2023.
- 1661 Muis, S., Apecechea, M. I., Dullaart, J., de Lima Rego, J., Madsen, K. S., Su, J., Yan, K., and Verlaan,
1662 M.: A high-resolution global dataset of extreme sea levels, tides, and storm surges, including future
1663 projections, *Front. Mar. Sci.*, 7, <https://doi.org/10.3389/fmars.2020.00263>, 2020.
- 1664 Müller Schmied, H.: DDM30 river routing network for ISIMIP3,
1665 <https://doi.org/10.48364/ISIMIP.865475>, 2022.
- 1666 Earth observation group - defense meteorological satellite program, boulder:
1667 <https://www.ngdc.noaa.gov/eog/dmsp/downloadV4composites.html>.
- 1668 van Oldenborgh, G. J., van der Wiel, K., Sebastian, A., Singh, R., Arrighi, J., Otto, F., Haustein, K., Li,
1669 S., Vecchi, G., and Cullen, H.: Attribution of extreme rainfall from Hurricane Harvey, August 2017,
1670 *Environ. Res. Lett.*, 12, 124009, 2017.
- 1671 O'Neill, B., van Aalst, M., Z., Z. I., Berrang Ford, L., Bhadwal, S., Buhaug, H., Diaz, D., Frieler, K.,
1672 Garschagen, M., Magnan, A., Midgley, G., Mirzabaev, A., Thomas, A., and Warren, R.: Climate
1673 Change 2022: Impacts, Adaptation and Vulnerability. Key Risks Across Sectors and Regions, in:
1674 Contribution of Working Group II to the Sixth Assessment Report of the Intergovernmental Panel on
1675 Climate Change, edited by: Pörtner, H.-O., Roberts, D. C., Tignor, M., Poloczanska, E. S.,
1676 Mintenbeck, K., Alegría, A., Craig, M., Langsdorf, S., Löschke, S., Möller, V., Okem, A., and Rama,
1677 B., Cambridge University Press, Cambridge, UK and New York, NY, USA, 2411–2538, 2022.
- 1678 Patricola, C. M. and Wehner, M. F.: Anthropogenic influences on major tropical cyclone events,
1679 *Nature*, 563, 339–346, 2018.
- 1680 Peduzzi, P., Chatenoux, B., Dao, H., De Bono, A., Herold, C., Kossin, J., Mouton, F., and Nordbeck,
1681 O.: Global trends in tropical cyclone risk, *Nat. Clim. Chang.*, 2, 289–294, 2012.
- 1682 Portmann, F. T., Siebert, S., and Döll, P.: MIRCA2000-Global monthly irrigated and rainfed crop areas
1683 around the year 2000: A new high-resolution data set for agricultural and hydrological modeling,
1684 *Global Biogeochem. Cycles*, 24, <https://doi.org/10.1029/2008gb003435>, 2010.
- 1685 Reyer, C., Silveyra Gonzalez, R., Dolos, K., Hartig, F., Hauf, Y., Noack, M., Lasch-Born, P., Rötzer,
1686 T., Pretzsch, H., Meesenburg, H., Fleck, S., Wagner, M., Bolte, A., Sanders, T., Kolari, P., Mäkelä, A.,
1687 Vesala, T., Mammarella, I., Pumpanen, J., Matteucci, G., Collalti, A., D'Andrea, E., Foltýnová, L.,
1688 Krejza, J., Ibrom, A., Pilegaard, K., Loustau, D., Bonnefond, J.-M., Berbigier, P., Picart, D., Lafont, S.,
1689 Dietze, M., Cameron, D., Vieno, M., Tian, H., Palacios-Orueta, A., Cicuendez, V., Recuero, L., Wiese,
1690 K., Büchner, M., Lange, S., Volkholz, J., Kim, H., Weedon, G., Sheffield, J., Vega del Valle, I.,
1691 Suckow, F., Horemans, J., Martel, S., Bohn, F., Steinkamp, J., Chikalanov, A., Mahnken, M., Gutsch,
1692 M., Trotta, C., Babst, F., and Frieler, K.: The PROFOUND database for evaluating vegetation models
1693 and simulating climate impacts on European forests. V. 0.3. GFZ Data Services,
1694 <https://doi.org/10.5880/PIK.2020.006>, 2020a.
- 1695 Reyer, C. P. O., Silveyra Gonzalez, R., Dolos, K., Hartig, F., Hauf, Y., Noack, M., Lasch-Born, P.,
1696 Rötzer, T., Pretzsch, H., Meesenburg, H., Fleck, S., Wagner, M., Bolte, A., Sanders, T. G. M., Kolari,
1697 P., Mäkelä, A., Vesala, T., Mammarella, I., Pumpanen, J., Collalti, A., Trotta, C., Matteucci, G.,

- 1698 D'Andrea, E., Foltýnová, L., Krejza, J., Ibrom, A., Pilegaard, K., Loustau, D., Bonnefond, J.-M.,
 1699 Berbigier, P., Picart, D., Lafont, S., Dietze, M., Cameron, D., Vieno, M., Tian, H., Palacios-Orueta, A.,
 1700 Cicuendez, V., Recuero, L., Wiese, K., Büchner, M., Lange, S., Volkholz, J., Kim, H., Horemans, J. A.,
 1701 Bohn, F., Steinkamp, J., Chikalanov, A., Weedon, G. P., Sheffield, J., Babst, F., Vega del Valle, I.,
 1702 Suckow, F., Martel, S., Mahnken, M., Gutsch, M., and Frieler, K.: The PROFOUND Database for
 1703 evaluating vegetation models and simulating climate impacts on European forests, *Earth Syst. Sci.*
 1704 *Data*, 12, 1295–1320, 2020b.
- 1705 Reyer, C. P. O., Schelhaas, M.-J., Mäkelä, A., Peltoniemi, M., Gutsch, M., Mahnken, M., Loustau, D.,
 1706 Martel, S., Merganič, J., Merganičová, K., Meesenburg, H., Rötzer, T., Heym, M., Collalti, A.,
 1707 D'Andrea, E., Matteucci, G., Ibrom, A., and Kvist Johannsen, V.: Current Site-specific management
 1708 guidelines and schedules for the 9 PROFOUND forest sites of the regional forest sector in ISIMIP,
 1709 <https://doi.org/10.5281/zenodo.7622027>, 2023.
- 1710 Risser, M. D. and Wehner, M. F.: Attributable human-induced changes in the likelihood and
 1711 magnitude of the observed extreme precipitation during hurricane Harvey, *Geophys. Res. Lett.*, 44,
 1712 12,457–12,464, 2017.
- 1713 Rousseau, Y., Blanchard, J., Novaglio, C., Pinnell, K., Tittensor, D., Watson, R., and Ye, Y.: A data
 1714 base of mapped global fishing activity, 1950-2017, *Scientific Data*, submitted 2023.
- 1715 Rousseau, Y., Blanchard, J., Novaglio, C., Kirsty, P., Tittensor, D., Watson, R., and Ye, Y.: Global
 1716 Fishing Effort, <https://doi.org/10.25959/MNGY-0Q43>, 2022.
- 1717 Rust, H. W., Kruschke, T., Dobler, A., Fischer, M., and Ulbrich, U.: Discontinuous Daily Temperatures
 1718 in the WATCH Forcing Datasets, *J. Hydrometeorol.*, 16, 465–472, 2015.
- 1719 Sarmiento, J. L. and Gruber, N.: Ocean Biogeochemical Dynamics, *Geol. Mag.*, 144, 1034–1034,
 1720 2006.
- 1721 Seitzinger, S., Harrison, J. A., Böhlke, J. K., Bouwman, A. F., Lowrance, R., Peterson, B., Tobias, C.,
 1722 and Van Dreht, G.: Denitrification across landscapes and waterscapes: a synthesis, *Ecol. Appl.*, 16,
 1723 2064–2090, 2006.
- 1724 Sherman, K.: Large Marine Ecosystems, in: *Encyclopedia of Ocean Sciences*, Elsevier, 709–723,
 1725 2017.
- 1726 Sitch, S., Friedlingstein, P., Gruber, N., Jones, S. D., Murray-Tortarolo, G., Ahlström, A., Doney, S. C.,
 1727 Graven, H., Heinze, C., Huntingford, C., Levis, S., Levy, P. E., Lomas, M., Poulter, B., Viovy, N.,
 1728 Zaehle, S., Zeng, N., Arneeth, A., Bonan, G., Bopp, L., Canadell, J. G., Chevallier, F., Ciais, P., Ellis,
 1729 R., Gloor, M., Peylin, P., Piao, S. L., Le Quéré, C., Smith, B., Zhu, Z., and Myneni, R.: Recent trends
 1730 and drivers of regional sources and sinks of carbon dioxide, *Biogeosciences*, 12, 653–679, 2015.
- 1731 Slivinski, L. C., Compo, G. P., Whitaker, J. S., Sardeshmukh, P. D., Giese, B. S., McColl, C., Allan, R.,
 1732 Yin, X., Vose, R., Titchner, H., Kennedy, J., Spencer, L. J., Ashcroft, L., Brönnimann, S., Brunet, M.,
 1733 Camuffo, D., Cornes, R., Cram, T. A., Crouthamel, R., Domínguez-Castro, F., Freeman, J. E., Gergis,
 1734 J., Hawkins, E., Jones, P. D., Jourdain, S., Kaplan, A., Kubota, H., Blancq, F. L., Lee, T.-C., Lorrey,
 1735 A., Luterbacher, J., Maugeri, M., Mock, C. J., Moore, G. W. K., Przybylak, R., Pudmenzky, C.,
 1736 Reason, C., Slonosky, V. C., Smith, C. A., Tinz, B., Trewin, B., Valente, M. A., Wang, X. L., Wilkinson,
 1737 C., Wood, K., and Wyszyński, P.: Towards a more reliable historical reanalysis: Improvements for
 1738 version 3 of the Twentieth Century Reanalysis system, *Quart. J. Roy. Meteor. Soc.*, 145, 2876–2908,
 1739 2019.
- 1740 Slivinski, L. C., Compo, G. P., Sardeshmukh, P. D., Whitaker, J. S., McColl, C., Allan, R. J., Brohan,
 1741 P., Yin, X., Smith, C. A., Spencer, L. J., Vose, R. S., Rohrer, M., Conroy, R. P., Schuster, D. C.,
 1742 Kennedy, J. J., Ashcroft, L., Brönnimann, S., Brunet, M., Camuffo, D., Cornes, R., Cram, T. A.,
 1743 Domínguez-Castro, F., Freeman, J. E., Gergis, J., Hawkins, E., Jones, P. D., Kubota, H., Lee, T. C.,
 1744 Lorrey, A. M., Luterbacher, J., Mock, C. J., Przybylak, R. K., Pudmenzky, C., Slonosky, V. C., Tinz, B.,
 1745 Trewin, B., Wang, X. L., Wilkinson, C., Wood, K., and Wyszyński, P.: An Evaluation of the
 1746 Performance of the Twentieth Century Reanalysis Version 3, *J. Clim.*, 34, 1417–1438, 2021.
- 1747 Smil, V.: *Enriching the Earth: Fritz Haber, Carl Bosch and the Transformation of World Food*

- 1748 Production, MIT Press, 2001.
- 1749 Stock, C. A., Dunne, J. P., and John, J. G.: Global-scale carbon and energy flows through the marine
1750 planktonic food web: An analysis with a coupled physical–biological model, *Prog. Oceanogr.*, 120,
1751 1–28, 2014.
- 1752 Tian, H., Yang, J., Lu, C., Xu, R., Canadell, J. G., Jackson, R. B., Arneeth, A., Chang, J., Chen, G.,
1753 Ciais, P., Gerber, S., Ito, A., Huang, Y., Joos, F., Lienert, S., Messina, P., Olin, S., Pan, S., Peng, C.,
1754 Saikawa, E., Thompson, R. L., Vuichard, N., Winiwarter, W., Zaehle, S., Zhang, B., Zhang, K., and
1755 Zhu, Q.: The Global N₂O Model Intercomparison Project, *Bull. Am. Meteorol. Soc.*, 99, 1231–1251,
1756 2018.
- 1757 Tittensor, D. P., Eddy, T. D., Lotze, H. K., Galbraith, E. D., Cheung, W., Barange, M., Blanchard, J. L.,
1758 Bopp, L., Bryndum-Buchholz, A., Büchner, M., Bulman, C., Carozza, D. A., Christensen, V., Coll, M.,
1759 Dunne, J. P., Fernandes, J. A., Fulton, E. A., Hobday, A. J., Huber, V., Jennings, S., Jones, M.,
1760 Lehodey, P., Link, J. S., Mackinson, S., Maury, O., Niiranen, S., Oliveros-Ramos, R., Roy, T.,
1761 Schewe, J., Shin, Y.-J., Silva, T., Stock, C. A., Steenbeek, J., Underwood, P. J., Volkholz, J., Watson,
1762 J. R., and Walker, N. D.: A protocol for the intercomparison of marine fishery and ecosystem models:
1763 Fish-MIP v1.0, *Geoscientific Model Development*, 11, 1421–1442, 2018.
- 1764 Treu, S., Muis, S., Dangendorf, S., Wahl, S., Heinicke, S., Frieler, K., and M., M.: Reconstruction of
1765 hourly coastal water levels and counterfactuals without sea level rise for impact attribution, *Earth
1766 System Science Data Discussions*, 1-23, <https://doi.org/10.5194/essd-2023-112>, 2023.
- 1767 Tsujino, H., Urakawa, S., Nakano, H., Small, R. J., Kim, W. M., Yeager, S. G., Danabasoglu, G.,
1768 Suzuki, T., Bamber, J. L., Bentsen, M., Böning, C. W., Bozec, A., Chassignet, E. P., Curchitser, E.,
1769 Boeira Dias, F., Durack, P. J., Griffies, S. M., Harada, Y., Ilicak, M., Josey, S. A., Kobayashi, C.,
1770 Kobayashi, S., Komuro, Y., Large, W. G., Le Sommer, J., Marsland, S. J., Masina, S., Scheinert, M.,
1771 Tomita, H., Valdivieso, M., and Yamazaki, D.: JRA-55 based surface dataset for driving ocean–sea-
1772 ice models (JRA55-do), *Ocean Model.*, 130, 79–139, 2018.
- 1773 del Valle, I. V., Reyer, C., and Perrette, M.: ISIMIP3a wood harvesting input data,
1774 <https://doi.org/10.48364/ISIMIP.482888.1>, 2022.
- 1775 Wada, Y., Lo, M.-H., Yeh, P. J.-F., Reager, J. T., Famiglietti, J. S., Wu, R.-J., and Tseng, Y.-H.: Fate
1776 of water pumped from underground and contributions to sea-level rise, *Nat. Clim. Chang.*, 6, 777–780,
1777 2016a.
- 1778 Wada, Y., Flörke, M., Hanasaki, N., Eisner, S., Fischer, G., Tramberend, S., Satoh, Y., van Vliet, M. T.
1779 H., Yillia, P., Ringler, C., Burek, P., and Wiberg, D.: Modeling global water use for the 21st century:
1780 the Water Futures and Solutions (WFaS) initiative and its approaches, *Geoscientific Model
1781 Development*, 9, 175–222, 2016b.
- 1782 Wang, J., Walter, B. A., Yao, F., Song, C., Ding, M., Maroof, A. S., Zhu, J., Fan, C., McAlister, J. M.,
1783 Sikder, S., Sheng, Y., Allen, G. H., Crétaux, J.-F., and Wada, Y.: GeoDAR: georeferenced global
1784 dams and reservoirs dataset for bridging attributes and geolocations, *Earth Syst. Sci. Data*, 14,
1785 1869–1899, 2022.
- 1786 Wang, S.-Y. S., Zhao, L., Yoon, J.-H., Klotzbach, P., and Gillies, R. R.: Quantitative attribution of
1787 climate effects on Hurricane Harvey’s extreme rainfall in Texas, *Environ. Res. Lett.*, 13, 054014, 2018.
- 1788 Wang, T. and Sun, F.: Global gridded GDP data set consistent with the shared socioeconomic
1789 pathways, *Sci Data*, 9, 221, 2022.
- 1790 Watson, R.: Global Fisheries Landings V4.0, <https://doi.org/10.25959/5C522CADBEA37>, 2019.
- 1791 Watson, R. A. and Tidd, A.: Mapping nearly a century and a half of global marine fishing: 1869–2015,
1792 *Mar. Policy*, 93, 171–177, 2018.
- 1793 Whitehouse, P. L.: Glacial isostatic adjustment modelling: historical perspectives, recent advances,
1794 and future directions, *Earth Surf. Dyn.*, 6, 401–429, 2018.

1795 Wöppelmann, G. and Marcos, M.: Vertical land motion as a key to understanding sea level change
1796 and variability, *Rev. Geophys.*, 54, 64–92, 2016.

1797 Wyns, A.: COP27 establishes loss and damage fund to respond to human cost of climate change,
1798 *Lancet Planet Health*, 7, e21–e22, 2023.

1799 Xi, D., Lin, N., and Smith, J.: Evaluation of a Physics-Based Tropical Cyclone Rainfall Model for Risk
1800 Assessment, *J. Hydrometeorol.*, 21, 2197–2218, 2020.

1801 Yang, J. and Tian, H.: ISIMIP3a N-deposition input data, <https://doi.org/10.48364/ISIMIP.759077.1>,
1802 2020.

1803 Yang, J., Yan, F., and Chen, M.: Effects of sea level rise on storm surges in the south Yellow Sea: A
1804 case study of Typhoon Muifa (2011), *Cont. Shelf Res.*, 215, 104346, 2021.

1805 Sea Around Us Area Parameters and Definitions: <https://www.searoundus.org/sea-around-us-area-parameters-and-definitions/>.

1807 Zhang, X., Davidson, E. A., Mauzerall, D. L., Searchinger, T. D., Dumas, P., and Shen, Y.: Managing
1808 nitrogen for sustainable development, *Nature*, 528, 51–59, 2015.

1809 Zhao, N., Liu, Y., Cao, G., Samson, E. L., and Zhang, J.: Forecasting China’s GDP at the pixel level
1810 using nighttime lights time series and population images, *GISci. Remote Sens.*, 54, 407–425, 2017.

1811 Zhu, L., Quiring, S. M., and Emanuel, K. A.: Estimating tropical cyclone precipitation risk in Texas,
1812 *Geophys. Res. Lett.*, 40, 6225–6230, 2013.

1813

1814 GSWP3 soil texture map: <http://hydro.iis.u-tokyo.ac.jp/~sujan/research/gswp3/soil-texture-map.html>,
1815 upscaling method A., last access 28 April 2022

1816

1817 GGCMI-HWSD: https://github.com/AgMIP-GGCMI/processing_hwsd_for_GGCMI, last access: 9
1818 February 2023

1819

1820 Tractebel: Filling of the reservoir of the Grand Renaissance Dam: <https://tractebel->
1821 [engie.com/en/news/2020/ethiopia-first-stage-of-the-filling-of-the-reservoir-of-the-grand-renaissance-](https://tractebel-)
1822 [dam](https://tractebel-), September 2020, last access: 10 February 2023.

1823

1824 UN 2019 World Population Prospects (WPP) Database 2019: <https://population.un.org/wpp/>, last
1825 access: 15 February 2023

1826 Malle, Johanna. 2023. w5e5_downscale. Github. https://github.com/johanna-malle/w5e5_downscale.

1827 IFASTAT: Statistics, International Fertilizer Association, IFASTAT Database [data set], available at:
1828 <https://www.ifastat.org>, last access: 21 January 2015.

1829

1830 ISIMIP organigram: <https://www.isimip.org/about/#organisational-structure>, last access: 7 March, 2023

1831 Technical University of Denmark (DTU): Global Wind Atlas 3.0, released in partnership with World
1832 Bank Group, utilising data provided by Vortex, using funding provided by Energy Sector Management
1833 Assistance Program (ESMAP) [data set], available at: <https://globalwindatlas.info>, 2023.

1834 United Nations, Department of Economic and Social Affairs: Population Division (2019), World
1835 Population Prospects 2019, archive [data set],
1836 <https://population.un.org/wpp/Download/Archive/Standard/>, 2019.

1837